ON THE VIBRATIONS OF A SHAFT CARRYING AN UNSYMMETRICAL ROTOR

Toshio YAMAMOTO and Hiroshi ŌTA

Department of Mechanical Engineering

(Received August 31, 1968)

CONTENTS

Page

Nomenclature 2
General Introduction 4
Chapter 1. Fundamental Equations 6
1.1. Introduction 6
1.2. Experimental apparatus and methods of experiments 7
1.3. Fundamental equations of motion 8
Chapter 2. Forced Vibrations without Damping and Unstable Vibrations near Major Critical Speed ω_c 13
2.1. Introduction 13
2.2. Major critical speeds and response curves 13
2.3. Unstable region near major critical speed 14
2.4. Natural frequencies and amplitude ratios of free vibrations 16
2.5. Experimental results 18
2.6. Conclusions 20
Chapter 3. Forced Vibrations with Viscous Damping 20
3.1. Introduction 20
3.2. Damping effect on unstable region 20
3.3. Forced vibrations due to eccentricity e 24
3.4. Forced vibrations due to deviational angle τ 26
3.5. Uncoupled system of two degrees of freedom ($\gamma=0$) 27
3.6. Conclusions 29
Chapter 4. Forced Vibrations Having the Circular Frequencies Differing from the Rotating Angular Velocity of the Shaft 30
4.1. Introduction 30
4.2. Solutions for the forced vibrations 30
4.3. Amplitude ratio of forced vibrations 33
4.4. Experimental apparatus and experimental results 38
4.5. Conclusions 41
Chapter 5. Unstable Vibrations Induced by Flexibility of Bearing Pedestals 42
5.1. Introduction 42
5.2. Existence of zones of instability, motions in the unstable zones 42
5.3. Effects of the damping force 48
5.4. Coupled system of four degrees of freedom ($\gamma\neq 0$) 49
5.5. Experimental results 50
5.6. Conclusions 53
Chapter 6. Unstable Vibrations near Rotating Speed ω_n 53
6.1. Introduction 53
6.2. Frequency equation and existence of unstable vibrations 54
6.3. Unstable region 55

6.4. Range of unstable region and value of negative damping coefficient 57
6.5. Approximation methods 59
6.6. Experimental results 60
6.7. Conclusions 63
Chapter 7. Effects of a Distributed Mass of Shaft, and of Non-linear Characteristics of Shaft Stiffness on Unstable Vibrations 64
7.1. Introduction 64
7.2. Equations of motion and frequency equation 65
7.3. Unstable vibrations (experiment I) 67
7.4. Unstable vibrations (experiment II) 71
7.5. Conclusions 73
Chapter 8. Unstable Vibrations of a Shaft with Unsymmetrical Stiffness 73
8.1. Introduction 73
8.2. Equations of motion and forced vibrations 73
8.3. Unstable vibrations near ω_e and ω_d 75
8.4. Conclusions 76
References 77

Nomenclature

The following nomenclature is used in this paper:

A, B, C. D, a, b, c, d, e=amplitudes of shaft vibration,

E, F, $\overline{E}$, $\overline{F}$, E_f, F_f, $\overline{E}_f$, $\overline{F}_f$=amplitudes of natural frequencies p, $\overline{p}$,

A_0, B_0, C_0, D_0=amplitudes of stationary forced vibrations,

E, F, E_0, F_0, A, B, C, D=amplitudes of forced vibrations with circular frequency ω_0,

E', F', E_0', F_0', A', B', C', D'=amplitudes of forced vibrations with circular frequency ω_0',

A_{ij}=cofactor of element a_{ij},

$a:b$=ratio representing the position of a rotor put on the shaft,

$c_1[c_1' = c_1\sqrt{g/(W\alpha)}]^*$=damping coefficient for deflections x, y,

$c_2[c_2' = c_2\sqrt{W/(\alpha g)}/I]$=damping coefficient for inclination angles θ_x, θ_y,

c_{c_1}, c_{c_2}=critical damping coefficients,

D=discriminant of biquadratic equation,

d=diameter of shaft,

det (a_{ij})=determinant consisting of element a_{ij},

$e[e' = e\sqrt{W/(Ig)}]$=statical unbalance (eccentricity),

F=dissipation function,

f, $\overline{f}$, f_i, f_j, f_0, $\overline{f}_0$, Φ, Φ_0=frequency equations,

G=gravitational center of rotor,

$G=\delta+i_p\omega p-p^2$, $\overline{G}=\delta+i_p\omega\overline{p}-\overline{p}^2$,

g=gravitational acceleration,

$H=1-p^2$, $\overline{H}=1-\overline{p}^2$,

H_i=Hurwitz's determinant of the i th order,

$I_z=\pi d^4/64$=moment of inertia of circular cross section of shaft,

I_1=principal moment of inertia about MY_2-axis,

I_2=principal moment of inertia about MX_2-axis,

$I=(I_1+I_2)/2$=mean value of diametral moments of inertia,

$I_p[i_p=I_p/I]$=polar moment of inertia about MZ_1-axis,

$i=\sqrt{-1}$=imaginary unit,

$j=M_t\sqrt{W/(Ig)}/P$ [$=M_t'/P'$],
i, j, k=integers,
K_i, K_i'=the i th order coefficients of the characteristic equation,
l=length of the shaft,
M=geometrical center of rotor,
M_t, [$M_t'=M_tW/(\alpha gI)$]=external moment acting on rotor with circular frequency ω_0,
m[$m'=m\sqrt{W/(\alpha g)}$]=negative damping coefficient,
$m_{\max}$=maximum value of negative damping coefficient,
o-x, y, z=rectangular coordinate system fixed in space,
P[$P'=P\sqrt{W/(Ig)}/\alpha$]=external force acting on rotor with circular frequency ω_0,
P_i, P_j=frequencies of unstable vibrations in unstable region,
p, p_i, p_j, p_{i0}[$p'=p\sqrt{W/(\alpha g)}$]=natural frequencies of lateral vibrations of the shaft,
$\overline{p}=2\omega-p$=natural frequency coupled with p,
P', p'=natural frequencies referred to the coordinate system rotating with shaft,
Q_s=generalized force,
q_s=generalized coordinate,
$r=\sqrt{x^2+y^2}$=lateral displacement of rotor,
s=eigenvalue or complex root of characteristic equation,
t[$t'=t\sqrt{\alpha g/W}$]=time,
T, T_1, T_2=kinetic energy of the system,
V, V'=potential energy of the system,
W=weight of rotor,
$X=\delta+(i_p-1)\omega^2$, $X_1=\delta+(i_p-1-\Delta)\omega^2$, $X_2=\delta+(i_p-1+\Delta)\omega^2$,
x, y, z[x', $y'=x$, $y\sqrt{W/(Ig)}$]=rectangular coordinates of the point M,
x_G, y_G, z_G=coordinates of the point G,
α, α_0=spring constants of shaft,
α', α'', β_i, β_j=phase differences,
$\tan\alpha$, $\tan\beta$, $\tan\alpha'$, $\tan\beta'$=gradients of p, p' in $p-\omega$ and $p'-\omega$ diagrams,
γ, γ_0[$\gamma'=\gamma\sqrt{W/(Ig)}/\alpha$]=spring constants of shaft,
$\Delta I=(I_1-I_2)/2$ [$\Delta=\Delta I/I$]=inertia asymmetry of rotor,
$\Delta\alpha$, $\Delta\gamma$, $\Delta\delta$=rotating or stationary half differences between maximum and minimum value of α, γ, and δ,
$\Delta_{11}=\Delta\alpha/\alpha$, $\Delta_{12}=\Delta\gamma/\gamma$, $\Delta_{22}=\Delta\delta/\delta$=rotating asymmetries of stiffness due to unsymmetrical shaft,
Δ_s=uniform asymmetry of flat shaft,
δ, δ_0[$\delta'=\delta W/(\alpha gI)$]=spring constants of shaft,
$\varepsilon=\Delta\alpha/\alpha$, $\varepsilon_{12}=\Delta\gamma/\gamma$, $\varepsilon_{22}=\Delta\delta/\delta$=stationary asymmetries of stiffness due to flexibility of bearing pedestals,
$\kappa_{12}=\varepsilon_{12}/\varepsilon$, $\kappa_{22}=\varepsilon_{22}/\varepsilon$,
η=angular position of τ, or deviation of p from p_0,
$\Theta=\varphi+\psi=\omega t-\pi/2$, $\Theta_1=\varphi_1+\psi_1$,
θ, θ_1, φ, φ_1, ψ, ψ_1=Eulerian angles denoting the angular position of the rotor and disc surface,
θ_x, θ_y, θ_{x_1}, θ_{y_1}=components of θ, θ_1 in x- and y-directions respectively,
ξ=angular position of e, or deviation of ω from ω_0,

$2|\xi_0|$=width of unstable region,
$\xi_{1,2}$, $\eta_{1,2}$=deviations from stationary forced vibration,
τ=dynamic unbalance, small deviational angle between MZ_1-axis and tangent MZ_0 of the deflection curve of the shaft at the point M,
$\varphi = -(1-p^2)(1-\overline{p}^2)p^2\overline{p}^2$, or phase difference,
$\omega = \dot{\Theta} = \dot{\varphi} + \dot{\psi}[\omega' = \omega\sqrt{W/(\alpha g)}]$ = angular velocity of the rotating shaft,
ω_0=circular frequency of external disturbance,
$\omega_0' = 2\omega - \omega_0$=circular frequency of coupled vibration with excitation ω_0,
ω_c, $\omega_{c_{1,2,3}}$ = major critical speeds,
ω_a, ω_d=rotating speeds of the cross points A, D,
ω_{d_2}, ω_{d1}=upper and lower limits of unstable region near ω_d,
ω_f, ω_g=rotating speeds where the relations $p_1=2\omega$ and $p_1=2\omega-1$ hold,
ω_{X_2}, ω_{Y_2}, ω_{Z_1} = components of angular velocity of rotor in MX_2-, MY_2-, and MZ_1-directions.

* Dimensionless quantity c_1' is shown in the bracket, and the prime on it is often omitted.

General Introduction

The number of revolutions of rotary machine has been increased gradually, and higher performance has been demanded for machinery, and, as the result, the problem of preventing vibration of the rotating shaft becomes of vital importance in this age of high speed mechinery.

A peculiar and seemingly hopeless complex whirling of rotating shaft sometimes takes place at a specified rotating speed due to various causes, and this speed is called "critical speed". If the amplitude of whirling during the rotation of shaft near the critical speed is large, it is a life and death matter to rotary machinery and to humans whose lives often depend on the proper function of rotary machinery. If the amplitude is not so large, the shaft is broken down by fatigue due to repeated stress during long time operation, and the machine containing the shaft is fatally damaged sometimes. Moreover, there are some cases that it is difficult to pass over the critical speed even when the shaft is designed to rotate at higher speed than the critical one. Even though it does not develop into a serious accident, the vibration of the shaft makes the performance of machine lower, causes noise, or is transmitted to near other machines, and, as the result, many troubles take place.

In order to get rid of the shaft vibration, the causes of vibration must be cleared up. Various vibrations of shaft investigated hitherto can be classified into the following four groups according to the cause of initiation.

(1) Forced vibrations

When there is a small eccentricity e of rotor or a slight deviation τ between the polar axis of inertia and the tangent of shaft, resonant whirling is violently induced at the vicinity of the angular velocity of rotating shaft which coincides with the natural circular frequency of the shaft system because centrifugal force by e and centrifugal moment by τ act on the rotating body periodically. This critical speed is called "major critical speed", at which whirling is the most furious and takes place generally, and has been investigated[1] in detail by W. J. Rankin (1869), S. Dunkerley (1894), A. Stodola (1903), S. Timoshenko (1928), L.

Föppl (1929), D. Robertson (1933), and J. P. Den Hartog (1934). Furthermore, such forced vibration can take place as secondary critical speed[2)3)4)] caused in a horizontal shaft having unsymmetrical bending rigidity, synchronous backward precession[5)] caused by directionally unequal flexibility of bearing pedestals, and two types of forced whirling[5)] of forward and backward precessions due to difference in diameter between steel balls of ball bearing.

(2) *Forced vibrations generated by non-linear spring characteristics*

Since there is an "angular clearance" in single-row radial ball bearing, asymmetric non-linearity takes place in the spring constants of shaft, and, as the result, sub-harmonic and "summed and differential hamonic" oscillations are induced[6)7)].

(3) *Self-excited vibrations*

There are three types of self-excited vibration of shaft. From the view point of "rotating field of resistance"[5)], the resistance acting to shaft is negative damping force that promotes the development of whirling. Oil whip or oil whirl discovered by B. L. Newkirk[9)] is induced by pressure of oil film in bearing, and the preventive method for it has been investigated for long time[10)]. A new stability criterion[11)] has been derived recently that can explain clearly many inconsistent experimental results concerning oil whip. Hysteresis whirl generated due to internal friction of shaft is induced not only by hysteresis of the shaft material[12)], but also by sliding friction at a sleeve or a hub to the shaft or between parts of a built-up rotor[13)]. Further qualitative investigation has been carried out by J. G. Baker[14)], F. M. Dimentberg[15)], and A. Tondl[16)]. Moreover, backward whirling due to dry friction between the shaft and guard ring is also investigated[17)].

(4) *Unstable vibrations induced by inequality rotating together with shaft*

(4.1) For a flat shaft or shaft with key way, the spring constant of the shaft is not equal in all directions. When lateral vibration of a disc located at the middle of shaft is constrained by a guide groove into only one direction, the equation of motion of the disc is expressed as Mathieu equation with parametric excitation, and some domains of the number of revolutions appear, in which the vibration of the disc becomes unstable near the major critical speed[18)]. Even if the guide groove is removed, similar unstable vibration takes place[3)4)19)]. There are some investigations[20)21)22)] concerning the combined effect of the inequality of the spring constant of rotating shaft and that of bearing pedestals.

(4.2) For a shaft with such unsymmetrical rotor as two-bladed propeller or armature of two-pole generator, similar unstable vibration with that of shaft with non-uniform elasticity also takes place. D. M. Smith[19)] (1933), Y. Yamada[22)] (1954), L. Y. Banaf and F. M. Dimentberg[23)] (1960), and S. Aiba[24)] (1963) report that unstable vibration appears in the vicinity of the major critical speed. O. N. Romaniv[25)] (1960), S. H. Crandall and P. J. Brosens[26)] (1961) report the effect of combination of unsymmetric rotor and flat shaft on the range of the unstable domain near the major critical speed.

In this paper the authors treat experimentally and analytically several kinds of forced and free vibrations of a shaft carrying an unsymmetrical rotor. The

vibratory character of the shaft system with an unsymmetrical rotor is found to be differ considerably from that with a symmetrical rotor.

This paper consists of eight chapters. In Chapter 1, a simple experimental apparatus and methods of experiments are shown. Then fundamental four differential equations of motion are introduced for lateral vibrations of the shaft[27].

In Chapter 2, upon use of the equations established in Chapter 1, forced and free vibrations with the modes of whirling are obtained. Unstable regions near the major critical speeds and natural frequencies of the system without damping are shown[27].

In Chapter 3, response curves, unstable region and phase difference of forced vibrations with viscous damping are calculated, and the effects of magnitudes of damping coefficients and of angular position between static unbalance e, dynamic unbalance τ and the inertia axis MY_2 of rotor are studied[29].

In Chapter 4, two forced vibrations of frequencies ω_0 and $\omega_0' = 2\omega - \omega_0$ are shown to take place simultaneously, when an unsymmetrical rotor with angular velocity ω is excited by a periodic external force having frequency ω_0. Depending on the circumstances, the amplitudes of the vibration of frequency ω_0' become remarkably larger than the amplitudes of the harmonic oscillations, *i.e.*, the forced vibration of frequency ω_0[31].

In Chapter 5, new regions of instability to occur due to coexistence of rotating asymmetry in inertia of rotor and stational small dissimilarity in stiffness of bearing pedestals are shown analytically by using "approximation method". These unstable vibrations are experimentally ascertained by adopting a bearing pedestal which is nearly rigid in x-direction, but somewhat flexible in y-direction[28].

In Chapter 6, it is shown that in the neighborhood of the rotating speed ω_d, where the relation $p_1+p_2=2\omega$ is satisfied, there is another unstable region in which two unstable lateral vibrations with frequencies $P_1(\fallingdotseq p_1)$ and $P_2(\fallingdotseq p_2)$ take place simultaneously and grow up steadily. Generally, frequencies P_1 and P_2 are not equal to the rotating speed ω of the shaft, and sum of these P_1+P_2 is always equal to 2ω[30].

In Chapter 7, new unstable regions are shown to occur due to a distributed mass of shaft[32]. This distributed mass of shaft itself has sometimes a rather low natural frequency of fundamental mode, and must not be always neglected, though it is fully neglected through Chapter 1~6.

In Chapter 8, it is shown that a shaft with unsymmetrical stiffness has similar unstable regions to those treated in Chapter 2 and 6, and approximation methods found useful in Chapter 6 are also applicable. The general system with gyroscopic terms and with a symmetrical rotor not mounted at the middle of the unsymmetrical shaft is discussed[27][34].

Chapter 1. Fundamental Equations[27]

1.1. Introduction

There are three principal moments of inertia I_p, I_1, and I_2 about the three principal axes passing through the geometrical center M of a rotor. The polar moment of inertia I_p is a principal moment of inertia about the rotating axis of the rotor, and I_1 and I_2 are principal moments of inertia about the axes perpendicular to the rotating axis. Rotors with I_1 and I_2 of equal magnitude, such as

the cylindrical ones, are called symmetrical rotors. The rotors having I_1 and I_2 of unequal magnitude, such as two-pole generator or two-bladed propeller, are known as unsymmetrical rotors.

1.2. Experimental apparatus and methods of experiments

Various sorts of lateral vibrations take place in the vertical shaft S carrying an unsymmetrical rotor R as shown in Figs. 1.1 and 1.2. Self-aligning double-row ball bearings with a bore of 10ϕ (#1200) are used. The rotor R is driven by a V-belt, power supplied by a 5-HP, DC motor with speed variations of from 0 to 6000 rpm. In order to remove the disturbance from the velt, a coupling S_p consisting of a helical spring is inserted between the pulley V and the shaft S. A guard ring G just above R is equipped to check the increase of deflections of the shaft. The upper surface of the rotor R is made of disc, then the whirling of the shaft is measured optically by recording simultaneously lateral motions of the disc edge both in x-direction and y-direction. A small piece of celluloid P is attached to the disc edge. The two beams of light from lamps F_1, F_2 are intercepted by this piece at each revolution of the shaft and thus the record both of rotating speed and of rotating direction of the shaft is obtained at the same time.

As shown in Fig. 1.2, the light from a lamp F_2, passing through a condensing lens L_1' placed before the disc, goes to a point B on the disc edge and is bent 90° by a prism P_3 and focused on a rotating film F by a lens L_2'. A slit S_l is placed before F in order to make sharp images. At the same time another light

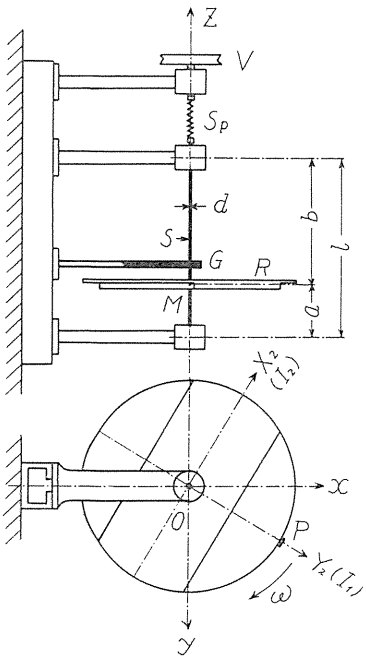

FIG. 1.1. Experimental apparatus

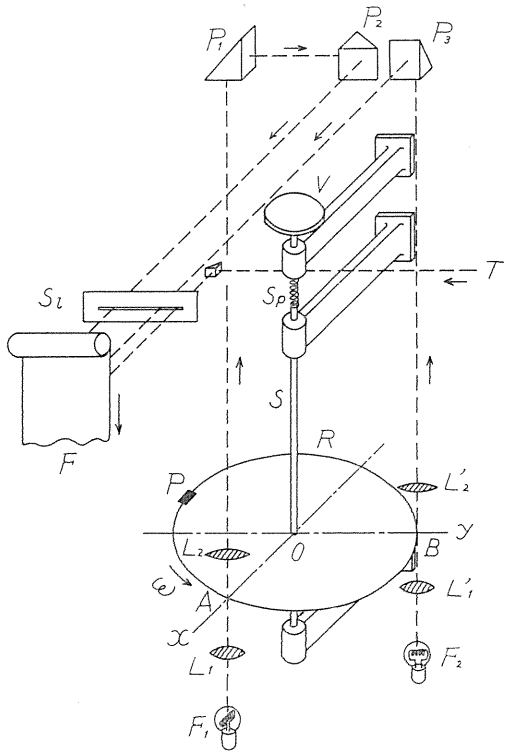

FIG. 1.2. Optical method of experiments

from F_1, passing through a point A and reflected by prisms P_1 and P_2, is focused by a lens L_2. A time mark T of 1/100 seconds is recorded on the film F at the same time. In experiments the direction of OA (which is the direction of the center line of bearing pedestal) is selected as x-axis, and the direction OB as y-axis.

The dimensions of an unsymmetrical rotor mainly used in experiments are as follows:

Diameter of disc edge=478.8 mm,

Weight $W=9.746$ kg,

Polar moment of inertia $I_p=2.390$ kg cm s^2,

Diametral moment of inertia about MY_2-axis $I_1=1.590$ kg cm s^2,

Diametral moment of inertia about MX_2-axis $I_2=0.815$ kg cm s^2.

Four shafts used in experiments are shown in the following Table 1.1, where the spring constants of the shaft made of mild steel α, γ, and δ may be calculated by "Strength of Material". Both ends of shaft are supported freely to incline by self-aligning double-row ball bearings.

$$\left.\begin{aligned}\alpha &= 3lEI_z(a^2-ab+b^2)/(a^3b^3),\\ \gamma &= 3lEI_z(a-b)/(a^2b^2),\\ \delta &= 3lEI_z/(ab),\end{aligned}\right\} \tag{1.1}$$

in which $E=2.1\times10^6$ kg/cm^2 is Young's modulus of shaft, $I_z=\pi d^4/64$ is moment of inertia of the area of cross section of shaft, d is diameter of round shaft, a, b are distances of the rotor from the lower and upper shaft ends, and shaft length $l=a+b$.

For an over-hang shaft which is supported only at the upper shaft end and used in experiments of chapter 6, spring constants α, γ, and δ are

$$\left.\begin{aligned}\alpha &= 6EI_z(2mn+6)/l^3(4mn+3),\\ \gamma &= -6EI_z(2mn+3)/l^2(4mn+3),\\ \delta &= 6EI_z(2mn+2)/l(4mn+3),\end{aligned}\right\} \tag{1.2}$$

in which $n=l_0/l$, l_0 is the center distance between the upper and lower ball bearings, l is the length of shaft from the lower bearing to the rotor, and n may be considered to reduce to 0 if the shaft end is fixed to incline, $m=I_z/I_{z0}$, I_{z0} is moment of inertia of the area of cross section of shaft between two ball bearings.

1.3. Fundamental equations of motion

We treat with the rotating shaft system consisting of a light elastic shaft and an unsymmetrical rotor with a weight W. Let o be the position of the geometrical center M of the rotor when no whirl exists and consider the right-handed rectangular coordinate system o-xyz fixed in space as shown in Fig. 1.3 in which z-axis is the bearing center line. Let M $(x, y, 0)$ be the shaft center where the rotor is mounted, and let $G(x_G, y_G, z_G)$ be the gravitational center of the rotor. The point M remains always on the xy-plane when shaft whirls and the rotor has five degrees of freedom. Now let us define the following five rectangular systems passing through the geometrical center M as follows:

M-XYZ is the rectangular coordinate system through M paralleling the

TABLE 1.1. Dimensions and Spring Constants of Shafts

No.	$a:b$	l mm	d mm	a mm	b mm	α kg/cm	$-\gamma$ kg/rad	δ kgcm/rad
1	1 : 3	508.2	11.80	131.9	376.3	2.725×10^2	3.023×10^3	6.139×10^4
2	1 : 4	505.5	11.60	101.9	403.6	5.375	5.047	6.881
3	3 : 7	507.0	11.88	151.2	355.8	2.055	2.204	5.787
4	1 : 5	506.1	11.67	84.5	421.6	9.570	7.700	8.137

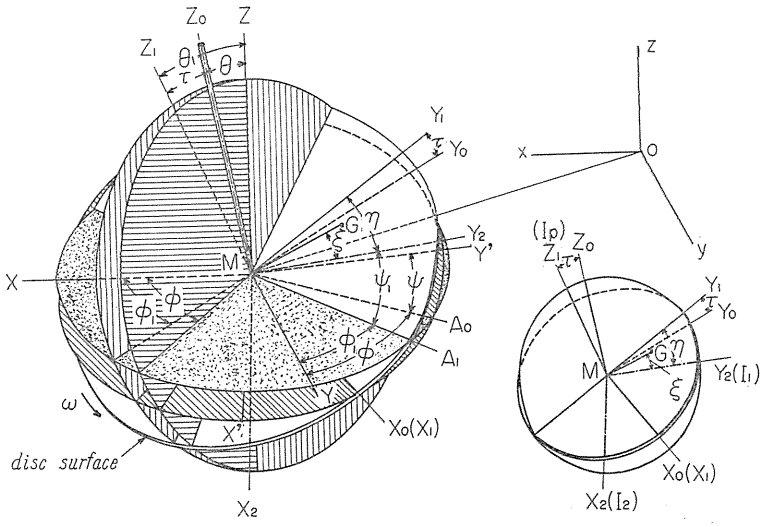

FIG. 1.3. Rectangular coordinates and Eulerian angles

system *o-xyz*.

M-$X_2Y_2Z_1$ is the rectangular coordinate system which consists of three principal axes passing through M, and the inclination of which is denoted by using Eulerian angles θ_1, φ_1, and ϕ_1. In Fig. 1.3, the X_2Y_2-plane is named as the disc surface.

M-$X_1Y_1Z_1$ is the system in which the X_1Y_1-plane coincides with the disc surface. A small deviational angle τ (*i.e.*, dynamic unbalance) from an ideal mounting is the angle between the principal axis MZ_1 and the tangent MZ_0 of deflection curve at M. The intersecting line MX_0 of the disc surface and the $X'Y'$-plane is perpendicular to the Z_0MZ_1 plane and Y_0MY_1 plane.

M-$X_0Y_0Z_0$ coincides with the system M-$X_1Y_1Z_1$ provided that the shaft is mounted perpendicular to the disc surface, *i.e.*, $\tau=0$.

M-$X'Y'Z_0$ coincides with the system M-$X_2Y_2Z_1$ provided $\tau=0$, and the inclination of the system M-$X'Y'Z_0$ is denoted by using Eulerian angles θ, φ, and ϕ.

Let principal moments of inertia about the principal axes MZ_1, MY_2, and MX_2 be I_p, I_1, and I_2 $(I_1>I_2)$, respectively, and let $I=(I_1+I_2)/2$, $\Delta I=(I_1-I_2)/2$. These principal moments of inertia regarding M differ only by the order of e^2 from the principal moments of inertia regarding the geometrical center G. The advanced angles $\xi=\angle Y_2MG$, and $\eta=\angle Y_2MY_1$ are the proceeding angles from the axis MY_2 to the direction to which the eccentricity $\overline{MG}=e$, and the small angle $\tau=\angle Y_0MY_1$ exist.

We proceed to obtain the differential equations of motion by using Lagrange's equation. Kinetic energy of translation T_1 is expressed in the form,

$$T_1 = \frac{W}{2g}(\dot{x}_G^2 + \dot{y}_G^2 + \dot{z}_G^2). \tag{1.3}$$

Let the rotating speed of shaft be ω, and let the components of the angular velocity in the MX_2-, MY_2-, and MZ_1-directions be ω_{X2}, ω_{Y2}, and ω_{Z1}, severally. Kinetic energy of rotation T_2 is represented as follows:

$$T_2 = \frac{1}{2}(I_p\omega_{Z_1}^2 + I_1\omega_{Y_2}^2 + I_2\omega_{X_2}^2). \tag{1.4}$$

Since the angular velocities of the rotor in the directions of MZ, MA_1 (*i.e.*, the intersecting line between the X_1Y_1-disc surface and the XY-plane), and MZ_1 are $\dot{\varphi}_1$, $\dot{\theta}_1$, and $\dot{\psi}_1$, respectively, ω_{X_2}, ω_{Y_2}, ω_{Z_1} are expressed as

$$\left.\begin{aligned} \omega_{X_2} &= \dot{\theta}_1\sin\psi_1 - \dot{\varphi}_1\sin\theta_1\cos\psi_1, \\ \omega_{Y_2} &= \dot{\theta}_1\cos\psi_1 + \dot{\varphi}_1\sin\theta_1\sin\psi_1, \\ \omega_{Z_1} &= \dot{\psi}_1 + \dot{\varphi}_1\cos\theta_1. \end{aligned}\right\} \tag{1.5}$$

We may neglect the terms of powers higher than 3rd order of small quantities e, τ, small variables x, y, θ_1, and their time derivatives which are all usually enough small compared with unity. We now introduce new variables as follows:

$$\left.\begin{aligned} &\Theta_1 = \varphi_1 + \psi_1, \quad \Theta = \varphi + \psi, \\ &\theta_{x_1} = \theta_1\cos\varphi_1, \quad \theta_x = \theta\cos\varphi, \\ &\theta_{y_1} = \theta_1\sin\varphi_1, \quad \theta_y = \theta\sin\varphi, \end{aligned}\right\} \tag{1.6}$$

where θ_x, θ_y are the projectional angles of inclination θ to xz-, and yz-planes.

Substituting Eqs. (1.5) and (1.6) into Eq. (1.4) we have

$$\begin{aligned} T_2 = \frac{1}{2}[&I_p\{\dot{\Theta}_1^2 + \dot{\Theta}_1(\dot{\theta}_{x_1}\theta_{y_1} - \dot{\theta}_{y_1}\theta_{x_1})\} + I(\dot{\theta}_{x_1}^2 + \dot{\theta}_{y_1}^2) \\ &+ \Delta I\{2\dot{\theta}_{x_1}\dot{\theta}_{y_1}\sin 2\Theta_1 + (\dot{\theta}_{x_1}^2 - \dot{\theta}_{y_1}^2)\cos 2\Theta_1\}]. \end{aligned} \tag{1.7}$$

The total kinetic energy of the rotor T is

$$T = T_1 + T_2. \tag{1.8}$$

The potential energy of the shaft V should be represented by the following form

$$V = \frac{1}{2}\alpha(x^2 + y^2) + \gamma(x\theta_x + y\theta_y) + \frac{1}{2}\delta(\theta_x^2 + \theta_y^2) \tag{1.9}$$

where spring constants α, γ, and δ are given in Eq. (1.1) or (1.2). And the dissipation function F is defined as follows:

$$F = \frac{1}{2}c_1(\dot{x}^2 + \dot{y}^2) + \frac{1}{2}c_2(\dot{\theta}_x^2 + \dot{\theta}_y^2) \tag{1.10}$$

where c_1 is viscous damping coefficient regarding deflection x, y, and c_2 is that regarding projectional angles θ_x, θ_y. Upon using the geometrical relationship of G and the direction cosines of the three sets of axis M-$X_0Y_0Z_0$, M-$X_1Y_1Z_1$, and M-XYZ with respect to each other, we obtain the following eight equations:

$$\dot{x}_G^2+\dot{y}_G^2+\dot{z}_G^2=\dot{x}^2+\dot{y}^2-2e\dot{\Theta}\{\dot{x}\cos(\Theta+\xi)+\dot{y}\sin(\Theta+\xi)\}+e^2\dot{\Theta}^2, \tag{1.11}$$

$$\left.\begin{aligned}
&\dot{\Theta}_1=\dot{\Theta}+\frac{\tau}{2}\dot{\Theta}\{\theta_x\sin(\Theta+\eta)-\theta_y\cos(\Theta+\eta)\}-\frac{\tau}{2}\{\dot{\theta}_x\cos(\Theta+\eta)+\dot{\theta}_y\sin(\Theta+\eta)\},\\
&\dot{\theta}_{x_1}\theta_{y_1}-\dot{\theta}_{y_1}\theta_{x_1}=\dot{\theta}_x\theta_y-\dot{\theta}_y\theta_x-\tau^2\dot{\Theta}-\tau\dot{\Theta}\{\theta_x\sin(\Theta+\eta)-\theta_y\cos(\Theta+\eta)\}\\
&\qquad\qquad-\tau\{\dot{\theta}_x\cos(\Theta+\eta)+\dot{\theta}_y\sin(\Theta+\eta)\},\\
&\dot{\theta}_{x_1}^2+\dot{\theta}_{y_1}^2=\dot{\theta}_x^2+\dot{\theta}_y^2+\tau^2\dot{\Theta}^2+2\tau\dot{\Theta}\{\dot{\theta}_x\cos(\Theta+\eta)+\dot{\theta}_y\sin(\Theta+\eta)\},\\
&\dot{\theta}_{x_1}\dot{\theta}_{y_1}=(1-\tau^2)\dot{\theta}_x\dot{\theta}_y+\tau\dot{\Theta}\{\dot{\theta}_x\sin(\Theta+\eta)+\dot{\theta}_y\cos(\Theta+\eta)\}+\frac{1}{2}\tau^2\dot{\Theta}^2\sin(2\Theta+2\eta),\\
&\dot{\theta}_{x_1}^2-\dot{\theta}_{y_1}^2=(1-\tau^2)(\dot{\theta}_x^2-\dot{\theta}_y^2)+2\tau\dot{\Theta}\{\dot{\theta}_x\cos(\Theta+\eta)-\dot{\theta}_y\sin(\Theta+\eta)\}\\
&\qquad\qquad+\tau^2\dot{\Theta}^2\cos(2\Theta+2\eta),\\
&\sin2\Theta_1=\sin2\Theta+\frac{\tau}{2}[\theta_y\{\sin(\Theta-\eta)-\sin(3\Theta+\eta)\}\\
&\qquad\qquad-\theta_x\{\cos(\Theta-\eta)+\cos(3\Theta+\eta)\}],\\
&\cos2\Theta_1=\cos2\Theta+\frac{\tau}{2}[\theta_x\{\sin(\Theta-\eta)+\sin(3\Theta+\eta)\}\\
&\qquad\qquad+\theta_y\{\cos(\Theta-\eta)-\cos(3\Theta+\eta)\}].
\end{aligned}\right\} \tag{1.12}$$

Substituting Eq. (1.11) into Eq. (1.3), and Eq. (1.12) into Eq. (1.7), we can express T of Eq. (1.8) as follows:

$$\begin{aligned}
T=&\frac{W}{2g}[\dot{x}^2+\dot{y}^2-2e\dot{\Theta}\{\dot{x}\cos(\Theta+\xi)+\dot{y}\sin(\Theta+\xi)\}+e^2\dot{\Theta}^2]\\
&+\frac{1}{2}I_p[(1-\tau^2)\dot{\Theta}^2-2\tau\dot{\Theta}\{\dot{\theta}_x\cos(\Theta+\eta)+\dot{\theta}_y\sin(\Theta+\eta)\}\\
&+\dot{\Theta}(\dot{\theta}_x\theta_y-\dot{\theta}_y\theta_x)]\\
&+\frac{1}{2}I[\dot{\theta}_x^2+\dot{\theta}_y^2+\tau^2\dot{\Theta}^2+2\tau\dot{\Theta}\{\dot{\theta}_x\cos(\Theta+\eta)+\dot{\theta}_y\sin(\Theta+\eta)\}]\\
&+\frac{1}{2}\Delta I[(\dot{\theta}_x^2-\dot{\theta}_y^2)\cos2\Theta+2\dot{\theta}_x\dot{\theta}_y\sin2\Theta+\tau^2\dot{\Theta}^2\cos2\eta\\
&+2\tau\dot{\Theta}\{\dot{\theta}_x\cos(\Theta-\eta)+\dot{\theta}_y\sin(\Theta-\eta)\}].
\end{aligned} \tag{1.8a}$$

Substituting Eqs. (1.8a), (1.9), and (1.10) into Lagrange's equation of motion (1.13)

$$\frac{d}{dt}\left(\frac{\partial T}{\partial\dot{q}_s}\right)-\frac{\partial T}{\partial q_s}+\frac{\partial V}{\partial q_s}+\frac{\partial F}{\partial\dot{q}_s}=Q_s \tag{1.13}$$

in which q_s is a generalized coordinate, and Q_s is a generalized force besides

restoring force. The equation of motion regarding Θ becomes

$$\{(1-\tau^2)I_p+\frac{We^2}{g}+(I+\Delta I\cos 2\eta)\tau^2\}\ddot{\Theta}$$
$$=\frac{We}{g}\{\ddot{x}\cos(\Theta+\xi)+\ddot{y}\sin(\Theta+\xi)\}+(I_p-I)\tau\{\ddot{\theta}_x\cos(\Theta+\eta)$$
$$+\ddot{\theta}_y\sin(\Theta+\eta)\}+\frac{1}{2}I_p(\ddot{\theta}_y\theta_x-\ddot{\theta}_x\theta_y)+\Delta I[2\dot{\theta}_x\dot{\theta}_y\cos 2\Theta$$
$$-(\dot{\theta}_x^2-\dot{\theta}_y^2)\sin 2\Theta-\tau\{\ddot{\theta}_x\cos(\Theta-\eta)+\ddot{\theta}_y\sin(\Theta-\eta)\}]. \tag{1.14}$$

Since all quantities of $\ddot{x}$, $\ddot{y}$, $\ddot{\theta}_x$, $\ddot{\theta}_y$, $\dot{\theta}_x$, $\dot{\theta}_y$, θ_x, θ_y, e, and τ are enough small compared with unity, we may neglect the higher powers of them in Eq. (1.14), so Eq. (1.14) is approximately expressed as follows:

$$I_p\ddot{\Theta}=0 \tag{1.14a}$$

and it leads to

$$\dot{\Theta}=\dot{\varphi}+\dot{\phi}=\omega, \qquad \Theta=\omega t-\pi/2. \tag{1.14b}$$

This conclusion (1.14a) or (1.14b) coincides with the usual assumption taken by most researchers. Eq. (1.14) means that the angular velocity of rotation $\dot{\Theta}$ is constant and that the rotation Θ is independent on the whirling motion x, y. It is recently insisted by A. Watari[1] that the assumption of constant angular speed of rotation is not general, and that it introduces many misleading and incomplete explanations, and that the whirl and the rotation relate with each other by eccentricity and the motion is exactly decided only by using non-linear equations. But the assumption (1.14a) or (1.14b) is kept enough, especially for the experimental apparatus shown in Figs. 1.1 and 1.2 where the twisting rigidity of coupling spring S_p is very small and the couple between the rotation of shaft Θ and lateral vibrations x, y, θ_x, and θ_y can be neglected as shown in Eq. (1.14).

Using the foregoing relationship (1.14b), we obtain the equations of motion regarding x, y, θ_x, and θ_y as follows[27]:

$$\frac{W}{g}\ddot{x}+c_1\dot{x}+\alpha x+\gamma\theta_x=\frac{W}{g}e\omega^2\cos(\omega t+\xi), \tag{1.15}$$

$$\frac{W}{g}\ddot{y}+c_1\dot{y}+\alpha y+\gamma\theta_y=\frac{W}{g}e\omega^2\sin(\omega t+\xi), \tag{1.16}$$

$$I\ddot{\theta}_x+I_p\omega\dot{\theta}_y+c_2\dot{\theta}_x+\gamma x+\delta\theta_x-\Delta I\cdot\frac{d}{dt}(\dot{\theta}_x\cos 2\omega t+\dot{\theta}_y\sin 2\omega t)$$
$$=\tau\omega^2\{(I_p-I)\cos(\omega t+\eta)-\Delta I\cos(\omega t-\eta)\}, \tag{1.17}$$

$$I\ddot{\theta}_y-I_p\omega\dot{\theta}_x+c_2\dot{\theta}_y+\gamma y+\delta\theta_y-\Delta I\cdot\frac{d}{dt}(\dot{\theta}_x\sin 2\omega t-\dot{\theta}_y\cos 2\omega t)$$
$$=\tau\omega^2\{(I_p-I)\sin(\omega t+\eta)-\Delta I\sin(\omega t-\eta)\}. \tag{1.18}$$

Putting $\Delta I=0$, $\Theta=\omega t-\pi/2-\xi$, and $\beta=\eta-\xi$ in Eqs. (1.15), (1.16), (1.17), and (1.18) we obtain the equations of motion of the shaft carrying a symmetrical rotor[5].

Chapter 2. Forced Vibrations without Damping and Unstable Vibrations near Major Critical Speed ω_c[27]

2.1. Introduction

The character of the vibratory shaft system with an unsymmetrical rotor differs considerably from that of the shaft system mounting a symmetrical rotor. In this chapter we study forced vibrations without damping and unstable regions near major critical speed ω_c, natural frequencies and amplitude ratios of free vibrations of the system.

2.2. Major critical speeds and response curves

Particular solutions of Eqs. (1.15)~(1.18), when $c_1=c_2=0$ are

$$\left.\begin{aligned} x &= E\cos(\omega t+\beta_1) = A\cos\omega t - B\sin\omega t,\\ y &= E\sin(\omega t+\beta_1) = A\sin\omega t + B\cos\omega t,\\ \theta_x &= F\cos(\omega t+\beta_2) = C\cos\omega t - D\sin\omega t,\\ \theta_y &= F\sin(\omega t+\beta_2) = C\sin\omega t + D\cos\omega t. \end{aligned}\right\} \tag{2.1}$$

Eq. (2.1) represent the forced vibrations induced by periodic disturbing forces caused by e or τ, and in Eq. (2.1) angles β_1 and β_2 are the phase differences between the vibrations and MY_2-axis. Substituting Eq. (2.1) into Eqs. (1.15)~(1.18) when $c_1=c_2=0$, we can obtain the amplitudes A, B, C, and D;

$$\left.\begin{aligned} A &= \frac{We\omega^2/g\{\delta+(I_p-I-\Delta I)\omega^2\}\cos\xi - (I_p-I-\Delta I)\tau\omega^2\gamma\cos\eta}{(\alpha-W\omega^2/g)\{\delta+(I_p-I-\Delta I)\omega^2\}-\gamma^2},\\ B &= \frac{We\omega^2/g\{\delta+(I_p-I+\Delta I)\omega^2\}\sin\xi - (I_p-I+\Delta I)\tau\omega^2\gamma\sin\eta}{(\alpha-W\omega^2/g)\{\delta+(I_p-I+\Delta I)\omega^2\}-\gamma^2},\\ C &= \frac{-(W/g)e\omega^2\gamma\cos\xi + (I_p-I-\Delta I)\tau\omega^2(\alpha-W\omega^2/g)\cos\eta}{(\alpha-W\omega^2/g)\{\delta+(I_p-I-\Delta I)\omega^2\}-\gamma^2},\\ D &= \frac{-(W/g)e\omega^2\gamma\sin\xi + (I_p-I+\Delta I)\tau\omega^2(\alpha-W\omega^2/g)\sin\eta}{(\alpha-W\omega^2/g)\{\delta+(I_p-I+\Delta I)\omega^2\}-\gamma^2}. \end{aligned}\right\} \tag{2.2}$$

When the amplitudes A and C become infinite, the rotating speed ω coincides with the major critical speeds ω_{c21}, ω_{c11}, and when B and D become infinite, ω agrees with the major critical speeds ω_{c22}, ω_{c12}. At the major critical speeds, the next relation holds,

$$\begin{aligned} K_0 = {} & [(\alpha-W\omega^2/g)\{\delta+(I_p-I-\Delta I)\omega^2\}-\gamma^2]\\ & \times[(\alpha-W\omega^2/g)\{\delta+(I_p-I+\Delta I)\omega^2\}-\gamma^2]=0. \end{aligned} \tag{2.3}$$

Solving Eq. (2.3), we have ω_{c21}, ω_{c22}, ω_{c11}, and ω_{c12};

$$\left.\begin{aligned} \frac{\omega_{c21}^2}{\omega_{c11}^2} &= \frac{\alpha(I_p-I-\Delta I)-W\delta/g \pm \sqrt{\{\alpha(I_p-I-\Delta I)+W\delta/g\}^2-4(I_p-I-\Delta I)W\gamma^2/g}}{2W(I_p-I-\Delta I)/g},\\ \frac{\omega_{c22}^2}{\omega_{c12}^2} &= \frac{\alpha(I_p-I+\Delta I)-W\delta/g \pm \sqrt{\{\alpha(I_p-I+\Delta I)+W\delta/g\}^2-4(I_p-I+\Delta I)W\gamma^2/g}}{2W(I_p-I+\Delta I)/g}. \end{aligned}\right\} \tag{2.4}$$

Putting $\Delta I=0$ in Eq. (2.4), we obtain the major critical speeds ω_c for the

vibratory shaft system with a symmetrical rotor ($I=I_1=I_2$). Critical speeds ω_{c21}, ω_{c22} are the lower major critical speeds and ω_{c11}, ω_{c12} are the higher. Critical speeds ω_{c11}, ω_{c12} can appear only when I_p is smaller than I_1. In Figs. 2.1 (a), (b), the response curves and the phase difference curves in the neighbourhood of the major critical speeds ω_{c21}, ω_{c22} are shown. As amplitudes C and D of inclination angle are remarkably small compared with ampitudes A and B of deflection, we show here A, B and β_1 only. Amplitude E and phase difference φ in Eq. (2.1) are expressed by

$$\left.\begin{aligned} E &= \sqrt{A^2+B^2}, \\ \varphi &= \xi - \beta_1 = \xi - \tan^{-1} A/B. \end{aligned}\right\} \tag{2.5}$$

Calculation is performed for the apparatus of Experiment II. As we see in Figs. 2.1 (a), (b), behaviors of vibrations are very much influenced by the magnitude of the angle ξ between the MG direction and the principal axis MY_2.

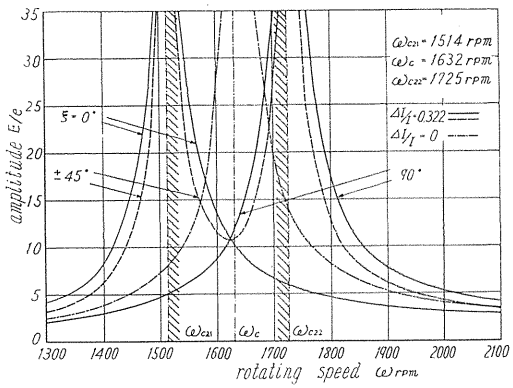

(a) Response curves

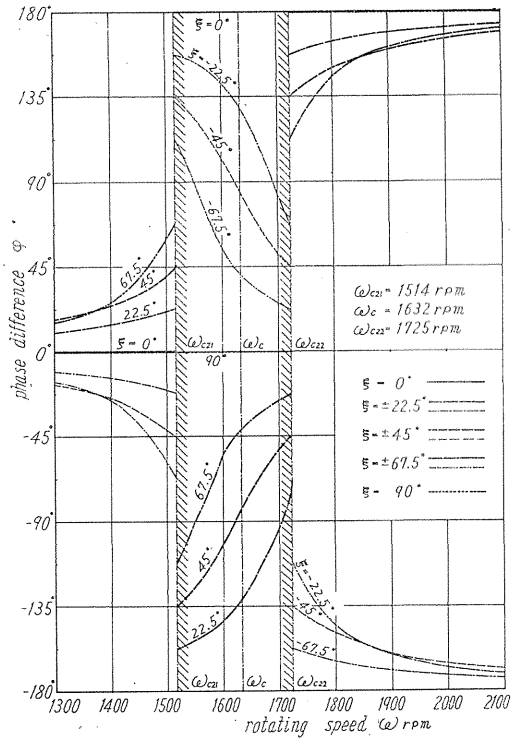

(b) Phase difference curves

FIG. 2.1. Forced vibrations near major critical speed ω_{c12}, ω_{c13} (Experiment II)

2.3. Unstable region near major critical speed

We treat the problems of stability of the system having an unsymmetrical rotor by Andronow—Witt method. Putting the stationary amplitudes as A_0, B_0, C_0, and D_0 in Eq. (2.1), and the small deviations from the stationary amplitudes as $\xi_{1,2}$, $\eta_{1,2}$, we have

$$\left.\begin{aligned} A &= A_0 + \xi_1, \quad B = B_0 + \xi_2, \\ C &= C_0 + \eta_1, \quad D = D_0 + \eta_2. \end{aligned}\right\} \tag{2.6}$$

Inserting Eqs. (2.1) and (2.6) into Eqs. (1.15)~(1.18) when $c_1 = c_2 = 0$, the differential equations for small deviations $\xi_{1,2}$, $\eta_{1,2}$ are

$$\left.\begin{aligned} &(W/g)\ddot{\xi}_1 + (\alpha - W\omega^2/g)\xi_1 - 2(W/g)\omega\dot{\xi}_2 + \gamma\eta_1 = 0, \\ &(W/g)\ddot{\xi}_2 + (\alpha - W\omega^2/g)\xi_2 + 2(W/g)\omega\dot{\xi}_1 + \gamma\eta_2 = 0, \\ &(I - \Delta I)\ddot{\eta}_1 + \{\delta + (I_p - I - \Delta I)\omega^2\}\eta_1 - (2I - I_p)\omega\dot{\eta}_2 + \gamma\xi_1 = 0, \\ &(I + \Delta I)\ddot{\eta}_2 + \{\delta + (I_p - I + \Delta I)\omega^2\}\eta_2 + (2I - I_p)\omega\dot{\eta}_1 + \gamma\xi_2 = 0. \end{aligned}\right\} \tag{2.7}$$

Substituting

$$\begin{matrix} \xi_1 \\ \xi_2 \end{matrix} = \begin{matrix} \xi_{10} \\ \xi_{20} \end{matrix} e^{st}, \quad \begin{matrix} \eta_1 \\ \eta_2 \end{matrix} = \begin{matrix} \eta_{10} \\ \eta_{20} \end{matrix} e^{st}, \tag{2.7a}$$

into Eq. (2.7), we can obtain the characteristic equation for s

$$K_8 s^8 + K_6 s^6 + K_4 s^4 + K_2 s^2 + K_0 = 0, \tag{2.8}$$

where coefficients $K_8 \sim K_0$ are functions of ω as shown in Eq. (2.3) and Eq. (2.9).

$$\left.\begin{aligned} K_8 &= (W/g)^2(I + \Delta I)(I - \Delta I), \\ K_6 &= (W/g)^2(I + \Delta I)\{\delta + (I_p - I - \Delta I)\omega^2\} + (W/g)^2(I - \Delta I)\{\delta + (I_p - I + \Delta I)\omega^2\} \\ &\quad + 2(W/g)(I + \Delta I)(I - \Delta I)(\alpha + W\omega^2/g) + (W/g)^2(2I - I_p)^2\omega^2, \\ K_4 &= (W/g)^2\{\delta + (I_p - I - \Delta I)\omega^2\}\{\delta + (I_p - I + \Delta I)\omega^2\} \\ &\quad + 2(W/g)(I + \Delta I)(\alpha + W\omega^2/g)\{\delta + (I_p - I - \Delta I)\omega^2\} \\ &\quad + 2(W/g)(I - \Delta I)(\alpha + W\omega^2/g)\{\delta + (I_p - I + \Delta I)\omega^2\} \\ &\quad + (I + \Delta I)(I - \Delta I)(\alpha - W\omega^2/g)^2 + 2(W/g)(2I - I_p)^2(\alpha + W\omega^2/g)\omega^2 - 2WI\gamma^2/g, \\ K_2 &= 2(W/g)(\alpha + W\omega^2/g)\{\delta + (I_p - I - \Delta I)\omega^2\}\{\delta + (I_p - I + \Delta I)\omega^2\} \\ &\quad + (I + \Delta I)(\alpha - W\omega^2/g)^2\{\delta + (I_p - I - \Delta I)\omega^2\} \\ &\quad + (I - \Delta I)(\alpha - W\omega^2/g)^2\{\delta + (I_p - I + \Delta I)\omega^2\} \\ &\quad - 2\gamma^2\{I\alpha + W\delta/g - 3(2I - I_p)W\omega^2/g\} + (2I - I_p)^2(\alpha - W\omega^2/g)^2\omega^2. \end{aligned}\right\} \tag{2.9}$$

Since $K_8 > 0$, Eq. (2.8) has at least one positive root for the rotating speed ω satisfying $K_0 < 0$ and the system becomes statically unstable. When $K_0 = 0$, ω has the critical values between stable and unstable ranges, and its values just coincide with ω_c given by Eq. (2.4). Consequently in the regions $[\omega_{c21}, \omega_{c22}]$ and $[\omega_{c11}, \omega_{c12}]$ the vibrations become statically unstable, because $K_0 < 0$.

Generally the next relation (2.10) between three moments of inertia I_p, I_1, and I_2 about principal axes through the gravitational center of rotor does hold

$$I_1 + I_2 \geqq I_p \geqq I_1 - I_2 \quad (i.e., \ 2I \geqq I_p \geqq 2\Delta I). \tag{2.10}$$

Unstable regions are classified into the next three cases (a), (b), and (c) for

various values of I_p/I and $\Delta I/I$.

(a) $I_p \geqq I_1 > I_2$ (*i.e.*, $I_p \geqq I + \Delta I$). Since $I_p - I \pm \Delta I \geqq 0$, Eq. (2.3) has two real roots ω_{c21}, ω_{c22}, and only one unstable region $[\omega_{c21}, \omega_{c22}]$ takes place.

(b) $I_1 > I_2 > I_p$ (*i.e.*, $I - \Delta I > I_p$). Since $I_p - I \pm \Delta I < 0$, Eq. (2.3) has all four real roots $\omega_{c_{2_1}}$, $\omega_{c_{22}}$, $\omega_{c_{11}}$, and $\omega_{c_{12}}$, then two unstable regions $[\omega_{c_{21}}, \omega_{c_{22}}]$ and $[\omega_{c_{11}}, \omega_{c_{12}}]$ appear.

(c) $I_1 > I_p \geqq I_2$ (*i.e.*, $I + \Delta I > I_p \geqq I - \Delta I$). As $I_p - I + \Delta I \geqq 0$ and $I_p - I - \Delta I < 0$, Eq. (2.3) has three real roots $\omega_{c_{21}}$, $\omega_{c_{22}}$, and $\omega_{c_{11}}$, and then two unstable regions $[\omega_{c_{21}}, \omega_{c_{22}}]$ and $[\omega_{c_{11}}, \infty]$ exist.

Boundaries between stable and unstable regions given by the relation $K_0 = 0$ are shown in Fig. 2.2 where unstable regions represented by shaded areas are shown for various values of parameter I_p/I and $\Delta I/I$. When $I_p/I = 2.0$, 1.0, and 0.4, for any $\Delta I/I$, unstable regions belong to (a), (c), and (b) respectively. When $I_p/I = 1.5$, (a) for $0 < \Delta I/I \leqq 0.5$, and (c) for $0.5 < \Delta I/I \leqq 0.75$. When $I_p/I = 0.8$, (b) for $0 < \Delta I/I < 0.2$ and (c) for $0.2 \leqq \Delta I/I \leqq 0.4$. The width of the lower unstable region $[\omega_{c_{21}}, \omega_{c_{22}}]$ increases approximately proportional to the asymmetry $\Delta I/I$ as seen from Fig. 2.2.

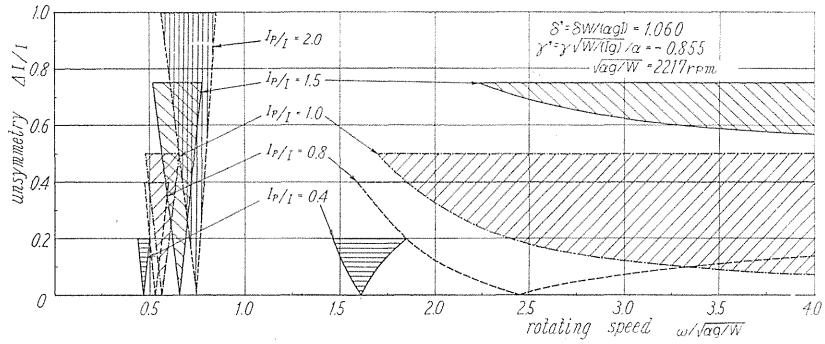

FIG. 2.2. Unstable regions $[\omega_{c21}, \omega_{c22}]$ and $[\omega_{c11}, \omega_{c12}]$

2.4. Natural frequencies and amplitude ratios of free vibrations

For convenience, we introduce the dimensionless quantities as follows;

$$\left.\begin{aligned} &I_p/I = i_p,\ \Delta I/I = \Delta,\ x\sqrt{W/(Ig)} = x',\ y\sqrt{W/(Ig)} = y',\ t\sqrt{\alpha g/W} = t', \\ &\omega\sqrt{W/(\alpha g)} = \omega',\ p\sqrt{W/(\alpha g)} = p',\ \gamma\sqrt{W/(Ig)}/\alpha = \gamma',\ \delta W/(\alpha g I) = \delta'. \end{aligned}\right\} \quad (2.11)$$

Substituting Eq. (2.11) into Eqs. (1.15)~(1.18) when $c_1 = c_2 = 0$, $e = \tau = 0$, and omitting primes on the dimensionless quantities, we have the equations of free vibrations,

$$\left.\begin{aligned} &\ddot{x} + x + \gamma\theta_x = 0, \\ &\ddot{y} + y + \gamma\theta_y = 0, \\ &\ddot{\theta}_x + i_p\omega\dot{\theta}_y + \gamma x + \delta\theta_x - \Delta\cdot\frac{d}{dt}(\dot{\theta}_x\cos 2\omega t + \dot{\theta}_y\sin 2\omega t) = 0, \\ &\ddot{\theta}_y - i_p\omega\dot{\theta}_x + \gamma y + \delta\theta_y - \Delta\cdot\frac{d}{dt}(\dot{\theta}_x\sin 2\omega t - \dot{\theta}_y\cos 2\omega t) = 0, \end{aligned}\right\} \quad (2.12)$$

where p is the natural frequency of the system.

Though the present system is a four degrees of freedom system with gyroscopic terms $i_p\omega\dot{\theta}_y$, $-i_p\omega\dot{\theta}_x$, there are eight natural frequencies p_i, $\bar{p}_i=2\omega-p_i$ $(i=1, 2, 3, 4)$ because of asymmetry of rotor, and a whirling motion of forward or backward precession takes place. Consequently, free vibrations are represented by

$$\left.\begin{matrix} x \\ y \end{matrix}\right\} = E\begin{matrix}\cos \\ \sin\end{matrix} pt + \bar{E}\begin{matrix}\cos \\ \sin\end{matrix} \bar{p}t, \quad \left.\begin{matrix} \theta_x \\ \theta_y \end{matrix}\right\} = F\begin{matrix}\cos \\ \sin\end{matrix} pt + \bar{F}\begin{matrix}\cos \\ \sin\end{matrix} \bar{p}t. \tag{2.13}$$

Inserting Eq. (2.13) into Eq. (2.12), we have the frequency equation

$$\det\ (a_{ij}) = \begin{vmatrix} 1-p^2 & 0 & \gamma & 0 \\ 0 & 1-\bar{p}^2 & 0 & \gamma \\ \gamma & 0 & G & -\Delta p\bar{p} \\ 0 & \gamma & -\Delta p\bar{p} & \bar{G} \end{vmatrix} = 0, \tag{2.14}$$

where $G=\delta+i_p\omega p-p^2$, $\bar{G}=\delta+i_p\omega\bar{p}-\bar{p}^2$. The determinant Eq. (2.14) is expanded to the equation of eight degrees for p.

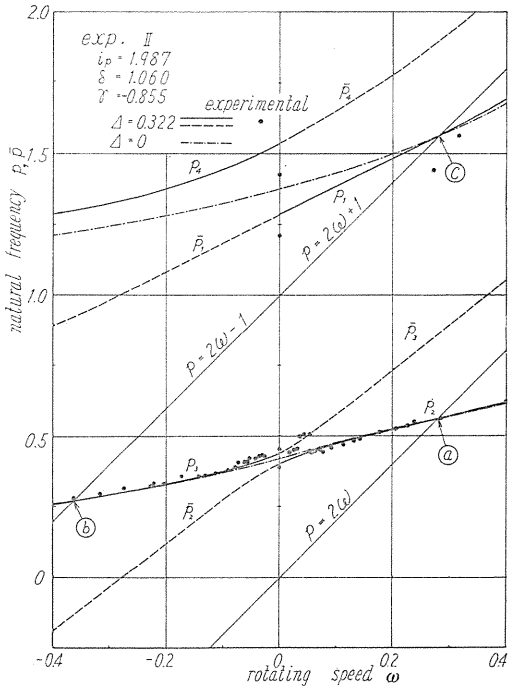

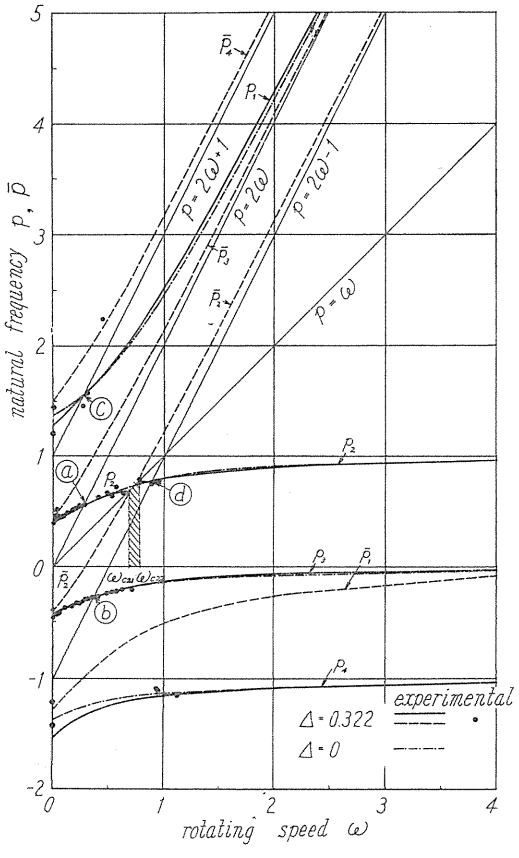

FIG. 2.3. Natural frequency p, $\bar{p}$ (Experiment II, $i_p=1.987$, $\delta=1.060$, $\gamma=-0.855$, $\omega_{c_{21}}=0.683$, $\omega_c=0.736$, $\omega_{c_{22}}=0.778$)

$$\Phi(\omega, p) = \{(1-p^2)G - \gamma^2\}\{(1-\bar{p}^2)\bar{G} - \gamma^2\} - \Delta^2(1-p^2)(1-\bar{p}^2)p^2\bar{p}^2 = 0. \qquad (2.15)$$

Since $i_p=1.987$, $\Delta=0.322$, $\delta=1.060$, and $\gamma=-0.855$ for the apparatus of Experiment II, we calculated numerically the natural frequencies p, $\bar{p}$ by Eq. (2.15) using the above values and showed the results in Figs. 2.3 (a) and (b). When the asymmetry is decreased gradually, the natural frequency p_i would approach that of a symmetrical rotor. The relations $p_1>1>p_2>0>p_3>-1>p_4$ always hold, provided $\gamma\neq 0$.

When $\omega=0$, natural frequency $p_{i0}(=-\bar{p}_{i0})$ is given briefly from Eq. (2.15):

$$\left.\begin{aligned} p_{10}^2 \\ p_{20}^2 \end{aligned}\right\} = \frac{(1+\Delta+\delta) \pm \sqrt{(1+\Delta-\delta)^2+4(1+\Delta)\gamma^2}}{2(1+\Delta)},$$
$$\left.\begin{aligned} p_{40}^2 \\ p_{30}^2 \end{aligned}\right\} = \frac{(1-\Delta+\delta) \pm \sqrt{(1-\Delta-\delta)^2+4(1-\Delta)\gamma^2}}{2(1-\Delta)}. \qquad (2.16)$$

Though the frequency equation (2.15) is the algebraic equation of eight degrees in the variable p, Eq. (2.15) becomes the biquartic equation in the variable p' putting $p=\omega+p'$, $\bar{p}=\omega-p'$,

$$\left.\begin{aligned} &(A'^2-B'^2)(C'^2-D'^2-F'^2) - 2\gamma^2(A'C'+B'F') + \gamma^4 = 0, \\ &\text{where } A' = 1-\omega^2-p'^2,\ B' = 2\omega p',\ C' = \delta + (i_p-1)\omega^2 - p'^2, \\ &D' = \Delta(\omega^2-p'^2),\ F' = (2-i_p)\omega p'. \end{aligned}\right\} \qquad (2.17)$$

From Eq. (2.17), the natural frequency is $\pm p'$ referred to the rotatory coordinate system with the rotating speed ω.

To each of these solutions of Eq. (2.15) or (2.17) belongs a set of values E, $\bar{E}$, F, and $\bar{F}$ of free vibrations, which determines the configuration of vibration. The ratio of amplitudes E, $\bar{E}$, F, and $\bar{F}$ is equal to the ratio of the cofactors A_{ij} of a_{ij} $(j=1, 2, 3, 4)$, *i.e.*, $E:\bar{E}:F:\bar{F}=A_{11}:A_{12}:A_{13}:A_{14}$ in the determinant (2.14). The cofactors A_{ij} are

$$\left.\begin{aligned} A_{11} &= \gamma^2\{(1-\bar{p}^2)\bar{G} - \gamma^2\}/(1-p^2), \\ A_{12} &= \gamma^2\Delta p\bar{p}, \\ A_{13} &= \gamma^3 - \gamma(1-\bar{p}^2)\bar{G}, \\ A_{14} &= -\gamma\Delta(1-\bar{p}^2)p\bar{p}. \end{aligned}\right\} \qquad (2.18)$$

Because of $\Delta=0$ for a symmetrical rotor, the amplitudes $\bar{E}$, $\bar{F}$ of free vibrations with the natural frequency $\bar{p}$ are zero. Consequently we can see that one of the peculiar characteristics of the system having an unsymmetrical rotor is the very existence of vibration $\bar{p}$. Fig. 2.4 shows the ratios of amplitudes $\bar{E}/E$ or $\bar{F}/F$ for each natural frequency $p_{1,2,3,4}$ using the same numerical values of Fig. 2.3. In Fig. 2.4, both amplitudes $\bar{E}$ and $\bar{F}$ are zero at the rotating speed ω where $p=2\omega$ is satisfied (*i.e.*, ⓐ in Fig. 2.3), and amplitude $\bar{F}$ is zero at ω where $p=2\omega\pm1$ (*i.e.*, ⓑⓒⓓ in Fig. 2.3).

2.5. Experimental results

We carried out the experiments of a vertical shaft, both ends of which are supported by self-aligning double-row ball bearings (#1200) shown at Figs. 1.1

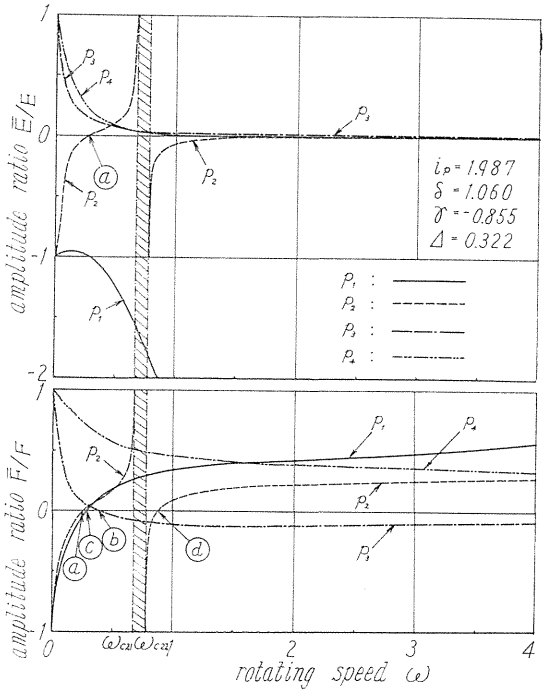

FIG. 2.4. Amplitude ratios of free vibrations (Experiment II)

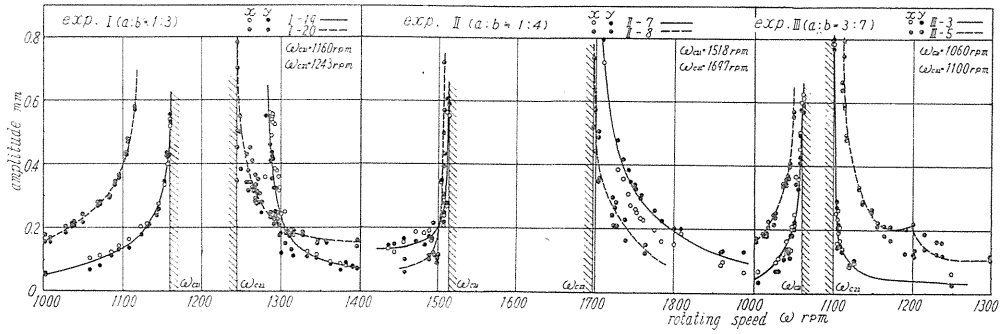

FIG. 2.5. Response curves near $\omega_{c_{21}}$, $\omega_{c_{22}}$

and 1.2. Polar moment of inertia $I_p=2.390$ kg cm s^2 and two other moments of inertia of the rotor used are $I_1=1.590$ kg cm s^2, $I_2=0.815$ kg cm s^2. Dimensions of three shafts used in Experiment I, II, and III are given in No. 1, 2, and 3 of Table 1.1, and spring constants α, γ, and δ are calculated by Eq. (1.1).

Moments of inertia of the rotor used are $I_p>I_1>I_2$, then the unstable region belongs to the case (a). Response curves obtained in Experiments I, II, and III are plotted on Fig. 2.5 in the vicinity of $\omega_{c_{21}}$, $\omega_{c_{22}}$ for two different conditions of balancing. The shaded regions are unstable regions. Comparisons of major critical speed $\omega_{c_{21}}$, $\omega_{c_{22}}$ obtained by experiments with those given by Eq. (2.4)

TABLE 2.1. Lower Major Critical Speeds ($\omega_{c_{21}}$, $\omega_{c_{22}}$) and Natural Frequencies (p_{20}, $\bar{p}_{30}$)

Experiment	$\omega_{c_{21}}$ rpm		$\omega_{c_{22}}$ rpm		p_{20} cpm		$\bar{p}_{30}$ cpm	
	Experimental	Calculated	Experimental	Calculated	Experimental	Calculated	Experimental	Calculated
I	1160	1165	1243	1244	889	871	979	961
II	1518	1514	1697	1725	908	861	1056	1006
III	1060	1112	1100	1155	907	922	977	986

are shown in Table 2.1, showing a good agreement. Also experimental results and calculated values by Eq. (2.16) of natural frequency p_{20} (vibration in the plane perpendicular to MY_2-axis), and $\bar{p}_{30}$ (perpendicular to MX_2-axis) are shown in Table 2.1. Natural frequencies p_i, $\bar{p}_i$ in Experiment II are shown by black mark ● in Figs. 2.3 (a), (b).

2.6. Conclusions

(1) The rotating shaft carrying an unsymmetrical rotor is statically unstable near its major critical speeds, and the unstable regions become wider as the asymmetry gets larger. The number of unstable regions is one or two according to the values of I_p, I_1, and I_2.

(2) The unstable region of the lower major critical speed ($p_2=\bar{p}_2=\omega$) vanishes as the mounting point of the rotor on the shaft comes to the center of the shaft.

(3) There are eight natural frequencies p_i, $\bar{p}_i$ ($i=1, 2, 3$, and 4) in the free vibrations of a four degrees of freedom system treated in this chapter, and the relation $\bar{p}_i=2\omega-p_i$ always exists.

(4) As the asymmetry disappears gradually, the natural frequency p_i approaches that of a symmetrical rotor, and the amplitudes $\bar{E}$, $\bar{F}$ of free vibrations peculiar to $\bar{p}_i$ disappear.

(5) Conclusions (1), (3), and (4) except (2) are the same of a shaft with unsymmetrical stiffness carrying a symmetrical rotor.

Chapter 3. Forced Vibrations with Viscous Damping[29]

3.1. Introduction

A shaft carrying an unsymmetrical rotor is statically unstable near its major critical speeds, and the unstable regions become smaller as damping forces are larger, and they vanish when the damping coefficients c_1, c_2 reach critical values. These critical damping coefficients c_{c_1}, c_{c_2} are given in the present chapter. Then, the response curves and phase differences of forced lateral vibrations are studied; they are found to depend very much upon angular positions of static and dynamic unbalances. The characteristics of the response curves and phase differences are very different from those of a usual vibratory system.

3.2. Damping effect on unstable region

The equations of motion of a shaft having an unsymmetrical rotor and damping forces are given in Eqs. (1.15)~(1.18). For simplicity of calculation, dimensionless quantities of Eqs. (2.11) and (3.1) are introduced:

$$e\sqrt{W/(Ig)}=e',\quad c_1\sqrt{g/(W\alpha)}=c_1',\quad c_2\sqrt{W/(\alpha g)}/I=c_2'. \tag{3.1}$$

Substituting Eqs. (2.11) and (3.1) into Eqs. (1.15)~(1.18), we have

$$\left.\begin{aligned}
&\ddot{x}+c_1\dot{x}+x+\gamma\theta_x=e\omega^2\cos(\omega t+\xi),\\
&\ddot{y}+c_1\dot{y}+y+\gamma\theta_y=e\omega^2\sin(\omega t+\xi),\\
&\ddot{\theta}_x+i_p\omega\dot{\theta}_y+c_2\dot{\theta}_x+\gamma x+\delta\theta_x-\Delta\cdot\frac{d}{dt}(\dot{\theta}_x\cos 2\omega t+\dot{\theta}_y\sin 2\omega t)\\
&\qquad=\tau\omega^2\{(i_p-1)\cos(\omega t+\eta)-\Delta\cos(\omega t-\eta)\},\\
&\ddot{\theta}_y-i_p\omega\dot{\theta}_x+c_2\dot{\theta}_y+\gamma y+\delta\theta_y-\Delta\cdot\frac{d}{dt}(\dot{\theta}_x\sin 2\omega t-\dot{\theta}_y\cos 2\omega t)\\
&\qquad=\tau\omega^2\{(i_p-1)\sin(\omega t+\eta)-\Delta\sin(\omega t-\eta)\}.
\end{aligned}\right\}\tag{3.2}$$

When the rotor is excited by periodic disturbing forces due to e and τ, the shaft whirls with the same angular velocity as the rotating speed of the shaft ω.

$$\left.\begin{aligned}
&x=E\cos(\omega t+\beta_1)=A\cos\omega t-B\sin\omega t,\quad \theta_x=F\cos(\omega t+\beta_2)=C\cos\omega t-D\sin\omega t,\\
&y=E\sin(\omega t+\beta_1)=A\sin\omega t+B\cos\omega t,\quad \theta_y=F\sin(\omega t+\beta_2)=C\sin\omega t+D\cos\omega t.
\end{aligned}\right\}\tag{3.3}$$

Substituting Eq. (3.3) into Eq. (3.2), we have simultaneous linear equations of A, B, C, and D of amplitudes of forced vibration.

$$\left.\begin{aligned}
&(1-\omega^2)A-c_1\omega B+\gamma C=e\omega^2\cos\xi,\\
&c_1\omega A+(1-\omega^2)B+\gamma D=e\omega^2\sin\xi,\\
&\gamma A+\{\delta+(i_p-1-\Delta)\omega^2\}C-c_2\omega D=(i_p-1-\Delta)\tau\omega^2\cos\eta,\\
&\gamma B+c_2\omega C+\{\delta+(i_p-1+\Delta)\omega^2\}D=(i_p-1+\Delta)\tau\omega^2\sin\eta.
\end{aligned}\right\}\tag{3.4}$$

Let the determinant consisting of coefficients a_{ij} in Eq. (3.4) be $K_0'=\det(a_{ij})$. The major critical speed ω_c is given by putting $K_0'=0$. When K_0' is negative, motions of the shaft become unstable and amplitudes A, B, C, and D build up exponentially. The motion of the shaft is in a critical condition between stable and unstable when $K_0'=0$:

$$K_0'=\{(1-\omega^2)X_1-\gamma^2\}\{(1-\omega^2)X_2-\gamma^2\}+c_1^2\omega^2X_1X_2+c_2^2\omega^2(1-\omega^2)^2+2c_1c_2\gamma^2\omega^2+c_1^2c_2^2\omega^4=0,\tag{3.5}$$

where $X=\delta+(i_p-1)\omega^2$, $X_{1,2}=\delta+(i_p-1\mp\Delta)\omega^2$. Eq. (3.5) can be rewritten as follows:

$$\omega^4\{(1-\omega^2)^2+c_1^2\omega^2\}\Delta^2=\{(1-\omega^2)X-\gamma^2\}^2+c_1^2\omega^2X^2+c_2^2\omega^2(1-\omega^2)^2+2c_1c_2\gamma^2\omega^2+c_1^2c_2^2\omega^4\tag{3.6}$$

which represents the relation between asymmetry Δ and the rotating speed ω.

Differential equations for small deviations $\xi_{1,2}$, $\eta_{1,2}$ from the stationary amplitudes are obtained in the same manner as Eq. (2.7), and substitution of Eq. (2.7a) gives the following characteristic equation[33] with damping for s:

$$\begin{vmatrix} s^2+c_1s+(1-\omega^2) & -2\omega s-c_1\omega & \gamma & 0 \\ 2\omega s+c_1\omega & s^2+c_1s+(1-\omega^2) & 0 & \gamma \\ \gamma & 0 & (1-\Delta)s^2+c_2s+\{\delta+(i_p-1-\Delta)\omega^2\} & -(2-i_p)\omega s-c_2\omega \\ 0 & \gamma & (2-i_p)\omega s+c_2\omega & (1+\Delta)s^2+c_2s+\{\delta+(i_p-1+\Delta)\omega^2\} \end{vmatrix}=0. \tag{3.7}$$

Expansion of Eq. (3.7) gives the equation of eight degrees for s.

$$K_8's^8+K_7's^7+K_6's^6+K_5's^5+K_4's^4+K_3's^3+K_2's^2+K_1's+K_0'=0. \tag{3.8}$$

When there is no damping, the coefficients K_8', K_6', K_4', K_2', and K_0' in Eq. (3.8) coincide with K_8, K_6, K_4, K_2, and K_0 of Eq. (2.9) which can be made to dimensionless form of Eq. (6.4) by putting $I_p=i_p$, $\Delta I=\Delta$, and $W/g=\alpha=I=1$, and also $K_7'=K_5'=K_3'=K_1'=0$. Constant term K_0' in Eq. (3.8) is the same as Eq. (3.5).

Because of $K_8'=K_8>0$, Eq. (3.8) has always one real positive root m at the rotating speed ω satisfying $K_0'<0$, then the unstable whirling motions of shaft occur in the following forms

$$\begin{matrix} x \\ y \end{matrix}=Ee^{mt}\begin{matrix}\cos \\ \sin\end{matrix}(\omega t+\beta_1),\quad \begin{matrix}\theta_x \\ \theta_y\end{matrix}=Fe^{mt}\begin{matrix}\cos \\ \sin\end{matrix}(\omega t+\beta_2). \tag{3.9}$$

Neglecting the higher terms than 3rd order of asymmetry Δ in Eq. (3.8), negative damping coefficient m at major critical speed ω_c is approximately obtained as follows:

$$K_2'm^2+K_1'm+K_0'=0. \tag{3.10}$$

The experimental data used in Experiment II stated in Chapter 2 are as follows:

$$\left.\begin{aligned} &I_p=2.390\ \text{kg cm s}^2,\ I_1=1.590\ \text{kg cm s}^2,\ I_2=0.815\ \text{kg cm s}^2,\\ &W=9.746\ \text{kg},\ l=50.55\ \text{cm},\ a:b=1:3.960,\ \alpha=5.375\times10^2\ \text{kg/cm},\\ &\gamma=-5.047\times10^3\ \text{kg/rad},\ \delta=6.881\times10^4\ \text{kg cm/rad},\ \sqrt{\alpha g/W}=2217\ \text{rpm},\\ &\sqrt{Ig/W}=11.00\ \text{cm}. \end{aligned}\right\} \tag{3.11}$$

These values can be represented by dimensionless quantities of Eq. (2.11) as follows:

$$i_p=1.987,\ \Delta=0.322,\ \gamma=-0.855,\ \text{and}\ \delta=1.060. \tag{3.11a}$$

The relations between the asymmetry Δ and the unstable range are given in Fig. 3.2, where the curve AA furnishes the boundary curve for no damping system, the curve BB for the system with damping coefficients $c_1=c_2=0.05$, and the curve CC for $c_1=c_2=0.10$. Horizontal line DD ($\Delta=0.322$) intersects the curve AA at $A_1(\omega=\omega_{c_{21}})$, $A_2(\omega=\omega_{c22})$ and the curve BB at $B_1(\omega_{c_{21d}})$, $B_2(\omega_{c_{22d}})$, but it does not cross the curve CC.

The major critical speeds of a damped system can be determined not analytically but by numerical calculation of Eq. (3.5) or graphical procedure by Fig. 3.2, while major critical speeds ω_{ci1}, ω_{ci2} $(i=1, 2)$ for no damping system are furnished analytically as Eq. (2.4).

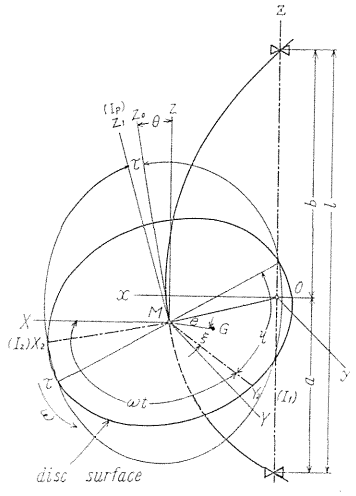

FIG. 3.1. Angular positions of ξ, η

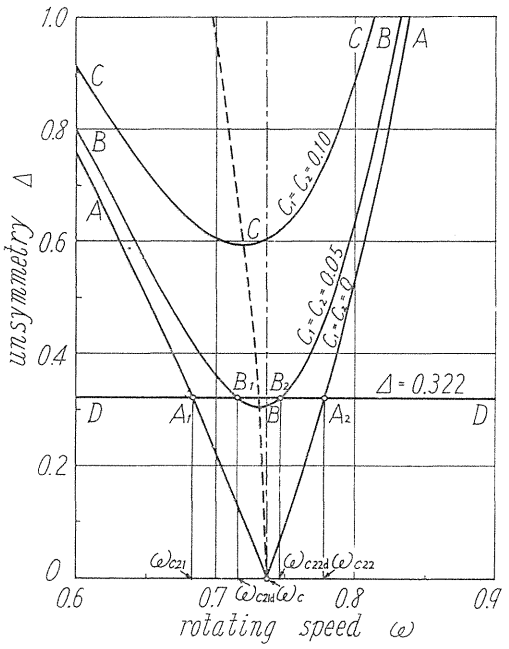

FIG. 3.2. Boundaries of unstable region near ω_c
$i_p=1.987$, $\gamma=-0.855$, $\delta=1.060$, $\omega_c=0.736$
$\omega_{c_{21}}=0.683$, $\omega_{c_{22}}=0.778$, $\omega_{c21d}=0.715$, $\omega_{c22d}=0.746$
$|\xi_0|/\Delta=0.148$, $m_{max}/\Delta=0.1056$

The motion of the shaft carrying an unsymmetrical rotor becomes always unstable near its major critical speeds provided $\gamma\neq 0$ and no damping. Thus for the shaft to run higher than the major critical speeds we must pass through the critical speed rapidly enough or give the system a sufficient damping force. When the damping coefficients c_1, c_2 are sufficiently large, the unstable regions near the major critical speeds vanish, that is, the relation $K_0'\geqq 0$ always holds. And we call the minimum values of damping coefficients which make K_0' always positive the critical damping coefficients c_{c_1}, c_{c_2}, which are shown in Fig. 3.3. Near the lower unstable region $[\omega_{c21}, \omega_{c22}]$, the deflections x, y are so much larger than the inclination angles θ_x, θ_y that c_1 is more effective than c_2. The points A, B, and C in Fig. 3.3 correspond to the curves AA, BB, and CC in Fig. 3.2 respectively. When Δ is sufficiently small, ω in Eq. (3.5) is approximately replaced by the value of ω_c given by Eq. (2.4) putting $\Delta=0$, and then an approximate equation for critical damping coefficients are as follows:

$$\frac{c_{c1}^2\gamma^4}{(1-\omega_c^2)^2}+c_{c2}^2(1-\omega_c^2)^2+2c_{c_1}c_{c_2}\gamma^2+c_{c1}^2c_{c2}^2\omega_c^2-\Delta^2\omega_c^2\{(1-\omega_c^2)^2+c_{c1}^2\omega_c^2\}=0. \quad (3.5a)$$

Approximate coefficients c_{c1}, c_{c2} are shown with broken lines in Fig. 3.3. Another approximate solution discussed in Chapter 5 and 6 gives directly $c_{c_1} = 0.164\,\Delta\,(c_1 = c_2)$, $c_{c1} = 0.211\,\Delta\,(c_2 = 0)$, and $c_{c2} = 0.740\,\Delta(c_1 = 0)$, and these values are shown with chain lines in Fig. 3.3.

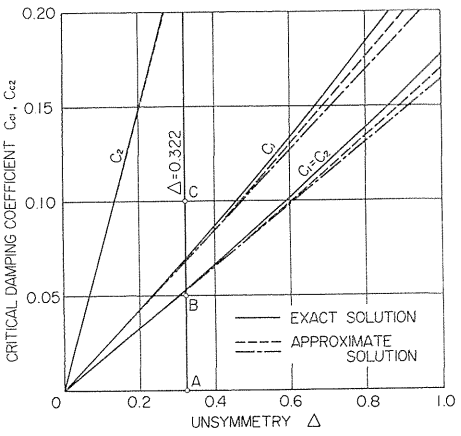

FIG. 3.3. Critical damping coefficients c_{c1}, c_{c2}

3.3. *Forced vibrations due to eccentricity e*

We can solve amplitudes A, B, C, and D by Eq. (3.4). The amplitude E of deflection being a vector sum of A and B always coexists with the amplitude F of inclination angle consisting of C and D, the former, however, predominates over the latter at the lower unstable range $[\omega_{c_{21}}, \omega_{c_{22}}]$ so that the amplitude E is only considered here.

The amplitude E induced by centrifugal force $e\omega^2$ and phase difference φ are

$$E/e = \sqrt{(A/e)^2 + (B/e)^2},\quad \varphi = \xi - \beta_1,\quad \tan\beta_1 = B/A, \tag{3.12}$$

$$\left.\begin{aligned} A/e &= \omega^2[\{(1-\omega^2)(X_1X_2 + c_2^2\omega^2) - \gamma^2 X_1\}\cos\xi + \{c_1\omega(X_1X_2 + c_2^2\omega^2) + \gamma^2 c_2\omega\}\sin\xi]/K_0', \\ B/e &= \omega^2[-\{c_1\omega(X_1X_2 + c_2^2\omega^2) + \gamma^2 c_2\omega\}\cos\xi + \{(1-\omega^2)(X_1X_2 + c_2^2\omega^2) - \gamma^2 X_2\}\sin\xi]/K_0'. \end{aligned}\right\} \tag{3.13}$$

Response curves and phase difference curves when $c_1 = c_2 = 0.10$ are shown in Fig. 3.4 (a), (b). When $c_1 = c_2 = 0.10$ the damping forces are too large for the motions to be unstable, and the amplitude E becomes maximum near ω_c as shown in Fig. 3.4. The behavior of vibration is very much affected by the value of angular position ξ. For instance, when $\xi = -45°$, the amplitude E is smaller than that of a symmetrical rotor. In a symmetrical rotor the phase difference φ is nearly 90° at the rotating speed ω where the maximum amplitude takes place, but not so in an unsymmetrical rotor. When the maximum amplitude appears, the phase difference φ is very different from 90°, and it is 145°, 56°, and 127° for $\xi = -45°$, 0°, and 90° respectively. The following Eq. (3.14) are easily derived from Eqs. (3.12) and (3.13):

$$(E)_{\xi+180°} = (E)_{\xi},\quad (\varphi)_{\xi+180°} = (\varphi)_{\xi}. \tag{3.14}$$

Then calculations may be done only for $90° \geqq \xi > -90°$. The relation between the maximum amplitude $(E/e)_{\max}$ and the angle ξ is shown in polar coordinates in Fig. 3.4 (c) which is nearly symmetrical about the axis $\xi = 45°$. Clearly the curve for symmetrical rotor ($\Delta = 0$) is a circle which is given by a broken line in Fig. 3.4 (c).

The points A_1, A_2 in Fig. 3.4 (b) are the intersections between a horizontal line $\varphi = 90°$ and vertical lines $\omega = \omega_{c21}$, ω_{c22}, and we can approximately conclude that curves φ for $\xi = 90°$ and 0° pass through these points A_1 and A_2 respectively. This fact is generally explained by Eqs. (3.12) and (3.13). That is, for $\xi = 0°$,

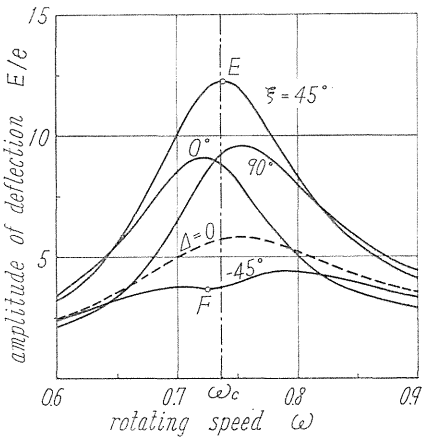

(a) Response curves ($c_1=c_2=0.10$)

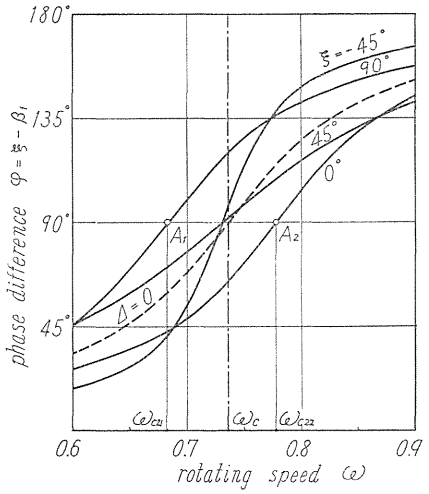

(b) Phase difference curves ($c_1=c_2=0.10$)

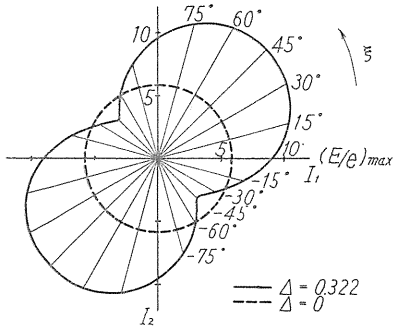

(c) Polar coordinate $[(E/e)_{\max}, \xi]$ ($c_1=c_2=0.10$)

FIG. 3.4.

the relation

$$\tan\beta_1 = -\frac{c_1\omega(X_1X_2+c_2^2\omega^2)+\gamma^2c_2\omega}{X_1\{(1-\omega^2)X_2-\gamma^2\}+c_2^2(1-\omega^2)\omega^2} \tag{3.15}$$

holds, while we have $(1-\omega^2)X_2-\gamma^2=0$ when $\omega=\omega_{c22}$ by Eq. (3.5). Consequently the denominator of Eq. (3.15) is almost zero and we get $\varphi=-\beta_1\fallingdotseq 90°$. It can be also seen that $\varphi\fallingdotseq 90°$ at $\omega=\omega_{c21}$ when $\xi=90°$ by the similar procedure.

In Fig. 3.5 (a), (b), the unstable range $[\omega_{c21d}, \omega_{c22d}]$ is represented by the shadowed region which is determined by the points B_1 and B_2 in Fig. 3.2. The amplitude E becomes larger as the rotating speed ω approaches ω_{c21d}, ω_{c22d} and no stable amplitude exists really in the unstable range. The phase difference φ is nearly zero at a sufficiently lower rotating speed than ω_c and nearly 180° at a sufficiently higher speed than ω_c, for all values of ξ, similarly to the general vibratory system. But φ changes discontinuously at $\omega=\omega_{c21d}$, ω_{c22d} and for $\xi=-45°$, it may be negative near the unstable range, that is, the forced vibration is ahead of the external force as seen in a flat shaft system[3].

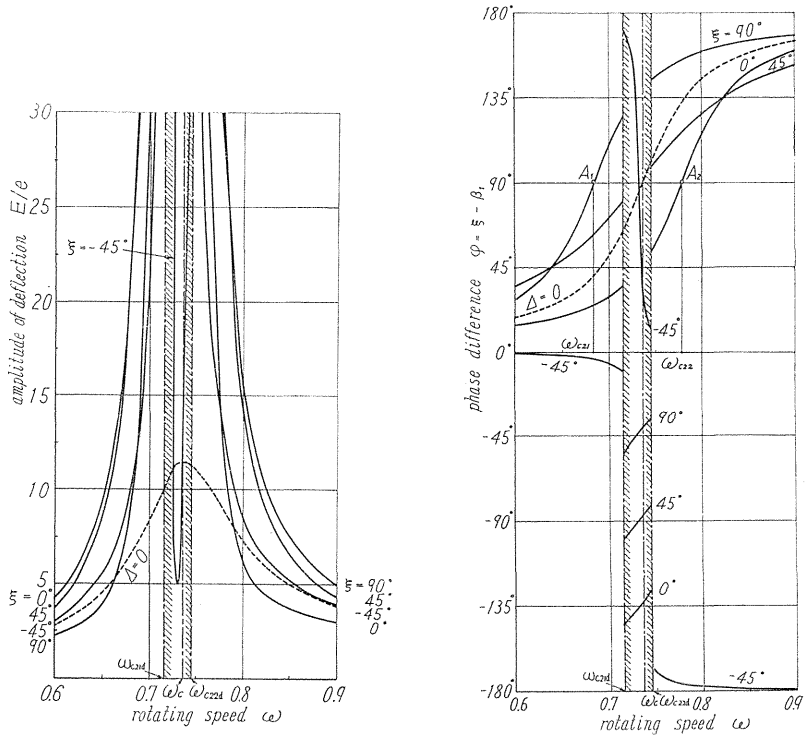

(a) Response curves ($c_1=c_2=0.05$) (b) Phase difference curves ($c_1=c_2=0.05$)

FIG. 3.5

3.4. Forced vibrations due to deviational angle τ

We can not perfectly eliminate e and τ in an actual rotor and the vibration that occurs is a vector sum of that induced by e and that by τ. Since the gyroscopic moment induced by τ lies in the direction $\omega t+\eta+90°$, the point M deflects in the direction $\omega t+\eta$. Now we consider the amplitude of deflection of forced vibration by τ. From Eqs. (3.3) and (3.4), we have

$$E/\tau=\sqrt{(A/\tau)^2+(B/\tau)^2},\quad \varphi=\eta-\beta_1,\quad \tan\beta_1=B/A, \tag{3.16}$$

$$\left.\begin{aligned} A/\tau &= \gamma\omega^2[-(i_p-1-\Delta)\{(1-\omega^2)X_2-c_1c_2\omega^2-\gamma^2\}\cos\eta \\ &\quad -(i_p-1+\Delta)\omega\{c_1X_1+c_2(1-\omega^2)\}\sin\eta]/K_0', \\ B/\tau &= \gamma\omega^2[(i_p-1-\Delta)\omega\{c_1X_2+c_2(1-\omega^2)\}\cos\eta \\ &\quad -(i_p-1+\Delta)\{(1-\omega^2)X_1-c_1c_2\omega^2-\gamma^2\}\sin\eta]/K_0', \end{aligned}\right\} \tag{3.17}$$

$$(E)_{\eta+180°}=(E)_\eta,\quad (\varphi)_{\tau+180°}=(\varphi)_\eta. \tag{3.18}$$

Amplitude E of deflection and phase difference φ are shown in Fig. 3.6 (a), (b) where damping coefficients c_1 and c_2 are 0.10. The maximum amplitude $(E/e)_{\max}$ for $\xi=90°$ is almost equal to that for $\xi=0°$ in Fig. 3.4 (a), but $(E/\tau)_{\max}$ is not in Fig. 3.6 (a) in which the former is much larger than the latter, because the gyroscopic moments for $\eta=90°$ and $\eta=0°$ are $(i_p-1+\Delta)\tau\omega^2$ and $(i_p-1-\Delta)\tau\omega^2$ respectively. The relation between the maximum amplitude $(E/\tau)_{\max}$ and the

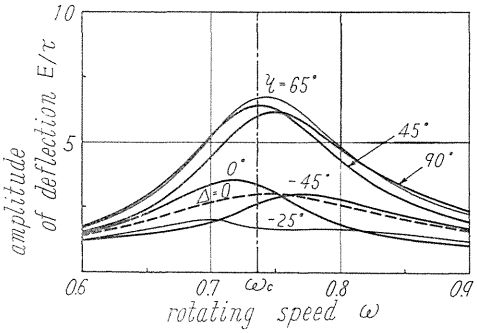

(a) Response curves ($c_1=c_2=0.10$)

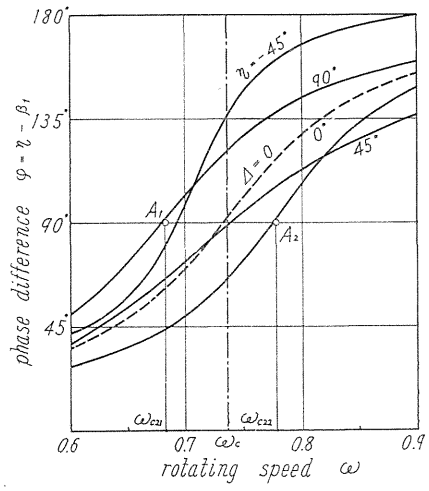

(b) Phase difference curves ($c_1=c_2=0.10$)

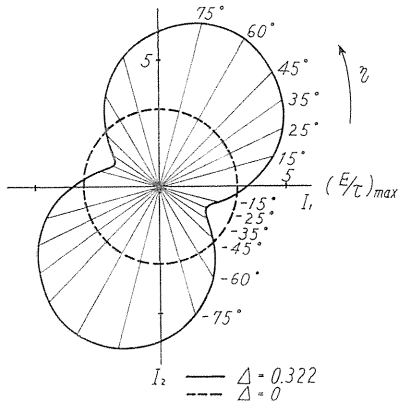

(c) Polar coordinate $[(E/\tau)_{max}, \gamma]$ ($c_1=c_2=0.10$)

FIG. 3.6

angle η is shown in Fig. 3.6 (c) in which the symmetrical axis of the figure is approximately the line $\eta=65°$. Fig. 3.6 (c) is somewhat different from Fig. 3.4 (c). Also E and φ are shown in Fig. 3.7 (a), (b) where both c_1 and c_2 are 0.05.

3.5. Uncoupled system of two degrees of freedom ($\gamma=0$)

So far we considered only the case of $i_p>1+\Delta$, in which there exists one unstable range $[\omega_{c21}, \omega_{c22}]$ and the forced vibrations of deflection take place in more remarkable amplitude than those of inclination angle in the unstable range $[\omega_{c21}, \omega_{c22}]$. In the case $i_p<1+\Delta$ treated here, however, there are two unstable regions, the lower being $[\omega_{c21}, \omega_{c22}]$, and the higher $[\omega_{c11}, \omega_{c12}]$. In the neighborhood of the unstable range $[\omega_{c11}, \omega_{c12}]$ the vibrations of inclination angle predominate over those of deflection.

Here is treated the simplest system where an unsymmetrical rotor is mounted at the middle point of the shaft, *i.e.*, $\gamma=0$, and the deflections x, y do not couple with inclination angles θ_x, θ_y. and the major critical speeds are $\omega_{c21}=\omega_{c22}=\omega_c=1$. This system is considered the same as a single degree of freedom system of a mass fixed to the middle of a beam with regard to deflection. The major critical speeds ω_{c11d}, ω_{c12d} for the system with damping coefficient c_2 are determined from Eq. (3.5). In Eq. (3.5), putting $\gamma=c_1=0$, we get

$$K_0' = X_1X_2 + c_2^2\omega^2 = 0, \tag{3.5b}$$

$$\frac{\omega_{c12d}^2}{\omega_{c11d}^2} = \frac{\delta\{(1-i_p)-c_2^2/(2\delta)\} \pm \delta\sqrt{\{(1-i_p)-c_2^2/(2\delta)\}^2-\{(1-i_p)^2-\Delta^2\}}}{(1-i_p)^2-\Delta^2}. \quad (3.19)$$

If the value with the radical sign of Eq. (3.19) vanishes or is imaginary, the unstable region $[\omega_{c11d}, \omega_{c12d}]$ disappears. When unsymmetry Δ is small, the critical damping coefficent c_{c2} is approximately gained by Eq. (3.5a) or (3.19) as follows:

$$c_{c2} = \Delta\sqrt{\delta/(1-i_p)} = \Delta\omega_c. \quad (3.20)$$

Boundary curves whether stable or unstable are shown in Fig. 3.8 for $i_p=2/3$, $\Delta=0\sim1/3$, and $\gamma=0$.

The amplitude F of inclination angle and the phase difference φ are obtained from the 3rd and 4th equations of Eqs. (3.3) and (3.4).

$$F/\tau = \sqrt{(C/\tau)^2+(D/\tau)^2},\ \varphi = \eta + 180^\circ - \beta_2,\ \tan\beta_2 = D/C, \quad (3.21)$$

$$\left.\begin{aligned} C/\tau &= \omega^2[(i_p-1-\Delta)X_2\cos\eta + (i_p-1+\Delta)c_2\omega\sin\eta]/K_0', \\ D/\tau &= \omega^2[-(i_p-1-\Delta)c_2\omega\cos\eta + (i_p-1+\Delta)X_1\sin\eta]/K_0'. \end{aligned}\right\} \quad (3.22)$$

Using the same values l and $\sqrt{Ig/W}$ as in Experiment II described in Chapter 2, dimensionless quantities $i_p=2/3$, $\Delta=0.1$, $\gamma=0$, $\delta=5.313$ and $c_2=0.7$ are given by calculation and the results are shown in Fig. 3.9 (a), (b).

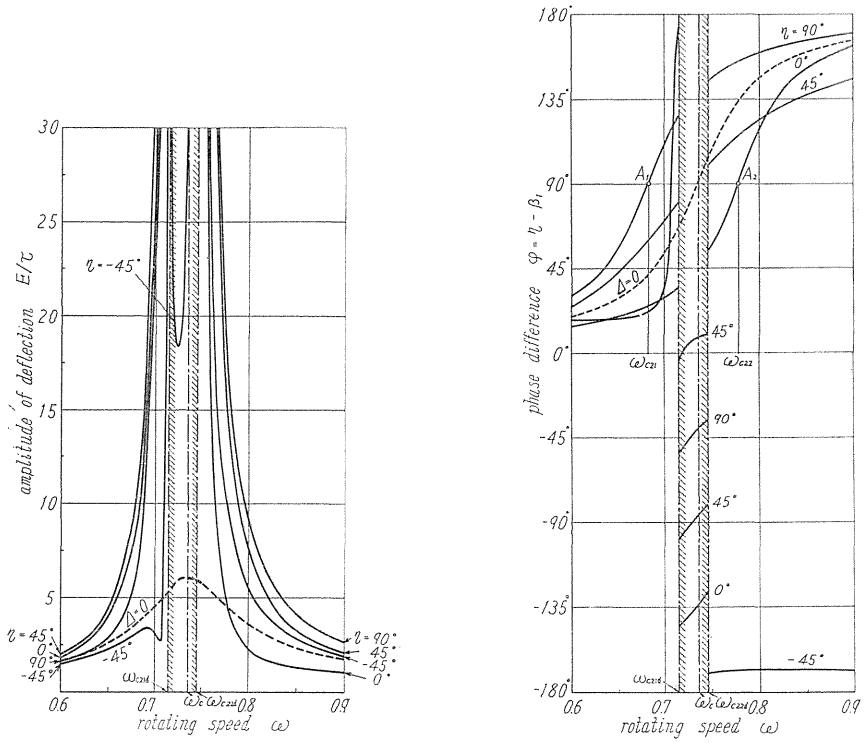

(a) Response curves ($c_1=c_2=0.05$) (b) Phase difference curves ($c_1=c_2=0.05$)

FIG. 3,7

In section 3.4, $(i_p-1\mp\Delta)$ is always positive and the positive moment $(i_p-1\mp\Delta)\tau\omega^2$ acting on the shaft $(a<b)$ results in inclining in the direction of $\omega t+\eta$, but in this section the moment $(i_p-1\mp\Delta)\tau\omega^2$ takes always a negative value, in the brackets of which the upper sign corresponds to $\eta=0°$ and the lower sign to $\eta=90°$ so the shaft inclines in the direction of $\omega t+\eta+180°$. Phase difference φ for $\eta=90°$, $0°$ just passes through the points A_3, A_4 which are intersections of lines $\omega=\omega_{c11}$, ω_{c12} and the horizontal line $\varphi=90°$.

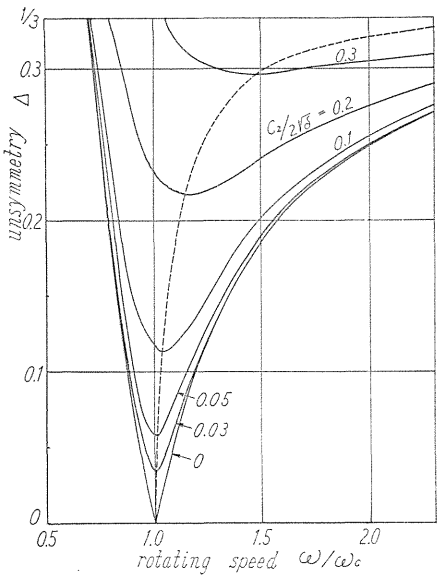

FIG. 3.8. Damping effect on unstable region [ω_{c11}, ω_{c12}]
($i_p=2/3$, $\Delta=0\sim1/3$, $\gamma=0$, $\omega_c=\sqrt{\delta/(1-i_p)}$)

3.6. Conclusions

(1) Unstable regions near major critical speeds become larger as the asymmetry of rotor becomes larger, but they become smaller as damping forces are larger.

(2) Unstable regions vanish when the damping coefficients c_1, c_2 reach the critical values c_{c1}, c_{c2} which are nearly in proportion to the asymmetry.

(3) Response curves and phase difference curves of forced vibrations induccd by static unbalance e and dynamic unbalance τ depend very much upon angular positions ξ of e and η of τ.

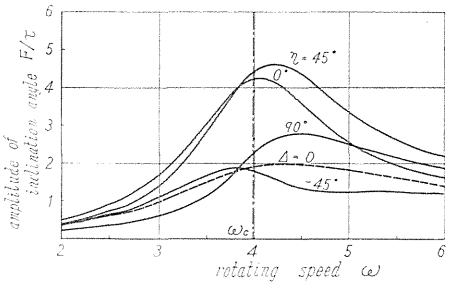

(a) Response curves

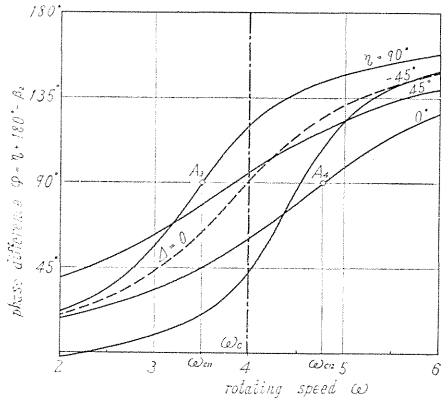

(b) Phase difference curves

FIG. 3.9. $i_p=2/3$, $\Delta=0.1$, $\gamma=0$, $\delta=5.313$, $c_{c2}=0.4$, $c_2=0.7$, $\omega_{c11}=3.502$, $\omega_{c12}=4.772$

Chapter 4. Forced Vibrations Having the Circular Frequencies Differing from the Rotating Angular Velocity of the Shaft[31]

4.1. Introduction

In the lateral vibrations of the shaft with an unsymmetrical rotor there are twice as many natural frequencies as the number of degrees of freedom because two free vibrations of natural frequencies p_i and $\bar{p}_i=2\omega-p_i$ appear simultaneously for each degree of freedom. Consequently, when the periodic disturbing force having the frequency ω_0 ($\neq\omega$) is applied to the unsymmetrical rotor, two forced vibrations of frequencies ω_0 and $\omega_0'=2\omega-\omega_0$ take place simultaneously. Depending on the circumstances, the amplitudes of the vibration of the frequency ω_0' become remarkably larger than the amplitudes of the harmonic oscillation with the frequency ω_0. Thus the idea generally accepted for the forced vibrations, that "the frequency of the forced vibration is equal or relates to that of the external force" is not always applicable for the forced vibrations of the shaft mounting an unsymmetrical rotor. In this chapter, the solutions for two forced vibrations,the response curves, and the amplitude ratio between two forced vibrations are treated theoretically and the results are verified through experiments.

4.2. Solutions for the forced vibrations

When the vibratory system consisting of a light shaft and an unsymmetrical rotor is excited by the disturbing forces with the frequency ω_0 ($\neq\omega$), the following dimensionless equations of motion are given:

$$\left.\begin{aligned}
&\ddot{x}+c_1\dot{x}+x+\gamma\theta_x=P\cos\omega_0 t,\\
&\ddot{y}+c_1\dot{y}+y+\gamma\theta_y=P\sin\omega_0 t,\\
&\ddot{\theta}_x+i_p\omega\dot{\theta}_y+c_2\dot{\theta}_x+\gamma x+\delta\theta_x-\Delta\cdot\frac{d}{dt}(\dot{\theta}_x\cos 2\omega t+\dot{\theta}_y\sin 2\omega t)=M_t\cos\omega_0 t,\\
&\ddot{\theta}_y-i_p\omega\dot{\theta}_x+c_2\dot{\theta}_y+\gamma y+\delta\theta_y-\Delta\cdot\frac{d}{dt}(\dot{\theta}_x\sin 2\omega t-\dot{\theta}_y\cos 2\omega t)=M_t\sin\omega_0 t.
\end{aligned}\right\}\qquad(4.1)$$

in which P and M_t are the magnitudes of the external force and moment with frequency ω_0, and we introduce the dimensionless quantities of Eqs. (2.11), (3.1) and (4.2), and omit primes on them for convenience.

$$\omega_0\sqrt{W/(\alpha g)}=\omega_0',\quad P\sqrt{W/(Ig)}/\alpha=P',\quad M_tW/(\alpha gI)=M_t'.\qquad(4.2)$$

Because of asymmetry Δ two forced vibrations of frequencies ω_0 and $\omega_0'=2\omega-\omega_0$ take place simultaneously.

$$\left.\begin{aligned}
&\begin{matrix}x\\y\end{matrix}=E\begin{matrix}\cos\\\sin\end{matrix}(\omega_0 t+\varphi_1)+E'\begin{matrix}\cos\\\sin\end{matrix}(\omega_0' t+\varphi_1')=A\begin{matrix}\cos\\\sin\end{matrix}\omega_0 t\mp B\begin{matrix}\sin\\\cos\end{matrix}\omega_0 t+A'\begin{matrix}\cos\\\sin\end{matrix}\omega_0' t\mp B'\begin{matrix}\sin\\\cos\end{matrix}\omega_0' t,\\
&\begin{matrix}\theta_x\\\theta_y\end{matrix}=F\begin{matrix}\cos\\\sin\end{matrix}(\omega_0 t+\varphi_2)+F'\begin{matrix}\cos\\\sin\end{matrix}(\omega_0' t+\varphi_2')=C\begin{matrix}\cos\\\sin\end{matrix}\omega_0 t\mp D\begin{matrix}\sin\\\cos\end{matrix}\omega_0 t+C'\begin{matrix}\cos\\\sin\end{matrix}\omega_0' t\mp D'\begin{matrix}\sin\\\cos\end{matrix}\omega_0' t.
\end{aligned}\right\}\qquad(4.3)$$

Substitution of Eq. (4.3) into Eq. (4.1) results in the following equations.

$$\left.\begin{aligned}
&(1-\omega_0^2)A - c_1\omega_0 B + \gamma C = P, && (1-\omega_0'^2)A' - c_1\omega_0' B' + \gamma C' = 0,\\
&c_1\omega_0 A + (1-\omega_0^2)B + \gamma D = 0, && c_1\omega_0' A' + (1-\omega_0'^2)B' + \gamma D' = 0,\\
&\gamma A + JC - c_2\omega_0 D - \Delta\omega_0\omega_0' C' = M_t, && -\Delta\omega_0\omega_0' C + \gamma A' + J'C' - c_2\omega_0' D' = 0,\\
&\gamma B + c_2\omega_0 C + JD + \Delta\omega_0\omega_0' D' = 0, && \Delta\omega_0\omega_0' D + \gamma B' + c_2\omega_0' C' + J'D' = 0.
\end{aligned}\right\} \tag{4.4}$$

$$\left.\begin{aligned}
&E = \sqrt{A^2+B^2},\ E' = \sqrt{A'^2+B'^2},\ F = \sqrt{C^2+D^2},\ F' = \sqrt{C'^2+D'^2},\\
&\tan\varphi_1 = B/A,\ \tan\varphi_1' = B'/A',\ \tan\varphi_2 = D/C,\ \tan\varphi_2' = D'/C'.
\end{aligned}\right\} \tag{4.5}$$

$$J = \delta + i_p\omega\omega_0 - \omega_0^2,\quad J' = \delta + i_p\omega\omega_0' - \omega_0'^2. \tag{4.6}$$

Let the amplitudes of forced vibrations with frequency ω_0 for deflection and inclination be E and F respectively; the amplitudes of forced vibrations with frequency $\omega_0' = 2\omega - \omega_0$ for deflection and inclination be E' and F' respectively; E, F, E' and F' when $c_1=0$, $c_2=0$ be E_0, F_0, E_0' and F_0' respectively; the amplitudes of free vibrations of frequency p without damping be E_f and F_f; the amplitudes of free vibrations of frequency $\overline{p}$ without damping be $\overline{E}_f$, $\overline{F}_f$. Though the amplitudes E, F, E' and F' can be calculated through Eqs. (4.4) and (4.5), they are not represented by rather simple formulae. The amplitudes when there is no damping force can be given by somewhat brief equations as follows:

$$\left.\begin{aligned}
E_0 &= \frac{P[(J-\gamma j)\{(1-\omega_0'^2)J' - \gamma^2\} - \Delta^2\omega_0^2\omega_0'^2(1-\omega_0'^2)]}{\{(1-\omega_0^2)J-\gamma^2\}\{(1-\omega_0'^2)J'-\gamma^2\} - \Delta^2\omega_0^2\omega_0'^2(1-\omega_0^2)(1-\omega_0'^2)},\\
E_0' &= \frac{P\gamma\Delta\omega_0\omega_0'\{\gamma - j(1-\omega_0^2)\}}{\{(1-\omega_0^2)J-\gamma^2\}\{(1-\omega_0'^2)J'-\gamma^2\} - \Delta^2\omega_0^2\omega_0'^2(1-\omega_0^2)(1-\omega_0'^2)},\\
F_0 &= \frac{-P\{(1-\omega_0'^2)J' - \gamma^2\}\{\gamma - j(1-\omega_0^2)\}}{\{(1-\omega_0^2)J-\gamma^2\}\{(1-\omega_0'^2)J'-\gamma^2\} - \Delta^2\omega_0^2\omega_0'^2(1-\omega_0^2)(1-\omega_0'^2)},\\
F_0' &= \frac{-P\Delta\omega_0\omega_0'(1-\omega_0'^2)\{\gamma - j(1-\omega_0^2)\}}{\{(1-\omega_0^2)J-\gamma^2\}\{(1-\omega_0'^2)J'-\gamma^2\} - \Delta^2\omega_0^2\omega_0'^2(1-\omega_0^2)(1-\omega_0'^2)}.
\end{aligned}\right\} \tag{4.7}$$

In this equation

$$j = (M_t/P). \tag{4.8}$$

When the dimensions of the rotor and the shaft, the condition of supports of the shaft at bearings and the position where the disturbance is exerted are known, the dimensionless quantity j is given by the formula of "beam theory". For the freely supported shaft the value of j is given by

$$\left.\begin{aligned}
j &= \sqrt{W/(Ig)}\,\frac{ab^2(l^2-3a^2-z^2) - ab(b-a)(l^2-a^2-z^2)}{(a^2-ab+b^2)(l^2-a^2-z^2) - b(b-a)(l^2-3a^2-z^2)} && \text{for } 0\leqq z\leqq b,\\
j &= \sqrt{W/(Ig)}\,\frac{-a^2b(3b^2-2zl+z^2) - ab(b-a)(b^2-2zl+z^2)}{(a^2-ab+b^2)(b^2-2zl+z^2) + a(b-a)(3b^2-2zl+z^2)} && \text{for } b\leqq z\leqq l,
\end{aligned}\right\} \tag{4.9}$$

in which z is the distance from the upper bearing to the position at which the disturbance is applied to the shaft system.

For the fixed shaft

$$j=\sqrt{W/(Ig)}\,\frac{2ab^2(2l^2-3al-2bz)-ab(b-a)(2az+3bl-3zl)}{2(a^2-ab+b^2)(2az+3bl-3zl)-3b(b-a)(2l^2-3al-2bz)} \quad \text{for } 0\leqq z\leqq b,$$

$$j=\sqrt{W/(Ig)}\,\frac{-2a^2b(bl-2az)-ab(b-a)(bl+2bz-3zl)}{2(a^2-ab+b^2)(bl+2bz-3zl)+3a(b-a)(bl-2az)} \quad \text{for } b\leqq z\leqq l. \tag{4.9a}$$

When the lower pedestal is forced to make a displacement,

$$j=-a\sqrt{W/(Ig)} \quad \text{for the freely supported shaft,} \tag{4.10}$$

$$j=-a\sqrt{W/(Ig)}/2 \quad \text{for the fixed shaft.} \tag{4.10a}$$

For our experimental apparatus, the dimensionless quantities are the values in Eq. (3.11a), and are used in numerical computations. The frequency equation for the system is given by Eq. (2.15). When the frequency ω_0 of the disturbance coincides with p or $\bar{p}$ given by Eq. (2.15), the denominator in Eq. (4.7) vanishes and the phenomenon of resonance takes place. As there are four p_i and $\bar{p}_i$ ($i=1, 2, 3, 4$) for each value of the rotating speed ω, as shown in Fig. 4.1, then there are eight values of ω_0 which satisfy the resonance conditions $\omega_0=p_i$ and $\omega_0=\bar{p}_i$.

The characteristics of forced vibrations when $\omega_0\fallingdotseq p_i$ (case I) considerably differ from those when $\omega_0\fallingdotseq\bar{p}_i$ (case II), as shown in Fig. 4.2. For experiments A and B which will be explained later in section 4.4, j in Eq. (4.8) takes the values -0.927 by Eq. (4.10) and 1.001 by Eq. (4.9) respectively. Response curves

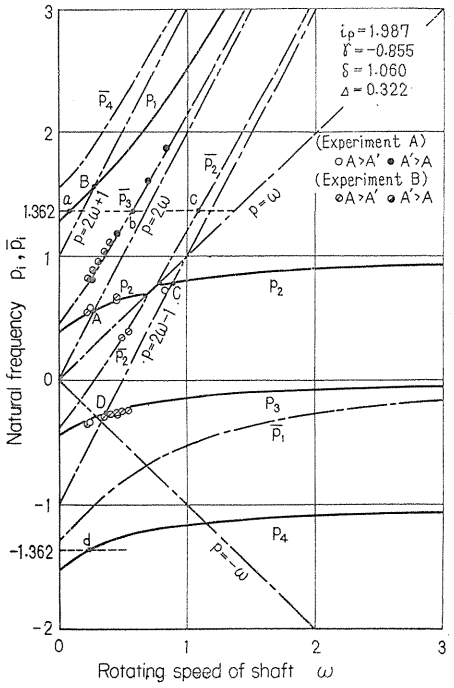

FIG. 4.1. Natural frequency-rotating speed ω diagram ($\omega=0.683\sim0.778$: unstable region)

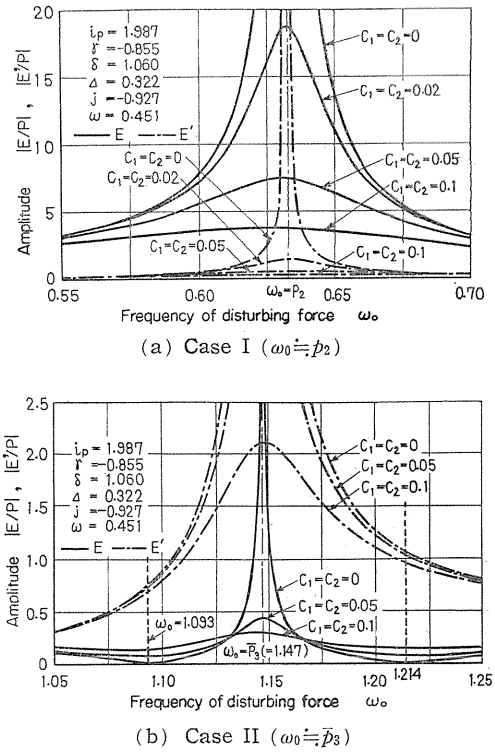

(a) Case I ($\omega_0\fallingdotseq p_2$)

(b) Case II ($\omega_0\fallingdotseq\bar{p}_3$)

FIG. 4.2. Respose curves (experiment A)

of experiment A for case I ($\omega_0 \fallingdotseq p_2$) and case II ($\omega_0 \fallingdotseq \bar{p}_3$) are given in Figs. 4.2 (a), (b) where ω is 0.451 (1000 rpm) and the vertical chain lines show the location of resonance $\omega_0 = p_2$, $\omega_0 = \bar{p}_3$ and the full and the chain lines give the amplitudes of forced vibrations with frequencies ω_0 and $\omega_0' = 2\omega - \omega_0$ respectively. In Fig. 4.2 (a) the amplitudes of ω_0 are larger than those of ω_0'. In Fig. 4.2 (b), however, the amplitudes of ω_0' are remarkably larger than those of ω_0 and it is seen that the periodic force having frequency ω_0 results in the forced vibrations with considerably large amplitudes and the frequency ω_0' which is not equal to the frequency ω_0 of the periodic force. Incidentally, in Fig. 4.2 (b), the amplitude E when $c_1 = c_2 = 0$ vanishes at $\omega_0 = 1.093$ and $\omega_0 = 1.214$, because the numerator in the first equation of Eq. (4.7) becomes zero at $\omega_0 = 1.093$ and 1.214.

4.3. Amplitude ratio of forced vibrations

4.3.1. Amplitude ratios without damping

From Eq. (4.7) we get the amplitude ratios

$$\frac{E_0'}{E_0} = \frac{\gamma \Delta \omega_0 \omega_0' \{\gamma - j(1-\omega_0^2)\}}{(J-\gamma j)\{(1-\omega_0'^2)J' - \gamma^2\} - \Delta^2 \omega_0^2 \omega_0'^2 (1-\omega_0'^2)}, \quad \frac{F_0'}{F_0} = \frac{\Delta \omega_0 \omega_0' (1-\omega_0'^2)}{(1-\omega_0'^2)J' - \gamma^2}. \tag{4.11}$$

Insertion of Eq. (2.15) into Eq. (4.11) yields

$$\left.\begin{aligned}
\left(\frac{E_0'}{E_0}\right)_{\omega_0 = p_i} &= \frac{\Delta p_i \bar{p}_i (1-p_i^2)}{(1-\bar{p}_i^2)(\delta + i_p \omega \bar{p}_i - \bar{p}_i^2) - \gamma^2} = \frac{\bar{E}_f}{E_f}, \\
\left(\frac{F_0'}{F_0}\right)_{\omega_0 = p_i} &= \frac{\Delta p_i \bar{p}_i (1-\bar{p}_i^2)}{(1-\bar{p}_i^2)(\delta + i_p \omega \bar{p}_i - \bar{p}_i^2) - \gamma^2} = \frac{\bar{F}_f}{F_f}, \\
\left(\frac{E_0'}{E_0}\right)_{\omega_0 = \bar{p}_i} &= \frac{\Delta p_i \bar{p}_i (1-\bar{p}_i^2)}{(1-p_i^2)(\delta + i_p \omega p_i - p_i^2) - \gamma^2} = \frac{E_f}{\bar{E}_f}, \\
\left(\frac{F_0'}{F_0}\right)_{\omega_0 = \bar{p}_i} &= \frac{\Delta p_i \bar{p}_i (1-p_i^2)}{(1-p_i^2)(\delta + i_p \omega p_i - p_i^2) - \gamma^2} = \frac{F_f}{\bar{F}_f}.
\end{aligned}\right\} \tag{4.12}$$

Eq. (4.12) mean that when there is no damping force, the amplitude ratios at the resonance are equal to those of free vibrations. Furthermore Eq. (4.12) yield the following reciprocal relations between cases I and II:

$$(E_0'/E_0)_{\omega_0 = p_i} \cdot (E_0'/E_0)_{\omega_0 = \bar{p}_i} = 1, \quad (F_0'/F_0)_{\omega_0 = p_i} \cdot (F_0'/F_0)_{\omega_0 = \bar{p}_i} = 1. \tag{4.13}$$

4.3.2. Amplitude ratios with damping

Substitution of Eq. (4.3) into Eq. (4.1) leads to

$$\left.\begin{aligned}
&(1-\omega_0^2)E + \gamma F \cos(\varphi_1 - \varphi_2) = P \cos \varphi_1, \\
&-c_1 \omega_0 E + \gamma F \sin(\varphi_1 - \varphi_2) = P \sin \varphi_1, \\
&(1-\omega_0'^2)E' + \gamma F' \cos(\varphi_1' - \varphi_2') = 0, \\
&-c_1 \omega_0' E' + \gamma F' \sin(\varphi_1' - \varphi_2') = 0, \\
&\gamma E \cos(\varphi_1 - \varphi_2) + JF - \Delta \omega_0 \omega_0' F' \cos(\varphi_2 + \varphi_2') = M_t \cos \varphi_2, \\
&-\gamma E \sin(\varphi_1 - \varphi_2) - c_2 \omega_0 F - \Delta \omega_0 \omega_0' F' \sin(\varphi_2 + \varphi_2') = M_t \sin \varphi_2, \\
&-\Delta \omega_0 \omega_0' F \cos(\varphi_2 + \varphi_2') + \gamma E' \cos(\varphi_1' - \varphi_2') + J'F' = 0, \\
&\Delta \omega_0 \omega_0' F \sin(\varphi_2 + \varphi_2') + \gamma E' \sin(\varphi_1' - \varphi_2') + c_2 \omega_0' F' = 0.
\end{aligned}\right\} \tag{4.14}$$

Eliminating $\varphi_1' - \varphi_2'$ from the 3rd and 4th equations of Eq. (4.14), we obtain

$$(E'/F')^2 = \gamma^2/\{(1-\omega_0'^2)^2 + c_1^2\omega_0'^2\}. \tag{4.15}$$

Eliminations of $\varphi_1' - \varphi_2'$, $\varphi_2 + \varphi_2'$ and E' from the 3rd, 4th, 7th and 8th equations of Eq. (4.14) result in

$$\left(\frac{F'}{F}\right)^2 = \frac{A^2\omega_0^2\omega_0'^2\{(1-\omega_0'^2)^2 + c_1^2\omega_0'^2\}^2}{[(1-\omega_0'^2)\{(1-\omega_0'^2)J' - \gamma^2\} + c_1^2\omega_0'^2 J']^2 + \{c_2\omega_0'(1-\omega_0'^2)^2 + c_1\omega_0'\gamma^2 + c_1^2c_2\omega_0'^3\}^2}. \tag{4.16}$$

Eliminating seven quantities $\varphi_1 - \varphi_2$, $\varphi_1' - \varphi_2'$, $\varphi_2 + \varphi_2'$, F, F', P and M_t from the eight relations of Eq. (4.14), we can obtain the equation of the amplitude ratio E'/E which is somewhat complicated. Consequently, using the relations of Eqs. (4.15) and (4.16) we have a rather simple equation of the amplitude ratio E'/E as follows:

$$\left(\frac{E'}{E}\right)^2 = \frac{\gamma^2(F/F')^2[\{\gamma - j(1-\omega_0^2)\}^2 + j^2c_1^2\omega_0^2]}{\{(1-\omega_0'^2)^2 + c_1^2\omega_0'^2\}[\{(J-\gamma j)(F/F')^2 + (1-\omega_0')^2(E'/F')^2 - J'\}^2 + \{c_1\omega_0'(E'/F')^2 + c_2\omega_0' - c_2\omega_0(F/F')^2\}^2]}. \tag{4.17}$$

Eqs. (4.16) and (4.17) give the amplitude ratios for forced vibrations with respect to deflection and inclination of the rotor respectively.

Computations through Eqs. (4.16) and (4.17) show that [1] the amplitude ratios E'/E and F'/F of forced vibrations have approximately constant magnitudes throughout the neighborhood of the resonance no matter how the magnitudes of amplitudes themselves remarkably change as the value of ω_0 changes as shown in Fig. 4.3, and [2] the amplitude ratios of forced vibrations in the neighborhood of the resonance, *i.e.*, at $\omega_0 \fallingdotseq p_i$ or $\omega_0 \fallingdotseq \bar{p}_i$, are approximately equal to those of free vibrations, provided that the coefficients of damping are not so large, as shown in Fig. 4.4. From the above facts [1] and [2], it can be concluded that the relations

$$\left.\begin{aligned} E'/E \fallingdotseq (E'/E)_{\omega_0 = p_i} \fallingdotseq (E_0'/E_0)_{\omega_0 = p_i} = \bar{E}_f/E_f \quad &\text{for case I } (\omega_0 \fallingdotseq p_i), \\ E'/E \fallingdotseq (E'/E)_{\omega_0 = \bar{p}_i} \fallingdotseq (E_0'/E_0)_{\omega_0 = \bar{p}_i} = E_f/\bar{E}_f \quad &\text{for case II } (\omega_0 \fallingdotseq \bar{p}_i), \end{aligned}\right\} \tag{4.18}$$

can be satisfied for the amplitude ratios of forced vibrations when $\omega_0 \fallingdotseq p_i$ or $\omega_0 \fallingdotseq \bar{p}_i$ and c_1, $c_2 = 10^{-2} \sim 10^{-3}$. For F'/F, the similar relations to Eq. (4.18) hold. In Figs. 4.4 (a) and (b), the amplitude ratios E'/E at the resonances $\omega_0 = \bar{p}_3$ and $\omega_0 = p_2$ are plotted against the coefficients of damping c_1, c_2 respectively. It can be seen that the ratio, when c_1 and c_2 are small, takes almost the same value as that of free vibrations. The value of $\bar{E}_f/E_f$ (case I) or $E_f/\bar{E}_f$ (case II) is indicated by mark ○ in Figs. 4.3 and 4.4. The curves of $(E'/E)_{\omega_0 = \bar{p}_2}$ represented in Fig. 4.4 (b) will be discussed later as an exceptional case. For comprehensive discussion of the amplitude ratio of forced vibrations, an analytical treatment of the amplitude ratio of free vibrations is more convenient because the relations of Eq. (4.18)

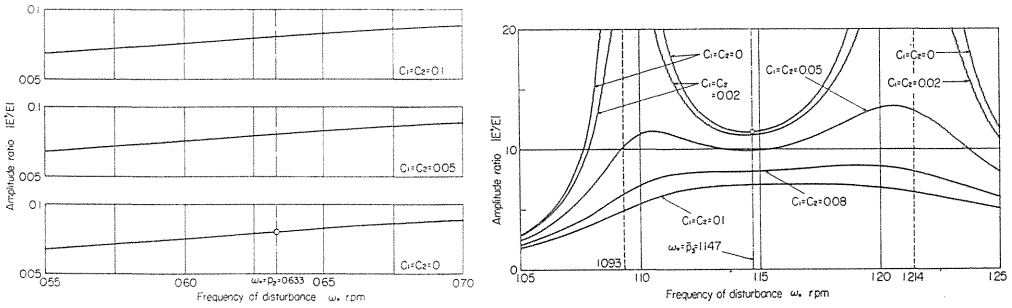

(a) Case I of $\omega_0 \fallingdotseq p_2$ (b) Case II of $\omega_0 \fallingdotseq \bar{p}_3$

FIG. 4.3. Amplitude ratio $|E'/E| - \omega_0$ diagrams
(experiment A, $j=-0.927$, $\omega=0.451$)
Mark ○ indicates $\bar{E}_f/E_f$ (case I), $E_f/\bar{E}_f$ (case II) of free vibrations without damping

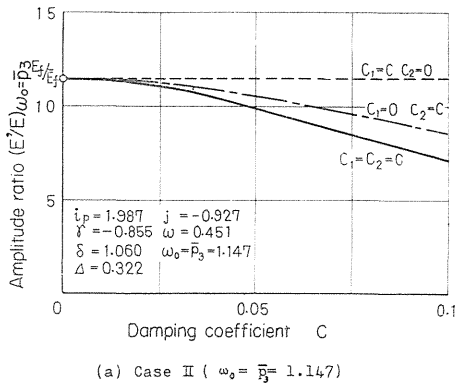

(a) Case II ($\omega_0 = \bar{p}_3 = 1.147$)

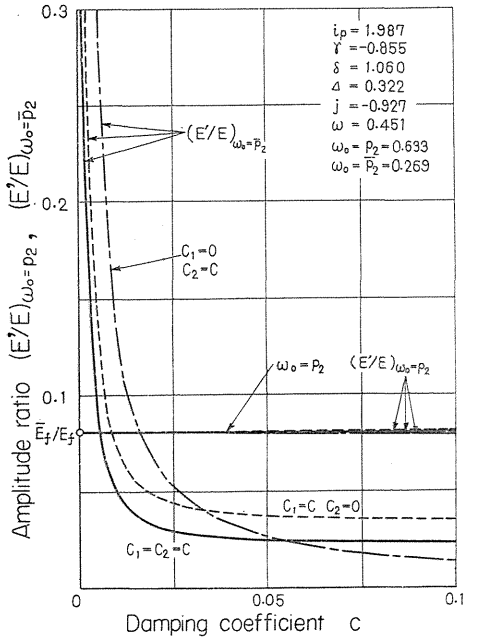

(b) Case I ($\omega_0 = p_2 = 0.633$) and
Case II ($\omega_0 = \bar{p}_2 = 0.269$)

FIG. 4.4. Effects of damping coefficient c on amplitude ratios $(E'/E)_{\omega_0=p_i}$, $(E'/E)_{\omega_0=\bar{p}_i}$ at resonance (experiment A)
$\bar{E}_f/E_f$: amplitude ratio of free vibrations without damping

can be satisfied. The values of the amplitude ratios $\bar{E}_f/E_f$ and $\bar{F}_f/F_f$ of free vibration are plotted against the rotating speed ω of the shaft in Fig. 4.5. Through Figs. 4.5 (a) and (b) all absolute values of $\bar{E}_f/E_f$ and $\bar{F}_f/F_f$ are smaller than unity, with an exception of curve $\widehat{EF}$ in Fig. 4.5 (a). It means that excluding this exception, in case I ($\omega_0 \fallingdotseq p_i$) the amplitudes of the forced vibrations with the same frequency ω_0 as the disturbing force are always larger than the amplitudes with the freqency $\omega_0' = 2\omega - \omega_0$, and vice versa in case II ($\omega_0 \fallingdotseq \bar{p}_i$).

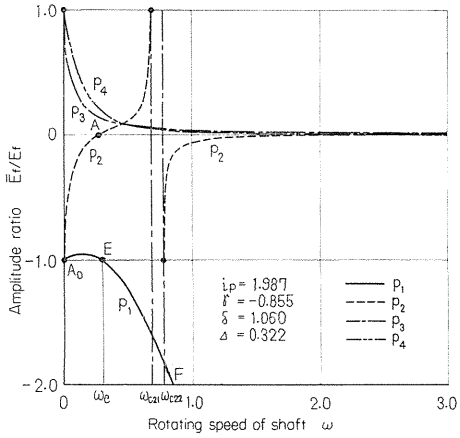

(a) Free vibrations of deflections x, y

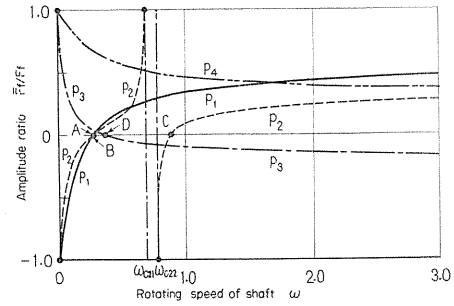

(b) Free vibrations of inclination angles θ_x, θ_y

FIG. 4.5. Amplitude ratio of free vibrations ($c_1=c_2=0$, major critical speeds: $\omega_{c21}=0.683$, $\omega_{c22}=0.778$)

There are the following exceptional cases (i) and (ii) in which the relations in Eq. (4.18) are not satisfied. When (i) the amplitude ratios of free vibrations and (ii) the magnitude of $\{\gamma - j(1-\omega_0^2)\}$ in Eqs. (4.11), (4.17) are nearly equal to zero, the approximation in Eq. (4.18) does not hold.

(i) For instance, at the points A ($\omega=0.278$), B ($\omega=0.281$), C ($\omega=0.888$), and D ($\omega=0.375$) in Fig. 4.5 as well as in Fig. 4.1 the numerator in Eq. (4.12) vanishes and the amplitude ratios of free vibrations become zero, because of $\bar{p}_2=0$ at A, $\bar{p}_1=-1$ at B, $\bar{p}_2=1$ at C, and $\bar{p}_3=1$ at D. The exceptional cases appearing near the points A, B, C, and D are shown in Figs. 4.6 (b), (a), (b), and (c) respectively. In Fig. 4.6, the amplitude ratios of forced vibrations for experiment B ($j=1.001$) are shown against the rotating velocity ω of the shaft and the vertical broken lines indicate ω at which the exceptional case (i) appears. In Figs. 4.6 (b), (a), (b), and (c), the amplitude ratios $|E'/E|$ or $|F'/F|$ for small damping coefficients of $c=c_1=c_2=0.01$, 0.05, 0.1 in the neighborhood of the points A, B, C, and D are remarkably smaller than the amplitude ratios for $c=0$ which are equal to the amplitude ratios of free vibrations as shown in Eq. (4.12).

(ii) For instance, since the value of $\{\gamma - j(1-\omega_0^2)\}$ vanishes at $\omega_0=\pm 0.279$ in experiment A because of $j=-0.927$, then it takes a quite small value 0.0064 for the value of $\omega_0=\bar{p}_2=0.269$ shown in Fig. 4.4 (b). Consequently the existence of only small damping coefficient c_1 or c_2 results in considerably smaller magnitude of the amplitude ratio $(E'/E)_{\omega_0=\bar{p}_2}$ than the value $E_f/\bar{E}_f=12.35$. In experiment B ($j=1.001$), the value of $\{\gamma - j(1-\omega_0^2)\}$ vanishes for $\omega_0=\pm 1.362$. Accordingly it becomes equal to zero at the points a ($\omega=0.079$), b ($\omega=0.573$), c ($\omega=1.085$), and d ($\omega=0.237$) in Fig. 4.1 where the horizontal lines $p=\pm 1.362$ cross the curves of p_1, $\bar{p}_3$, $\bar{p}_2$, and p_4 respectively. As examples, the amplitude ratios in the neighborhood of the points b and c just mentioned are shown in Figs. 4.6 (c) and (b) respectively, in which the remarkably small value of E'/E compared with that of $E_0'/E_0=(E'/E)_{c_1=c_2=0}$ is given near the points b and c. As there is the term $\{\gamma - j(1-\omega_0^2)\}$ only in Eq. (4.17) and not in Eq. (4.16), the exceptional case (ii) above discussed appears only in the amplitude ratio of deflection E'/E and not in F'/F of inclination angle.

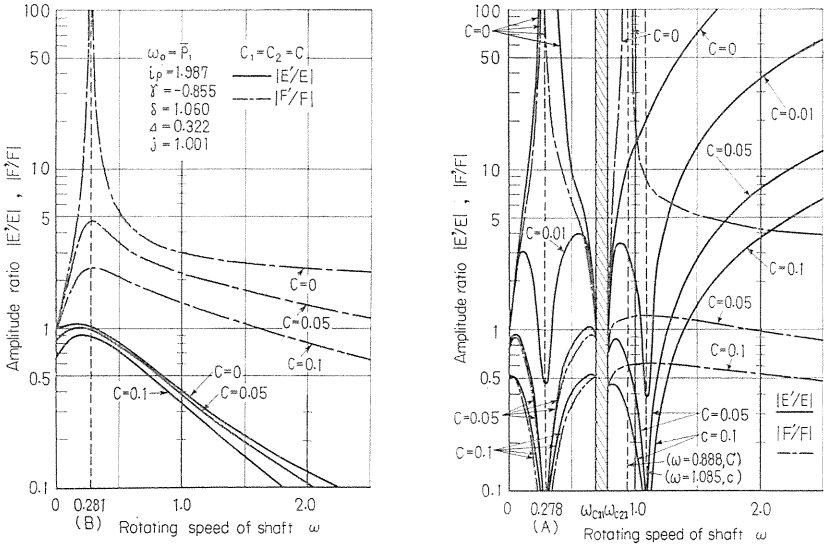

(a) $\omega_0=\bar{p}_1$ (b) $\omega_0=\bar{p}_2$

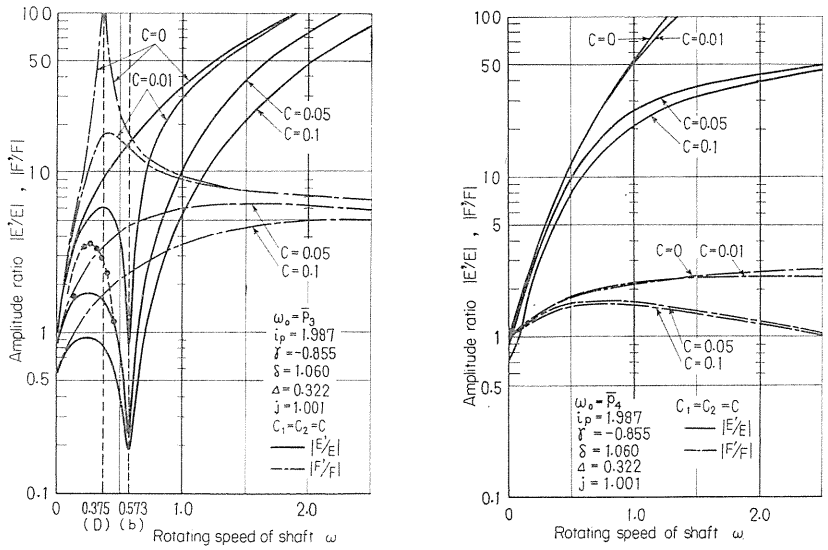

(c) $\omega_0=\bar{p}_3$ (d) $\omega_0=\bar{p}_4$

FIG. 4.6. Amplitude ratio-rotating speed ω diagrams
(experiment B, case II of $\omega_0=\bar{p}_1$)

The reason why such exceptional cases (i) and (ii) take place is as follows: Let ε and damping coefficient c be small, $[\varepsilon^2]_{1,2,3}$ and $[c^2]_{1,2}$ be small quantities having the same order as ε^2. In the exceptional case (i), for instance, since ω_0 becomes a small value ε in the neighborhood of the point A ($\omega=0.278$) because of $\omega_0=\bar{p}_2=\varepsilon\fallingdotseq 0$, then $\omega_0=\varepsilon$ results in $\{(1-\omega_0'^2)J'-\gamma^2\}=[\varepsilon^2]$ through Eq. (2.15). Consequently Eq. (4.16) takes the form of $(F'/F)^2=[\varepsilon^2]_1/\{[c^2]_1+[\varepsilon^4]+[c^2]_2\cdot[\varepsilon^2]_2\}\fallingdotseq [\varepsilon^2]_1/[c^2]_1$ which is remarkably smaller than $(F'/F)^2_{c_1=c_2=0}=[\varepsilon^2]_1/[\varepsilon^4]=1/[\varepsilon^2]_3$. In

exceptional case (ii), the term $\{(J-\gamma j)(F/F')^2+(1-\omega_0'^2)(E'/F')^2-J'\}$ in the denominator of Eq. (4.17) becomes small as ε when $\{\gamma-j(1-\omega_0^2)\}=\varepsilon\fallingdotseq 0$, and Eq. (4.17) takes the form of $(E'/E)^2\fallingdotseq\{[\varepsilon^2]_1+[c^2]_1\}/\{[\varepsilon^2]_2+[c^2]_2\}$ which is quite different from $(E'/E)^2_{c1=c2=0}\fallingdotseq(E_0'/E_0)^2=[\varepsilon^2]_1/[\varepsilon^2]_2$.

The amplitude ratios E'/E, F'/F—the rotating speed ω diagram in which the exceptional cases (i) and (ii) do not take place is shown in Fig. 4.6 (d) where the relations of Eq. (4.18) are satisfied and all E'/E and F'/F are approximately equal to the amplitude ratios of free vibrations, *i.e.*, $E_f/\bar{E}_f$ and $F_f/\bar{F}_f$ provided $c\ll 1$.

4.4. *Experimental apparatus and experimental results*

4.4.1. *Experiment A*

Experimental apparatus is shown in Fig. 4.7. The lower bearing pedestal A is somewhat flexible only in y-direction and its spring constant is 1.15×10^3 kg/cm. The pulley V_2 with the eccentric weight W_e put on the top of the pedestal A is driven with the rotating speed ω_0. Thus the forced deflection of the pedestal A due to the centrifugal force of W_e results in the disturbing force with the frequency ω_0 which can be changed by a stepless transmission. Accordingly the experiment A corresponds to the case when the disturbances having their sources in the machinery or the constructions near the shaft system induce the forced vibrations of the unsymmetrical rotor through the bearing pedestal. The value of j in experiment A computed by Eq. (4.10) is $j=-0.927$. Motions at the edge of the rotor are recorded optically in both x- and y-directions. By this method the whirl of the rotor can be measured. Small pieces of black celluloid P_1 and P_2 are attached to the disk edge and the edge of the pulley V_2 respectively and furnish the rotating marks for each revolution of the disk and the pulley. Dimensions of the experimental apparatus are the same as in Eq. (3.11) and the dimensionless quantities of Eq. (2.11) are given in Eq. (3.11a).

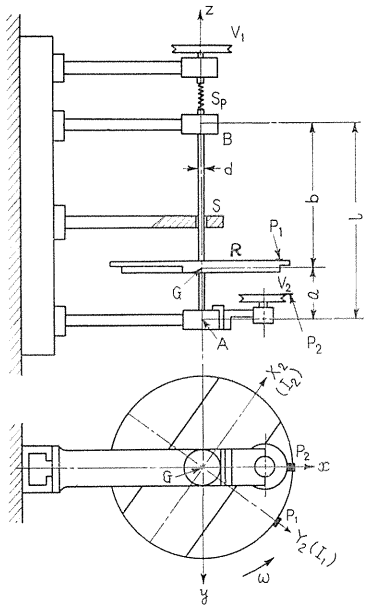

FIG. 4.7. Experimental apparatus (experiment A)

When at $\omega=0.455$ (1009 rpm) the eccentric weight $W_e=0.068$ kg attached at the radius 5.9 cm is rotated with $\omega_0\fallingdotseq p_2$, the response curves, *i.e.*, the amplitude —ω_0 diagrams and the amplitude ratio as shown in Figs. 4.8 (a) (b) are obtained by experiment. The experimental results in Figs. 4.8 correspond to Figs. 4.2 (a) and 4.3 (a), and for comparison the response curves, *i.e.*, E, E'—ω_0 diagrams and the amplitude ratio E_0'/E_0 which are analytically obtained are added in Fig. 4.8 (b). As the vibrations on the recording oscillographic papers are not simple vibrations of deflections but include the small component of vibrations of inclinations because

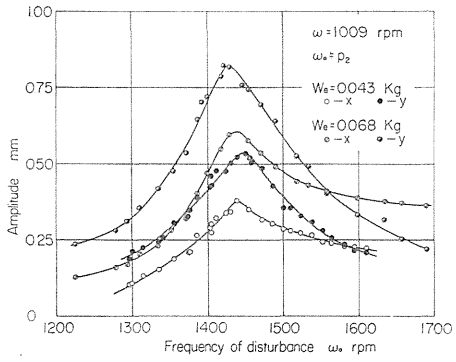

(a) Response curves of $\omega_0 \fallingdotseq p_2$

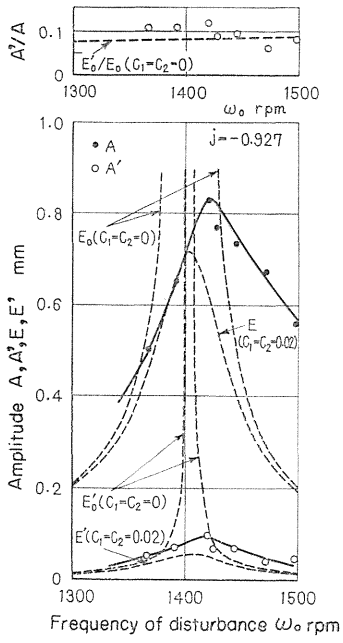

(b) A: amplitude of ω_0
A': amplitude of ω_0'

FIG. 4.8. Experimental results of response curves and amplitude ratio (experiment A, $\omega=$ 1009 rpm, case I of $\omega_0 \fallingdotseq p_2$)

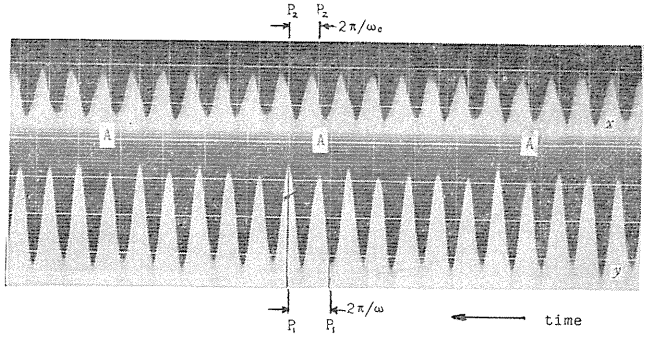

$\omega=1009.0$ rpm, $\omega_0=1418.7$ rpm, $\omega'_0=599.3$ rpm, $A'/A=0.12$

FIG. 4.9. Vibratory waves (experiment A, case I of $\omega_0 \fallingdotseq p_2$, $\omega : \omega_0 : \omega_0' \fallingdotseq 5 : 7 : 3$)

of the coupled system of deflection and inclination, in place of E, E', the notations A, A' are used for the amplitudes obtained through experiments in Figs. 4.1, 4.8, 4.9. An example of vibratory waves is illustrated in Fig. 4.9 where the vertical white lines are the rotating marks (of P_1 on the rotor R in x-, y-directions, and of P_2 on the pulley V_2 in x-direction), and the horizontal fine white lines are furnished on a scale of 1.0 mm for measuring the amplitudes. In Fig. 4.9 comparison of the rotating marks with the vibratory waves between marks AA leads to $\omega : \omega_0 : \omega_0' \fallingdotseq 5 : 7 : 3$ and it is seen that the relation $\omega_0' = 2\omega - \omega_0$ holds.

4.4.2. Experiment B

In experiment B, both lower and upper bearing pedestals are rigid and the

disturbance with frequency ω_0 is applied through an exciter which is attached to the shaft at $z=b/2$, and then the value j is 1.001. The centrifugal exciter is shown in Fig. 4.10. A rotor R_1 with unbalanced disc D' is driven by a rotor R_2 through three sets of pin P_2, curved leaf spring S_p and pin P_1. R_1 (R_2) is supported freely to rotate around the shaft S (stater S_t) by a single-row radial ball bearing B_1 (B_2). Response curves of experiment B are shown in Figs. 4.11 (a), (b).

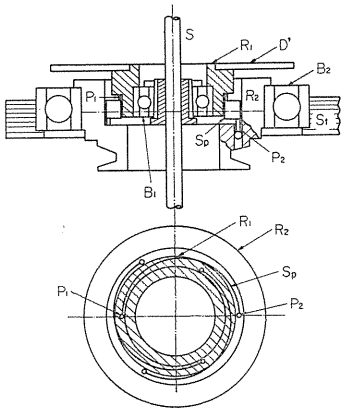

FIG. 4.10. Centrifugal exciter (experiment B)

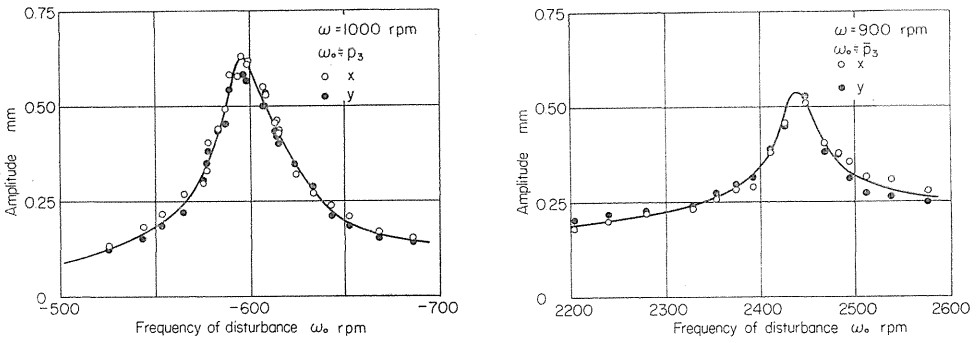

(a) case I of $\omega_0 \fallingdotseq p_3$ (b) case II of $\omega_0 \fallingdotseq \bar{p}_3$

FIG. 4.11. Response curves (experiment B)

Examples of vibratory waves in experiment B are illustrated in Figs. 4.12 (a), (b), (c) where vertical white lines both in x-, y-directions are the rotating marks made by two pieces of celluloid put on edges of the rotor R and the disc D'. As stated in section 4.3 the amplitudes of ω_0' are larger than those of ω_0 in Figs. 4.12 (b), (c) because of case II, and vice versa in Fig. 4.12 (a) of case I.

Marks in Fig. 4.6 (c) are obtained by experiment B and they verify experimentally the existence of the exceptional case (ii) discussed in section 4.3. The frequencies of the disturbances ω_0 at resonances in experiment A and experiment B are represented by marks ○, ●, ⊘ and ◪ in Fig. 4.1.

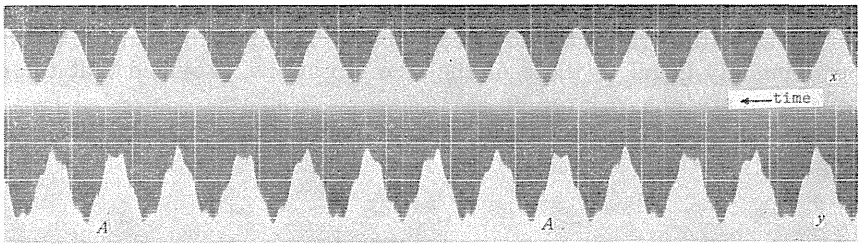

$\omega=1004.4$ rpm, $\omega_0=-593.8$ rpm, $\omega_0'=2602.6$ rpm
(a) case I of $\omega_0 \fallingdotseq p_3$ ($\omega:\omega_0:\omega_0' \fallingdotseq 12:-7:31$)

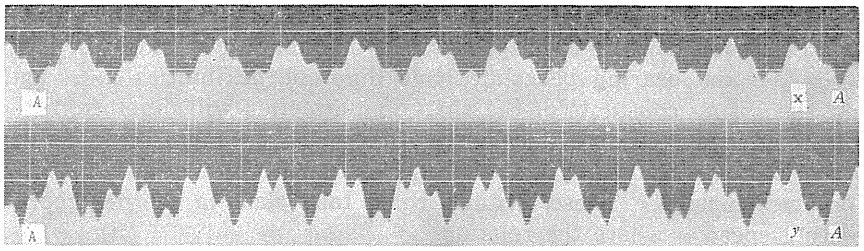

$\omega=888.0$ rpm, $\omega_0=2427.4$ rpm, $\omega_0'=-651.4$ rpm, $A'/A=2.4$
(b) case II of $\omega_0 \fallingdotseq \bar{p}_3$ ($\omega:\omega_0:\omega_0' \fallingdotseq 15:41:-11$)

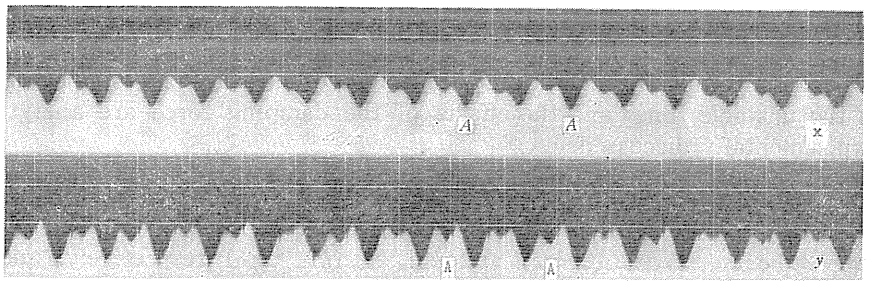

$\omega=1101.4$ rpm, $\omega_0=736.6$ rpm, $\omega_0'=1466.2$ rpm
(c) case II of $\omega_0 \fallingdotseq \bar{p}_2$ ($\omega:\omega_0:\omega_0' \fallingdotseq 3:2:4$)
FIG. 4.12. Vibratory waves (experiment B)

4.5. Conclusions

(1) In the vibratory shaft system with an unsymmetrical rotor, the disturbance of frequency ω_0 ($\neq\omega$) results in two forced vibrations with frequencies ω_0 and $\omega_0'=2\omega-\omega_0$.

(2) In case I when $\omega_0 \fallingdotseq p_i$, the amplitudes of frequency ω_0 are larger than those of ω_0'. On the other hand, in case II when $\omega \fallingdotseq \bar{p}_i$, the vibrations having the frequency ω_0' which is quite different from the frequency ω_0 of the disturbance build up remarkably and the amplitudes of the harmonic oscillations of frequency ω_0 are rather small.

(3) The fact stated in (2) has an exception corresponding to the curve $\widehat{EF}$ in Fig. 4.5 (a).

(4) At the resonances the reciprocal relation Eq. (4.13) of the amplitude

ratio between cases I and II holds.

(5) The amplitude ratios of the forced vibrations occurring near the resonances are approximately equal to those of the free vibrations, provided that the damping coefficients are not so large.

(6) The fact mentioned in (5) has two exceptional cases (i) and (ii) discussed in section 4.3.

Chapter 5. Unstable Vibrations Induced by Flexibility of Bearing Pedestals[28]

5.1. *Introduction*

In the lateral vibrations of a shaft carrying an unsymmetrical rotor, a free vibration of frequency p_i always appears with another free vibration of frequency $\overline{p}_i=2\omega-p_i$. If the bearing pedestals have different flexibilities in x- and y-directions, the spring constants of the shaft in x-direction will differ from those in y-direction. Coexistence of p_i and $\overline{p}_i$ and the small dissimilarity in spring constants result in new zones of instability where the whirling motions of the rotating shaft become unstable. These unstable zones take place in the neighborhood of the rotating speed ω where the relation

$$p_i=-p_j, \qquad \text{or} \qquad p_i=-\overline{p}_j=2\omega+p_j$$

is satisfied, in which p_i and p_j are the natural frequencies of the system. In the unstable zones, the system becomes dynamically unstable and vibrations with frequencies p_i, p_j, $\overline{p}_i$ and $\overline{p}_j$ build up steadily. In the present chapter, the cause of the occurrence of these vibrations, the extent of unstable zones, the motions within the unstable zones and the effects of the damping force are analytically and experimentally discussed.

5.2. *Existence of zones of instability, motions in the unstable zones*

Let the spring constants of lower bearing pedestal A and of upper bearing pedestal B be $k_{x\mathrm{A}}$, $k_{y\mathrm{A}}$ $(k_{x\mathrm{A}}>k_{y\mathrm{A}})$ and $k_{x\mathrm{B}}$, $k_{y\mathrm{B}}$ $(k_{x\mathrm{B}}>k_{y\mathrm{B}})$ respectively, and the spring constants of the shaft itself be α_0, γ_0, and δ_0 assuming the displacements of bearing pedestals and the inclination angle of bearing center line z to be negligibly smaller than x, y and θ_x, θ_y respectively, and then the equations of motions of the unsymmetrical rotating body supported by the flexible bearing pedestals are obtained[5],

$$\left.\begin{aligned}
&W/g\cdot\ddot{x}+(\alpha+\Delta\alpha)x+(\gamma+\Delta\gamma)\theta_x=0,\\
&W/g\cdot\ddot{y}+(\alpha-\Delta\alpha)y+(\gamma-\Delta\gamma)\theta_y=0,\\
&I\ddot{\theta}_x+I_p\omega\dot{\theta}_y+(\gamma+\Delta\gamma)x+(\delta+\Delta\delta)\theta_x-\Delta I\cdot\frac{d}{dt}(\dot{\theta}_x\cos 2\omega t+\dot{\theta}_y\sin 2\omega t)=0,\\
&I\ddot{\theta}_y-I_p\omega\dot{\theta}_x+(\gamma-\Delta\gamma)y+(\delta-\Delta\delta)\theta_y-\Delta I\cdot\frac{d}{dt}(\dot{\theta}_x\sin 2\omega t-\dot{\theta}_y\cos 2\omega t)=0,
\end{aligned}\right\} \tag{5.1}$$

where α, γ, and δ are spring constants of the shaft including flexibility of bearing pedestals; $\Delta\alpha$, $\Delta\gamma$, and $\Delta\delta$ are small differences in spring constants between x- and y-directions as follows:

$$\left.\begin{aligned}
\frac{\alpha_0-\alpha}{\Delta\alpha} &= \frac{1}{2l^2}\left\{(\alpha_0 b-\gamma_0)^2\left(\frac{1}{k_{y\mathrm{A}}}\pm\frac{1}{k_{x\mathrm{A}}}\right)+(\alpha_0 a+\gamma_0)^2\left(\frac{1}{k_{y\mathrm{B}}}\pm\frac{1}{k_{x\mathrm{B}}}\right)\right\},\\
\frac{\gamma_0-\gamma}{\Delta\gamma} &= \frac{1}{2l^2}\left\{(\alpha_0 b-\gamma_0)(\gamma_0 b-\delta_0)\left(\frac{1}{k_{y\mathrm{A}}}\pm\frac{1}{k_{x\mathrm{A}}}\right)+(\alpha_0 a+\gamma_0)(\gamma_0 a+\delta_0)\left(\frac{1}{k_{y\mathrm{B}}}\pm\frac{1}{k_{x\mathrm{B}}}\right)\right\},\\
\frac{\delta_0-\delta}{\Delta\delta} &= \frac{1}{2l^2}\left\{(\gamma_0 b-\delta_0)^2\left(\frac{1}{k_{y\mathrm{A}}}\pm\frac{1}{k_{x\mathrm{A}}}\right)+(\gamma_0 a+\delta_0)^2\left(\frac{1}{k_{y\mathrm{B}}}\pm\frac{1}{k_{x\mathrm{B}}}\right)\right\}.
\end{aligned}\right\} \tag{5.2}$$

For conveniene, we introduce the dimensionless quantities as follows:

$$\Delta\alpha/\alpha=\varepsilon,\quad \Delta\gamma/\gamma=\varepsilon_{12}=\kappa_{12}\varepsilon,\quad \Delta\delta/\delta=\varepsilon_{22}=\kappa_{22}\varepsilon. \tag{5.3}$$

Substituting Eqs. (2.11) and (5.3) into Eq. (5.1) and omitting primes on the dimensionless quantities, we have

$$\left.\begin{aligned}
&\ddot{x}+x+\gamma\theta_x+\varepsilon(x+\gamma\kappa_{12}\theta_x)=0,\\
&\ddot{y}+y+\gamma\theta_y-\varepsilon(y+\gamma\kappa_{12}\theta_y)=0,\\
&\ddot{\theta}_x+i_p\omega\dot{\theta}_y+\gamma x+\delta\theta_x+\varepsilon(\gamma\kappa_{12}x+\delta\kappa_{22}\theta_x)-\Delta\cdot\frac{d}{dt}(\dot{\theta}_x\cos 2\omega t+\dot{\theta}_y\sin 2\omega t)=0,\\
&\ddot{\theta}_y-i_p\omega\dot{\theta}_x+\gamma y+\delta\theta_y-\varepsilon(\gamma\kappa_{12}y+\delta\kappa_{22}\theta_y)-\Delta\cdot\frac{d}{dt}(\dot{\theta}_x\sin 2\omega t-\dot{\theta}_y\cos 2\omega t)=0.
\end{aligned}\right\} \tag{5.1 a}$$

In the first place, we consider a rather simple vibratory system in which the spring constant γ vanishes and motions of θ_x and θ_y do not couple with motions of x and y. Putting $\gamma=0$ and $\kappa_{12}=0$, and

$$t\sqrt{\delta}=t',\quad \omega/\sqrt{\delta}=\omega',\quad \kappa_{22}=1, \tag{5.4}$$

in Eq. (5.1 a) and omitting primes, we have the equations of motion of θ_x and θ_y for the system of $\gamma=0$.

$$\left.\begin{aligned}
&\ddot{\theta}_x+i_p\omega\dot{\theta}_y+\theta_x+\varepsilon\theta_x-\Delta\cdot\frac{d}{dt}(\dot{\theta}_x\cos 2\omega t+\dot{\theta}_y\sin 2\omega t)=0,\\
&\ddot{\theta}_y-i_p\omega\dot{\theta}_x+\theta_y-\varepsilon\theta_y-\Delta\cdot\frac{d}{dt}(\dot{\theta}_x\sin 2\omega t-\dot{\theta}_y\cos 2\omega t)=0.
\end{aligned}\right\} \tag{5.1 b}$$

If the bearing pedestals are rigid and the difference in spring constant ε vanishes, the free vibrations of the system are represented by

$$\left.\begin{aligned}
\theta_x &= \sum_{i=1}^{k}[A_i\cos(p_i t+\beta_i)+B_i\cos\{(2\omega-p_i)t-\beta_i\}],\\
\theta_y &= \sum_{i=1}^{k}[A_i\sin(p_i t+\beta_i)+B_i\sin\{(2\omega-p_i)t-\beta_i\}],
\end{aligned}\right\} \tag{5.5}$$

where k is the number of degrees of freedom[27]. For the present system, however, Eq. (5.5) do not satisfy Eq. (5.1 b) because of $\varepsilon\neq 0$. Since there is a difference in spring constant ε, the amplitudes of free vibrations in y-direction differ from those in x-direction. Accordingly, free vibrations take the form

$$\left.\begin{aligned}\theta_x &= A\cos pt = \frac{1}{2}(A+B)\cos pt + \frac{1}{2}(A-B)\cos(-p)t,\\ \theta_y &= B\sin pt = \frac{1}{2}(A+B)\sin pt + \frac{1}{2}(A-B)\sin(-p)t,\end{aligned}\right\} \tag{5.6}$$

and a free vibration of forward precession having frequency p and one of backward precession with frequency $-p$ take place simultaneously. Further, free vibrations of frequencies $\overline{p}=2\omega-p$ and $\overline{-p}=2\omega+p$ should coexist with vibrations of p and $-p$, because of unsymmetrical rotating body[27]. Furthermore, unequal amplitudes induced by unequal shaft rigidity ε in vibrations of $\overline{p}$ and $\overline{-p}$ result in vibrations of frequencies $-\overline{p}=p-2\omega$ and $-(\overline{-p})=-2\omega-p$ through the similar expression to Eq. (5.6). Repeating this procedure, free vibrations of the system with unsymmetrical rotating body and unequal spring constant are represent by the equations of infinite terms

$$\begin{aligned}\begin{matrix}\theta_x\\ \theta_y\end{matrix} &= A\begin{matrix}\cos\\ \sin\end{matrix}pt + a\begin{matrix}\cos\\ \sin\end{matrix}(2\omega-p)t + B\begin{matrix}\cos\\ \sin\end{matrix}(-p)t + b\begin{matrix}\cos\\ \sin\end{matrix}(2\omega+p)t\\ &+ C\begin{matrix}\cos\\ \sin\end{matrix}(p-2\omega)t + c\begin{matrix}\cos\\ \sin\end{matrix}(4\omega-p)t + D\begin{matrix}\cos\\ \sin\end{matrix}(-2\omega-p)t\\ &+ d\begin{matrix}\cos\\ \sin\end{matrix}(4\omega+p)t + E\begin{matrix}\cos\\ \sin\end{matrix}(p-4\omega)t + e\begin{matrix}\cos\\ \sin\end{matrix}(6\omega-p)t + \cdots .\end{aligned} \tag{5.7}$$

Since vibration of $-p$ is induced by small difference of spring constant ε, the value $(A-B)/(A+B)$ in Eq. (5.6) is as small as the order of ε. Thus, amplitudes of A and a in Eq. (5.7) are in the zero order of ε; and B, C, b and c are in the first order of ε; D, E, d and e in the second order of ε. Inserting Eq. (5.7) into Eq. (5.1 b) and comparing the coefficients, we obtain

$$\left.\begin{aligned}&G(p)\cdot A - \Delta p(2\omega-p)\cdot a + \varepsilon B = 0,\\ &G(2\omega-p)\cdot a - \Delta p(2\omega-p)\cdot A + \varepsilon C = 0,\\ &G(-p)\cdot B - \Delta(-p)(2\omega+p)\cdot b + \varepsilon A = 0,\\ &G(2\omega+p)\cdot b - \Delta(-p)(2\omega+p)\cdot B + \varepsilon D = 0,\\ &G(p-2\omega)\cdot C - \Delta(p-2\omega)(4\omega-p)\cdot c + \varepsilon a = 0,\\ &G(4\omega-p)\cdot c - \Delta(p-2\omega)(4\omega-p)\cdot C + \varepsilon E = 0,\\ &G(-2\omega-p)\cdot D - \Delta(-2\omega-p)(4\omega+p)\cdot d + \varepsilon b = 0,\\ &G(p-4\omega)\cdot E - \Delta(p-4\omega)(6\omega-p)\cdot e + \varepsilon c = 0,\end{aligned}\right\} \tag{5.8}$$

where

$$G(p) = 1 + i_p\omega p - p^2. \tag{5.9}$$

The ratios of amplitudes $A:a:B:b:\cdots$ in Eq. (5.7) are determined by Eq. (5.8), provided the natural frequency p is given. Neglecting terms smaller than ε^2, we have the relations

$$\left.\begin{aligned}b &= \Delta(-p)(2\omega+p)B/G(2\omega+p),\\ c &= \Delta(p-2\omega)(4\omega-p)C/G(4\omega-p),\end{aligned}\right\} \tag{5.10}$$

from the 4th and 6th equations in Eq. (5.8). Inserting Eq. (5.10) into the 3rd and 5th equations in Eq. (5.8) and eliminating b and c, we have the 1st, 2nd, 3rd and 5th equations of Eq. (5.8) containing only A, a, B and C. Using these four equations of A, a, B and C, the frequency equation

$$\Phi(\omega, p) = f_1 f_2 f_3 + \varepsilon^2 \varphi + \cdots = 0, \tag{5.11}$$

is given, where $\cdots$ represents small terms of higher powers than ε^3, and

$$\left.\begin{aligned} f_1 &= f(p) = G(p)G(2\omega - p) - \Delta^2 p^2 (2\omega - p)^2, \\ f_2 &= f(-p) = G(-p)G(2\omega + p) - \Delta^2 p^2 (2\omega + p)^2, \\ f_3 &= f(-\bar{p}) = G(p - 2\omega)G(4\omega - p) - \Delta^2 (p - 2\omega)^2 (4\omega - p)^2, \\ \varphi &= -\{G(p)G(4\omega - p)\cdot f_2 + G(2\omega - p)G(2\omega + p)\cdot f_3\}. \end{aligned}\right\} \tag{5.12}$$

The equation $f_1 = 0$ is the frequency equation when $\varepsilon = 0$[27], and the roots of $f_1 = 0$ are $p = p_1$, p_2, $\bar{p}_1$ and $\bar{p}_2$. At the major critical speed ω_c, the root p_1 becomes equal to $\bar{p}_1$ and a zone of instability appears[27][29]. For the present, neglecting the terms smaller than ε^2 in Eq. (5.11), we have

$$f_1 f_2 f_3 = 0. \tag{5.11a}$$

By observing Eq. (5.12) and Eq. (5.9), it can be seen that there are 12 roots of Eq. (5.11a), that is, we obtain roots $p = p_1$, $\bar{p}_1$, p_2 and $\bar{p}_2$ from $f_1 = 0$, and $p = -p_1$, $-\bar{p}_1$, $-p_2$ and $-\bar{p}_2$ from $f_2 = 0$, and $-\bar{p}_1 = p_1 + 2\omega$, $-\overline{\bar{p}_1} = p_1 - 2\omega = 4\omega - p_1$, $p_2 + 2\omega$ and $4\omega - p_2$ from $f_3 = 0$. When there are equal roots among the above 12 roots, the system becomes unstable, and new zones of instability take place in addition to that near the major critical speed ω_c. For instance, at the rotating speed ω where the relation

$$p_1 - p_2 = 2\omega \qquad (p_1 > p_2) \tag{5.13}$$

is satisfied, the roots $p = p_1$, $\bar{p}_2$ of $f_1 = 0$ become equal to the roots $p = p_2 + 2\omega$, $4\omega - p_1$ of $f_3 = 0$ respectively. Further the roots $p = p_2$, $\bar{p}_1$ of $f_1 = 0$ are equal to $p = p_1 - 2\omega$, $-p_2$ of $f_2 = 0$ respectively. Consequently unstable vibrations of frequencies p_1, p_2, $\bar{p}_1$ and $\bar{p}_2$ grow up steadily.

The range of unstable zone is determined by the following procedures. Let p_1, p_2 and ω which satisfy $f_1 f_2 f_3 = 0$ and Eq. (5.13) simultaneously be p_{10}, p_{20} and ω_0. In $p - \omega$ diagram of Fig. 5.1, the curve aa is a p_1 curve given by $f_1 = 0$, and the curve bb is a $p_2 + 2\omega$ curve furnished by $f_3 = 0$. As shown in Fig. 5.1, the curves aa and bb cross each other at the point A (ω_0, p_{10}) because of $p_1 = p_2 + 2\omega$. At the point $(\omega = \omega_0 + \xi, p = p_{10} + \eta_1)$ near the point A, the frequency equation $\Phi(\omega, p) = 0$ of Eq. (5.11) can be represented by

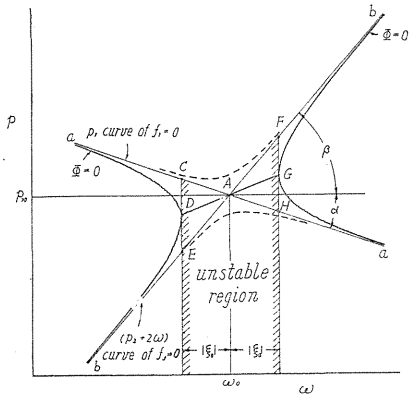

FIG. 5.1. $p - \omega$ curves

$$\Phi(\omega_0+\xi, p_{10}+\eta_1)=\Phi(\omega_0, p_{10})+\left(\frac{\partial\Phi}{\partial p}\eta_1+\frac{\partial\Phi}{\partial\omega}\xi\right)+\cdots$$

$$=f_2\left(\frac{\partial f_1}{\partial p}\eta_1+\frac{\partial f_1}{\partial\omega}\xi\right)\left(\frac{\partial f_3}{\partial p}\eta_1+\frac{\partial f_3}{\partial\omega}\xi\right)+\varepsilon^2\varphi(\omega_0, p_{10})+\cdots=0. \tag{5.14}$$

Neglecting small terms, we have

$$f_2\left\{\frac{\partial f_1}{\partial p}\frac{\partial f_3}{\partial p}\eta_1^2+\left(\frac{\partial f_1}{\partial p}\frac{\partial f_3}{\partial\omega}+\frac{\partial f_1}{\partial\omega}\frac{\partial f_3}{\partial p}\right)\xi\eta_1+\frac{\partial f_1}{\partial\omega}\frac{\partial f_3}{\partial\omega}\xi^2\right\}+\varepsilon^2\varphi(\omega_0, p_{10})=0. \tag{5.15}$$

Let the inclination angles of curves *aa* and *bb* at the point A be α and β respectively, as shown in Fig. 5.1, and we have

$$\tan\alpha=-\frac{\partial f_1}{\partial\omega}\Big/\left(\frac{\partial f_1}{\partial p}\right),\quad \tan\beta=-\frac{\partial f_3}{\partial\omega}\Big/\left(\frac{\partial f_3}{\partial p}\right). \tag{5.15a}$$

Then we obtain

$$\eta_1=\frac{1}{2}\left[(\tan\alpha+\tan\beta)\xi\pm\sqrt{(\tan\alpha-\tan\beta)^2\xi^2-4\varepsilon^2\varphi(\omega_0, p_{10})\Big/\left(\frac{\partial f_1}{\partial p}\frac{\partial f_3}{\partial p}\right)f_2}\right], \tag{5.16}$$

from Eqs. (5.15) and (5.15a). At the points D and G on the curve $\Phi=0$ in Fig. 5.1, equation $\Phi=0$ has equal roots, that is, terms within $\sqrt{\ }$ in Eq. (5.16) vanish and η_1 becomes an equal root. By putting $\sqrt{\ }=0$, we have ξ_0 as the values ξ at D and G.

$$\xi_0=\pm 2\varepsilon\sqrt{\varphi(\omega_0, p_{10})\Big/\left(\frac{\partial f_1}{\partial p}\frac{\partial f_3}{\partial p}\right)f_2}\Big/|\tan\alpha-\tan\beta|. \tag{5.17}$$

Eq. (5.14) has equal roots provided $\Phi\cdot\partial^2\Phi/\partial p^2=\varphi(\omega_0, p_{10})\left(\frac{\partial f_1}{\partial p}\frac{\partial f_3}{\partial p}\right)f_2>0$ at the point $A(\omega_0, p_{10})$. When $\Phi\cdot\partial^2\Phi/\partial p^2<0$, however, curves of $\Phi=0$ take the shape of dotted lines in Fig. 5.1, and equal roots do not appear near the point A. Inserting Eq. (5.17) into Eq. (5.16), we get

$$\eta_1=\frac{1}{2}\{(\tan\alpha+\tan\beta)\xi\pm\sqrt{(\tan\alpha-\tan\beta)^2(\xi^2-\xi_0^2)}\}. \tag{5.16a}$$

Accordingly, for $|\xi|<|\xi_0|$, the natural frequency p_1 is given by

$$p_1=p_{10}+\eta_1=P_1\pm im\qquad(i=\sqrt{-1}), \tag{5.18}$$

where

$$\left.\begin{aligned}P_1&=p_{10}+\frac{1}{2}(\tan\alpha+\tan\beta)\xi,\\ m&=\frac{1}{2}\sqrt{(\tan\alpha-\tan\beta)^2(\xi_0^2-\xi^2)},\end{aligned}\right\} \tag{5.19}$$

$$m_{\max}=\varepsilon\sqrt{\varphi(\omega_0, p_{10})\Big/\left(\frac{\partial f_1}{\partial p}\frac{\partial f_3}{\partial p}\right)f_2}. \tag{5.19a}$$

The range $|\xi_0|>\xi>-|\xi_0|$ represents clearly a zone of instability in which vib-

rations are expressed in the forms of $e^{mt}\cos P_1 t$ and $e^{mt}\sin P_1 t$ and build up exponentially. From Eqs. (5.17) and (5.19a) ξ_0 and $m_{\max}$ are seen to be in proportion to $\varepsilon\Delta$, because both $f_1=0$ and $f_3=0$ hold at the point A and $\varphi=-\Delta^2 p^2(2\omega-p)^2 f_2 \times G(4\omega-p)/G(2\omega-p)$ using Eq. (5.12). In Fig. 5.1, vertical lines at $\omega=\omega_0-|\xi_0|$ and $\omega=\omega_0+|\xi_0|$ intersect the curves $f_1=0$ and $f_3=0$ at C, E and H, F respectively. Let the middle points of CE and HF be D and G respectively, and we get

$$CD=DE=FG=GH=\varepsilon\sqrt{\varphi(\omega_0, p_{10})\Big/\left(\frac{\partial f_1}{\partial p}\frac{\partial f_3}{\partial p}\right)f_2}=m_{\max}. \tag{5.20}$$

Real part of p_1 in Eq. (5.18), *i.e.*, the frequency P_1 in the zone of instability is indicated by the line DAG in Fig. 5.1. Imaginary part m of p_1 vanishes at $\omega=\omega_0\pm|\xi_0|$ and takes a maximum value at ω_0, the middle of the zone of instability. Magnitude of value m in the unstable zone is shown in Fig. 5.2. Discussion of stability of free vibration with frequency p_2 is similar to that of frequency p_1 just mentioned. The curve $a'a'$ of p_2 given by $f_1=0$ and the curve $b'b'$ of $(p_1-2\omega)$ furnished by $f_2=0$ intersect each other at $\omega=\omega_0$ Let p_2 at $\omega=\omega_0$ be p_{20}, and calculating the value of Φ at the point $(\omega_0+\xi, p_{20}+\eta_2)$, and we get

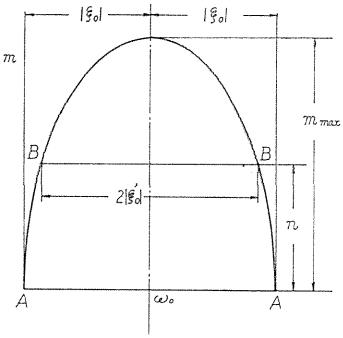

FIG. 5.2. Negative damping coefficient m

$$\eta_{/2}=\frac{1}{2}\left[(\tan\alpha'+\tan\beta')\xi\pm\sqrt{(\tan\alpha'-\tan\beta')^2\xi^2-4\varepsilon^2\varphi(\omega_0,p_{20})\Big/\left(\frac{\partial f_1}{\partial p}\frac{\partial f_2}{\partial p}\right)f_3}\right], \tag{5.16b}$$

in which α' and β' are the inclination angles of the curves $a'a'$ and $b'b'$ at the point (ω_0, p_{20}) respectively. We can prove $(\partial f_1/\partial p)_{p20}=(\partial f_3/\partial p)_{p10}$ and $(\partial f_2/\partial p)_{p20}=(\partial f_1/\partial p)_{p10}$ by calculation, and $\varphi(\omega_0, p_{10})/f_2=\varphi(\omega_0, p_{20})/f_3$ because of $p_{10}-p_{20}=2\omega_0$, and further we see clearly $\tan\alpha-\tan\beta=\tan\beta'-\tan\alpha'$. Thus the magnitudes of ξ_0 and m given by Eqs. (5.17) and (5.19) are common to both vibrations of frequencies p_1 and p_2. Consequently, range $2|\xi_0|$ of zone of instability of vibration p_1 is the same as that of vibration p_2, and the coefficient of negative damping m for vibration p_1 is equal to that of vibration p_2. This fact and the relations

$$\begin{pmatrix}\theta_x\\ \theta_y\end{pmatrix}=A\begin{matrix}\cos\\ \sin\end{matrix}(P+im)t+B\begin{matrix}\cos\\ \sin\end{matrix}(P-im)t=\frac{1}{2}(A+B)(e^{-mt}+e^{mt})\begin{matrix}\cos\\ \sin\end{matrix}Pt$$
$$-\frac{i}{2}(B-A)(e^{-mt}-e^{mt})\begin{matrix}\sin\\ \cos\end{matrix}Pt=a\left\{e^{-mt}\begin{matrix}\cos\\ \sin\end{matrix}(Pt-\beta)+e^{mt}\begin{matrix}\cos\\ \sin\end{matrix}(Pt+\beta)\right\}$$

result in the general solution within unstable range

$$\begin{pmatrix}\theta_x\\ \theta_y\end{pmatrix}=e^{-mt}\left\{A_1\begin{matrix}\cos\\ \sin\end{matrix}(P_1t-\beta_1)+a_1\begin{matrix}\cos\\ \sin\end{matrix}(\overline{P}_1t+\beta_1)+\cdots\right.$$
$$\left.+A_2\begin{matrix}\cos\\ \sin\end{matrix}(P_2t-\beta_2)+a_2\begin{matrix}\cos\\ \sin\end{matrix}(\overline{P}_2t+\beta_2)+\cdots\right\}$$

$$+e^{mt}\Big\{A_1\begin{matrix}\cos\\ \sin\end{matrix}(P_1t+\beta_1)+a_1\begin{matrix}\cos\\ \sin\end{matrix}(\overline{P}_1t-\beta_1)+\cdots$$

$$+A_2\begin{matrix}\cos\\ \sin\end{matrix}(P_2t+\beta_2)+a_2\begin{matrix}\cos\\ \sin\end{matrix}(P_2t-\beta_2)+\cdots\Big\}. \tag{5.21}$$

Values of amplitudes A_1, A_2 and phase angles β_1, β_2 are given by the initial conditions and the amplitudes a_1 and a_2 are determined by the magnitudes of A_1 and A_2.

For example, we calculate values ξ_0 and m for the system of $I_1:I_2:I_p=5:3:2$, *i.e.*, $i_p=1/2$, $\Delta=1/4$. For this vibratory system, we have $\omega_0=1.026$, $p_{10}=1.248$, $\overline{p}_{10}=0.804$, $p_{20}=-0.804$, $\overline{p}_{20}=2.856$, $|\xi_0|=0.0216\varepsilon$, and $m_{\max}=0.1835\varepsilon$. Incidentally, the zone of instability at the major critical speed ω_c is $\omega_{c11}=1.155\sim\omega_{c12}=2.000$.

5.3. Effects of the damping force

Now we consider the damping force and deal with the equation of motion having damping terms $c_2\dot{\theta}_x$ and $c_2\dot{\theta}_y$ in the 1st and 2nd equations of Eq. (5.1b) respectively. For this damped system, a free vibration takes the form

$$\begin{matrix}\theta_x\\ \theta_y\end{matrix}=e^{-mt}\Big[A\begin{matrix}\cos\\ \sin\end{matrix}pt+a\begin{matrix}\cos\\ \sin\end{matrix}(2\omega-p)t+B\begin{matrix}\cos\\ \sin\end{matrix}(-pt+\alpha')+b\begin{matrix}\cos\\ \sin\end{matrix}\{(2\omega+p)t-\alpha'\}$$

$$+C\begin{matrix}\cos\\ \sin\end{matrix}\{(p-2\omega)t+\alpha''\}+c\begin{matrix}\cos\\ \sin\end{matrix}\{(4\omega-p)t-\alpha''\}+\cdots\Big], \tag{5.7a}$$

in which the phase angles α' and α'' are as small as ε and c_2. Inserting Eq. (5.7a) into the equations of motion with damping terms and rejecting the higher powers than ε^2, we get

$$\left.\begin{aligned}
&\{G(p)+n^2-nc_2\}A-\Delta\{p(2\omega-p)+n^2\}a+\varepsilon B=0,\\
&\{G(2\omega-p)+n^2-nc_2\}a-\Delta\{p(2\omega-p)+n^2\}A+\varepsilon C=0,\\
&G(-p)\cdot B-\Delta(-p)(2\omega+p)\cdot b+\varepsilon A=0,\\
&G(2\omega+p)\cdot b-\Delta(-p)(2\omega+p)\cdot B=0,\\
&G(p-2\omega)\cdot C-\Delta(p-2\omega)(4\omega-p)\cdot c+\varepsilon a=0,\\
&G(4\omega-p)\cdot c-\Delta(p-2\omega)(4\omega-p)\cdot C=0,\\
&G(-2\omega-p)\cdot D-\Delta(-2\omega-p)(4\omega+p)\cdot d+\varepsilon b=0,\\
&G(p-4\omega)\cdot E-\Delta(p-4\omega)(6\omega-p)\cdot e+\varepsilon c=0.
\end{aligned}\right\} \tag{5.8a}$$

$$\left.\begin{aligned}
&(2np-c_2p-i_p\omega n)A+2n\Delta(\omega-p)\cdot a=0,\\
&\{2n(2\omega-p)-c_2(2\omega-p)-i_p\omega n\}a-2n\Delta(\omega-p)\cdot A=0,\\
&[\{2n(-p)-c_2(-p)-i_p\omega n\}-G(-p)\cdot\alpha']B\\
&\quad+\Delta\{2n(\omega+p)+(-p)(2\omega+p)\cdot\alpha'\}b=0,\\
&[\{2n(2\omega+p)-c_2(2\omega+p)-i_p\omega n\}+G(2\omega+p)\cdot\alpha']b\\
&\quad-\Delta\{2n(\omega+p)+(-p)(2\omega+p)\cdot\alpha'\}B=0,\\
&[\{2n(p-2\omega)-c_2(p-2\omega)-i_p\omega n\}-G(p-2\omega)\cdot\alpha'']C\\
&\quad+\Delta\{2n(3\omega-p)+(p-2\omega)(4\omega-p)\cdot\alpha''\}c=0,
\end{aligned}\right\} \tag{5.22}$$

$$\left.\begin{aligned}&[\{2n(4\omega-p)-c_2(4\omega-p)-i_p\omega n\}+G(4\omega-p)\cdot\alpha'']c\\&-\Delta\{2n(3\omega-p)+(p-2\omega)(4\omega-p)\cdot\alpha''\}C=0.\end{aligned}\right\}$$

Damping coefficient n is determined by the 1st and 2nd equations of Eq. (5.22) as follows:

$$n=c_2\frac{\{2p(2\omega-p)-i_p\omega^2\}+\sqrt{\{i_p^2\omega^2-4\Delta^2p(2\omega-p)\}(\omega-p)^2}}{(2p-i_p\omega)\{2(2\omega-p)-i_p\omega\}+4\Delta^2(\omega-p)^2}. \tag{5.23}$$

Phase angle α' is calculated by the 3rd and 4th equations of Eq. (5.22) and α'' is given by the 5th and 6th equations of Eq. (5.22). From Eq. (5.8a), we obtain the frequency equation

$$\Phi'(\omega,p)=f_1'f_2f_3+\varepsilon^2\varphi+\cdots=0, \tag{5.11b}$$

in which

$$f_1'=f_1+(n^2-nc_2)C(\omega,p),\quad C(\omega,p)=G(p)+G(2\omega-p). \tag{5.12a}$$

Developing Φ' at the point A (ω_0, p_{10}), we obtain

$$\begin{aligned}\Phi'(\omega_0+\xi,p_{10}+\eta_1)=f_2\Big[&\frac{\partial f_1}{\partial p}\eta_1+\frac{\partial f_1}{\partial\omega}\xi+(n^2-nc_2)\Big\{C(\omega_0,p_{10})\\&+\frac{\partial C}{\partial p}\eta_1+\frac{\partial C}{\partial\omega}\xi\Big\}\Big]\cdot\Big(\frac{\partial f_3}{\partial p}\eta_1+\frac{\partial f_3}{\partial\omega}\xi\Big)+\varepsilon^2\varphi(\omega_0,p_{10})+\cdots=0.\end{aligned} \tag{5.14a}$$

Neglecting small terms, Eq. (5.14a) reduces to Eq. (5.15). Consequently, when small damping coefficient n has the same order as ε, we also obtain the results of Eq. (5.16) to Eq. (5.19a) from $\Phi'(\omega,p)=0$. For the damped system, the solution in the unstable range is

$$\begin{aligned}\begin{matrix}\theta_x\\\theta_y\end{matrix}=&e^{-(n+m)t}\Big\{A_1\begin{matrix}\cos\\\sin\end{matrix}(P_1t-\beta_1)+a_1\begin{matrix}\cos\\\sin\end{matrix}(\overline{P}_1t+\beta_1)+\cdots\Big\}\\&+e^{(-n+m)t}\Big\{A_1\begin{matrix}\cos\\\sin\end{matrix}(P_1t+\beta_1)+a_1\begin{matrix}\cos\\\sin\end{matrix}(\overline{P}_1t-\beta_1)+\cdots\Big\}.\end{aligned} \tag{5.21a}$$

As shown in Fig. 5.2, the range of an unstable zone $AA=2|\xi_0|$ for an undamped system reduces to $BB=2|\xi_0'|$ when the damping forces exist. Clearly, the zone of instability vanishes when $n>m_{\max}$. The range $2|\xi_0'|$ decreases as the damping coefficient n increases as shown in Fig. 5.3 where the curve is a quarter of a circle.

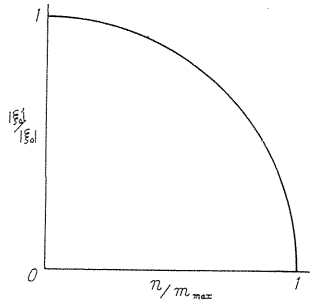

FIG. 5.3. Width of uustable region $2|\xi_0'|$ and damping n

5.4. *Coupled system of four degrees of freedom* ($\gamma\neq0$)

When the spring constant γ does not vanish, and the system is represented by Eq. (5.1a), expanding the following determinant (5.24)

$$\Phi(\omega, p)=\begin{vmatrix} H_1 & 0 & \varepsilon & 0 & \gamma & 0 & \varepsilon\gamma\kappa_{12} & 0 \\ 0 & \bar{H}_1 & 0 & \varepsilon & 0 & \gamma & 0 & \varepsilon\gamma\kappa_{12} \\ \varepsilon & 0 & H_2 & 0 & \varepsilon\gamma\kappa_{12} & 0 & \gamma & 0 \\ 0 & \varepsilon & 0 & H_3 & 0 & \varepsilon\gamma\kappa_{12} & 0 & \gamma \\ \gamma & 0 & \varepsilon\gamma\kappa_{12} & 0 & G_1 & -\Delta_1 & \varepsilon\delta\kappa_{22} & 0 \\ 0 & \gamma & 0 & \varepsilon\gamma\kappa_{12} & -\Delta_1 & \bar{G}_1 & 0 & \varepsilon\delta\kappa_{22} \\ \varepsilon\gamma\kappa_{12} & 0 & \gamma & 0 & \varepsilon\delta\kappa_{22} & 0 & B_2 & 0 \\ 0 & \varepsilon\gamma\kappa_{12} & 0 & \gamma & 0 & \varepsilon\delta\kappa_{22} & 0 & B_3 \end{vmatrix}=0 \quad (5.24)$$

gives the frequency equation which still takes the same form of Eq. (5.11), provied

$$\left.\begin{aligned} f_i &= (H_iG_i-\gamma^2)(\bar{H}_i\bar{G}_i-\gamma^2)-\Delta_i^2H_i\bar{H}_i, \qquad (i=1,2,3), \\ \varphi &= -f_2(\bar{H}_3\bar{G}_3-\gamma^2)[(H_1G_1-\gamma^2)\{\bar{G}_1B_3+(2\gamma^2+\bar{G}_1H_3+\bar{H}_1B_3)\gamma^2\kappa_{12}^2 \\ &\quad +\bar{H}_1H_3\delta^2\kappa_{22}^2-2\gamma^2(\bar{G}_1+B_3)\kappa_{12}+2\delta\gamma^2\kappa_{22}-2\delta\gamma^2(\bar{H}_1+H_3)\kappa_{12}\kappa_{22}\} \\ &\quad +H_1\Delta_1^2(-B_3-\gamma^2H_3\kappa_{12}^2+2\gamma^2\kappa_{12})] \\ &\quad -f_3(\bar{H}_2\bar{G}_2-\gamma^2)[(\bar{H}_1\bar{G}_1-\gamma^2)\{G_1B_2+(2\gamma^2+G_1H_2+H_1B_2)\gamma^2\kappa_{12}^2 \\ &\quad +H_1H_2\delta^2\kappa_{22}^2-2\gamma^2(G_1+B_2)\kappa_{12}+2\delta\gamma^2\kappa_{22}-2\delta\gamma^2(H_1+H_2)\kappa_{12}\kappa_{22}\} \\ &\quad +\bar{H}_1\Delta_1^2(-B_2-\gamma^2H_2\kappa_{12}^2+2\gamma^2\kappa_{12})], \end{aligned}\right\} \quad (5.25)$$

in which

$$\left.\begin{aligned} &H_1=1-p^2,\ \bar{H}_1=1-(2\omega-p)^2,\ G_1=\delta+i_p\omega p-p^2,\ \bar{G}_1=\delta+i_p\omega(2\omega-p)-(2\omega-p)^2, \\ &H_2=1-(-p)^2,\ \bar{H}_2=1-(2\omega+p)^2,\ G_2=\delta+i_p\omega(-p)-p^2, \\ &\bar{G}_2=\delta+i_p\omega(2\omega+p)-(2\omega+p)^2,\ H_3=1-(p-2\omega)^2=\bar{H}_1,\ \bar{H}_3=1-(4\omega-p)^2, \\ &G_3=\delta+i_p\omega(p-2\omega)-(p-2\omega)^2,\ \bar{G}_3=\delta+i_p\omega(4\omega-p)-(4\omega-p)^2, \\ &\Delta_1=p(2\omega-p)\Delta,\ \Delta_2=(-p)(2\omega+p)\Delta, \\ &\Delta_3=(p-2\omega)(4\omega-p)\Delta,\ B_{2,3}=G_{2,3}-\bar{H}_{2,3}\Delta_{2,3}^2/(\bar{H}_{2,3}\bar{G}_{2,3}-\gamma^2). \end{aligned}\right\} \quad (5.26)$$

In Fig. 5.4, $p_{1,2,3,4}-\omega$ curves and $\bar{p}_{1,2,3,4}-\omega$ curves, *i.e.*, curves $f_1=0$ of the vibratory system governed by Eq. (5.1a) are shown by thick full lines, and curves $f_2=0$ and $f_3=0$ are represented by dotted lines and fine lines respectively. Frequency equation $f_1f_2f_3=0$ has equal roots at $\omega=\omega_1, \omega_2, \ldots, \omega_8$ where curves $f_2=0$ and $f_3=0$ cross curves $f_1=0$.

5.5. Experimental results

Experiments were performed with vertical four shafts ($a:b=3:7$, $1:3$, $1:4$, and $1:5$ in Table 1.1) mounting an unsymmetrical rotor having $I_p=2.390$ kg cm s^2, $I_1=1.590$ kg cm s^2, and $I_2=0.815$ kg cm s^2. In order to give a small difference in flexibility ε, a somewhat flexible pedestal A is used in place of lower rigid pedestal as shown in Fig. 4.7. Measuring the deflection at the top of the pedestal, we find $k_{yA}=1.15\times10^3$ kg/cm[5].

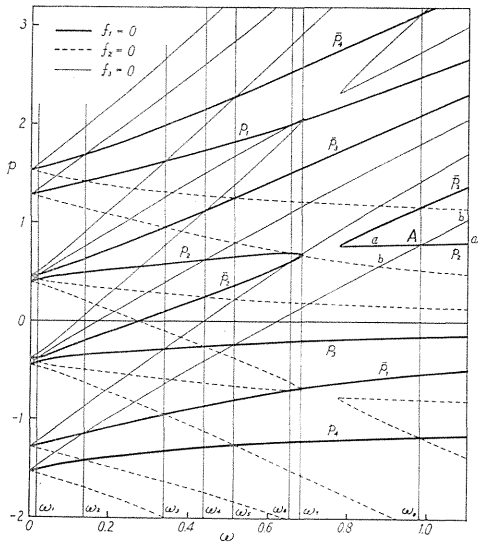

FIG. 5.4 $p-\omega$ curves ($a:b=1:4$, $\varepsilon\fallingdotseq 0$, $i_p=1.987$, $\Delta=0.322$, $\gamma=-0.860$, $\delta=1.040$)

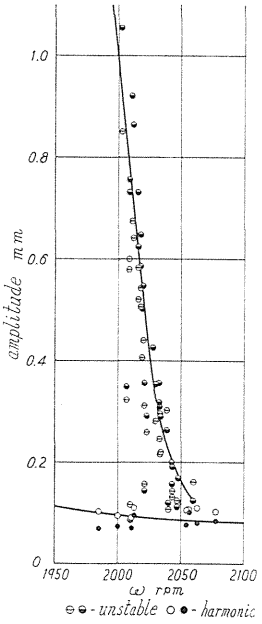

FIG. 5.5. Response curve ($a:b=1:4$, $\varepsilon\fallingdotseq 0$)

When No. 2 shaft ($a:b=1:4$) and a lower flexible pedestal A were used, $k_{yB}=1.05\times10^4$ kg/cm, $k_{yA}=1.15\times10^3$ kg/cm, $k_{xB}=k_{xA}=\infty$, and mean values of spring constants are $\alpha=4.54\times10^2$ kg/cm, $\gamma=-4.33\times10^3$ kg/rad, and $\delta=5.72\times10^4$ kg cm/rad ($i_p=1.987$, $\Delta=0.322$, $\gamma=-0.860$, $\delta=1.040$, $\varepsilon=0.199$, $\varepsilon_{12}=0.211$, $\varepsilon_{22}=0.157$, $\kappa_{12}=1.061$, and $\kappa_{22}=0.791$). Using these spring constants, natural frequency curves of the experimental apparatus are given by thick full lines, *i.e.*, $p_{1,2,3,4}$ and $\bar{p}_{1,2,,3,4}$ curves in Fig. 5.4, where ω and p are represented by dimensionless quantities, and multiplying $\sqrt{\alpha g/W}=2040$ rpm, we have values of ω and p in rpm. As shown in Fig. 5.4, in this vibratory system, p_2 is equal to $\bar{p}_2$ at $\omega_{c21}=0.685$ and $\omega_{c22}=0.780$, thus the zone of instability near the major critical speed ω_c takes place in the range of $\omega=0.685\sim0.780$ (1397$\sim$1591 rpm). Further unstable zones can appear at $\omega=\omega_1$, ω_2, ..., ω_8, where $f_1f_2f_3=0$ has equal roots. In Fig. 5.5, experimental results in the zone of instability near $\omega=\omega_8=0.98$ (1999 rpm) are shown. In this unstable zone, the aa curve of p_2 and the bb curve of $p_4+2\omega$ cross each other at the point A as shown in Fig. 5.4, and unstable vibrations with frequencies p_2, p_4, $\bar{p}_2$ and $\bar{p}_4$ appear. By calculation of amplitude ratio, however, we see that amplitudes of vibrations $\bar{p}_2$ and $\bar{p}_4$ are so small in this zone that only vibrations of p_2 and p_4 take place apparently as shown in Fig. 5.8. Further by calculation, we obtain $p_2=0.79$ (1612 rpm), $p_4=-1.17$ (-2386 rpm) for the values at the point A and $\tan\alpha=0.179$ (incline of p_2 curve), $\tan\beta=2.14$ (incline of $2\omega+p_4$ curve), negative damping coefficient $m_{\max}=0.0131$, and $\xi_0=\pm0.0134$ (±26.7 rpm). Both calculated and experimental results are given in Fig. 5.6 where the calculated frequency P_2 in the unstable zone changes along the curve cc and the calculated unstable range is BB, while the unstable range obtained by experiment is $B'B'$. Though there is a small difference between the curve cc and the experimental results $c'c'$

because of effects of accuracy of spring constants and neglect of shaft mass, we can see that the frequency P_2 obtained by experiment does not change its magnitude along the p_2 curve (curve aa) but along the values P_2 (curve cc) given by Eq. (5.19). Since the damping coefficient n in the experimental apparatus is about 0.005, there is sufficient possibility of an unstable vibration occurring at the negative damping coefficient $m_{max}=0.0131$.

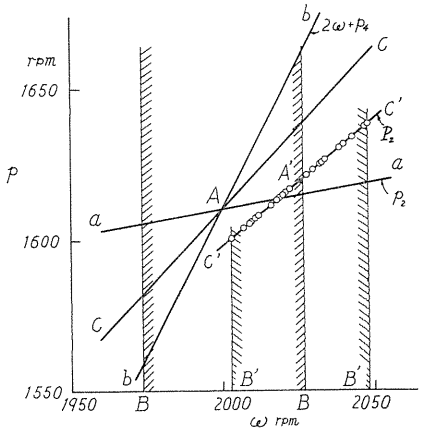

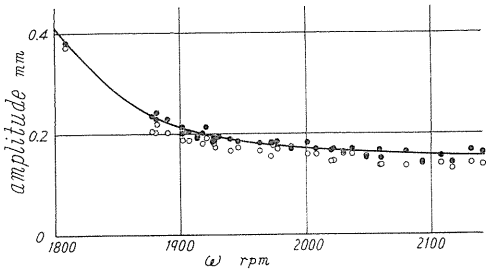

FIG. 5.7. Rosponse curve ($a:b=1:4$, $\varepsilon=0$)

← FIG. 5.6. P_2, $p_2-\omega$ diagram ($a:b=1:4$, $\varepsilon\fallingdotseq 0$)

Fig. 5.4 shows that zones of instability can take place at $\omega_1, \omega_2, \ldots, \omega_7$ but ω_8. Rotating speed $\omega_1=0.020$ (40 rpm), however, is too low for experiment and $\omega_6=0.658$ (1342 rpm), $\omega_7=0.681$ (1389 rpm) are too near the unstable range of ω_c to perform the experiment, and at $\omega_3=0.338$ (689 rpm) and $\omega_4=0.439$ (896 rpm) the negative damping m is too small to overcome the damping coefficient n. Further at $\omega_2=0.137$ (279.5 rpm) and $\omega_5=0.513$ (1046 rpm), the sign of $\varphi(\omega, p)$ differs from that of $(\partial f_1/\partial p)(\partial f_3/\partial p)f_2$ and a zone of instability cannot appear as mentioned in section 5.2. Consequently, unstable vibrations can occur only at $\omega_8=0.98$ (1999 rpm).

When rigid bearing pedestals are used both in the upper and lower pedestal, unstable vibrations do not take place even at ω_8 because of $\varepsilon=0$, as shown in Fig. 5.7.

In the procedure of analytical treatment in section 5.2, we can see that an external force, *i.e.*, unbalance of rotor has no effect on the unstable vibrations. Existence of an external force only results in superposition of harmonic vibrations on the unstable vibrations.

Vibratory waves of unstable vibrations appearing near ω_8 are given in Fig. 5.8 where vertical white lines are rotating marks recorded at each revolution. The lower bearing pedestal deflects in y-direction, and its rigidity is almost infinite in x-direction perpendicular to y-direction. In Fig. 5.8, the upper photograph shows waves in x-direction, and the lower does waves in y-direction. In Fig. 5.8, vibratory waves change periodically between the marks AA. At intervals of marks AA, the shaft rotates 16 times and vibration of P_2 (>0) and P_4 (<0) oscillate 13 times and 19 times respectively. So we can see that $P_2:P_4:\omega \fallingdotseq 13:-19:16$ and $P_2-P_4=2\omega$. As a vibration of P_2 is a forward precession and one

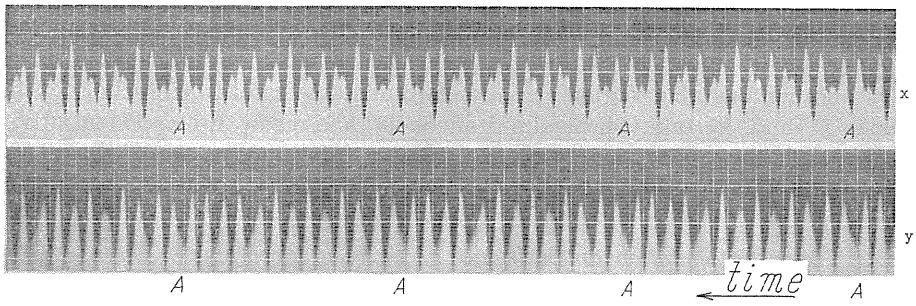

FIG. 5.8. Vibratory waves ($a:b=1:4$, $\varepsilon\fallingdotseq 0$, $P_2:P_4:\omega\fallingdotseq 13:-19:16$)

of P_4 a backward precession, the loop of beat in x-direction and the node of beat in y-direction occur at the same time.

When the position mounting the rotor comes nearer to the middle of the shaft, small differences in flexibility ε, ε_{12}, and ε_{22} due to the same flexible pedestal A, become smaller. Therefore, a zone of instability at $\omega=\omega_s$ where the relation $p_2-p_4=2\omega$ is satisfied is used to occur for the two shafts ($a:b=1:4$ and $a:b=1:5$), but can not appear for the shafts ($a:b=3:7$ and $a:b=1:3$).

5.6. Conclusions

(1) Coexistence of p_i, $\bar{p}_i$ due to an inertia asymmetry of rotor and of p_i, $-p_i$ due to small differences in spring constants between x- and y-directions result in new zones of instability. These zones appear at the rotating speed ω where the relation $p_i=-p_j$, or $p_i=-\bar{p}_j=2\omega+p_j$ is satisfied.

(2) In the unstable zones, the system is dynamically unstable and amplitudes of the vibrations with frequencies P_i, P_j, $\bar{P}_i$, P_j grow up exponentially.

(3) The approximately calculated values of width of unstable zone $2|\xi_0|$ and frequencies of vibrations P_i, P_j coincide well with experimental results.

(4) When there is damping, the width of unstable zone $2|\xi_0'|$ decreases with the increase of damping coefficient n, and unstable vibrations can not occur if n is larger than $m_{\max}$.

(5) $2|\xi_0|$ and $m_{\max}$ are in proportion to the product of dissimilarity in flexibility ε and inertia asymmetry of rotor Δ.

(6) Whether $\Phi\cdot\partial^2\Phi/\partial p^2$ is positive or negative at the point A (ω_0, p_0) where $f_i=0$ curve meets with $f_j=0$ curve, determines occurence or no occurence of unstable zones.

Chapter 6. Unstable Vibrations near Rotating Speed ω_d[30)33)]

6.1. Introduction

Although some studies have been made on the problems of unstable vibrations of a shaft system carrying an unsymmetrical rotor[22)~26)], it seems that the unstable vibration problems we discuss in this chapter have not been treated by other researchers. The rotating shaft becomes unstable near its major critical

speeds ω_c where the relation $p_i=\bar{p}_i$ holds and unstable vibrations of frequency ω build up[27)29)]. In this chapter it is shown that in the neighborhood of the rotating speed ω_d, where the relation $p_i=\bar{p}_j$ $(i\neq j)$, *i.e.*, $p_i+p_j=2\omega$ is satisfied, there is always another unstable region in which two unstable lateral vibrations with frequencies P_i and P_j take place simultaneously and grow up exponentially, and the sum of these P_i+P_j is always equal to 2ω. Also the nature of unstable vibrations is treated theoretically and the results are verified through experiments.

6.2. Frequency equation and existence of unstable vibrations

Here we treat the vibratory system which consists of a light shaft supported by rigid bearing pedestals and of an unsymmetrical rotor without any static and dynamic unbalances.

Inserting Eq. (2.13) of free vibrations into Eq. (2.12) we get the following frequency equation:

$$\Phi(\omega, p) = f\bar{f} + \Delta^2\varphi = 0. \tag{6.1}$$

In this equation

$$\left.\begin{aligned} &f=(1-p^2)(\delta+i_p\omega p-p^2)-\gamma^2,\quad \bar{f}=(1-\bar{p}^2)(\delta+i_p\omega\bar{p}-\bar{p}^2)-\gamma^2,\\ &\varphi=-(1-p^2)(1-\bar{p}^2)p^2\bar{p}^2. \end{aligned}\right\} \tag{6.2}$$

Also when the rotor is a symmetrical rotor $f=0$ as the frequency equation. Then, if we insert

$$p=\omega+p',\quad \bar{p}=2\omega-p=\omega-p', \tag{6.3}$$

Eq. (6.1) can be rewritten as follows:

$$K_8p'^8-K_6p'^6+K_4p'^4-K_2p'^2+K_0=0. \tag{6.4}$$

In this equation

$$\left.\begin{aligned} K_8&=1-\Delta^2,\\ K_6&=\{2\delta+(i_p^2-2i_p+2-2\Delta^2)\omega^2\}+2(1-\Delta^2)(1+\omega^2),\\ K_4&=\{\delta+(i_p-1-\Delta)\omega^2\}\{\delta+(i_p-1+\Delta)\omega^2\}\\ &\quad+2(1+\omega^2)\{2\delta+(i_p^2-2i_p+2-2\Delta^2)\omega^2\}+(1-\Delta^2)(1-\omega^2)^2-2\gamma^2,\\ K_2&=2(1+\omega^2)\{\delta+(i_p-1-\Delta)\omega^2\}\{\delta+(i_p-1+\Delta)\omega^2\}\\ &\quad+(1-\omega^2)^2\{2\delta+(i_p^2-2i_p+2-2\Delta^2)\omega^2\}-2\gamma^2\{1+\delta-3(2-i_p)\omega^2\},\\ K_0&=[(1-\omega^2)\{\delta+(i_p-1-\Delta)\omega^2\}-\gamma^2]\cdot[(1-\omega^2)\{\delta+(i_p-1+\Delta)\omega^2\}-\gamma^2]. \end{aligned}\right\} \tag{6.5}$$

When all the roots of the biquadratic equation (6.4) in p'^2 are positive the system is stable. When K_0 in Eq. (6.4) is negative, Eq. (6.4) has at least one negative root $p_i'^2=-m^2$ $(m>0)$ which results in $p_i'=\pm im$, $p_i=\omega+im$, $\bar{p}_i=\omega-im$ and unstable vibrations of Eq. (3.9)[27)29)].

If Eq. (6.4) with real coefficients has a pair of conjugate complex roots $p'^2=A+iB$, $p'^2=A-iB$ it follows that $p'=\pm(P'+im)$ and $p'=\pm(P'-im)$ respectively. By inserting $P'=\sqrt{(\sqrt{A^2+B^2}+A)/2}>0$ and $m=\sqrt{(\sqrt{A^2+B^2}-A)/2}>0$ it results in $p=\omega+P'\pm im$ and $\bar{p}=\omega-P'\pm im$. Inserting the foregoing results into Eq. (2.13) we obtain unstable vibrations, *e.g.*,

$$x=A_i\{e^{mt}\cos(P_it+\beta_i)+e^{-mt}\cos(P_it-\beta_i)\}+A_j\{e^{mt}\cos(P_jt+\beta_j)+e^{-mt}\cos(P_jt-\beta_j)\}. \tag{6.6}$$

In Eq. (6.6)

$$P_i=\omega+P',\ P_j=\omega-P',\ \text{and}\ P_i+P_j=2\omega. \tag{6.7}$$

At the boundaries of unstable ranges negative damping m in Eq. (6.6) vanishes and the imaginary part B is equal to zero. Then Eq. (6.4) has a double root $p'^2=A$. This then results in $p=P_i=\bar{P}_j$ and $p=P_j=\bar{P}_i$ in Eq. (6.1).

6.3. Unstable region

When the asymmetry Δ falls to zero the unstable region is reduced to zero. That is, its boundary shrinks to a point at a certain rotating speed ω_d, while the frequency equation (6.1) is reduced to $f\bar{f}=0$. Since this point is still said to be the boundary, the frequency equation $f\bar{f}=0$ has two double roots: $p=p_i=\bar{p}_j$ and $p=p_j=\bar{p}_i$. As was mentioned before, in $p-\omega$ diagram of $f\bar{f}=0$ (Fig. 6.1), curves p_i and $\bar{p}_j$ as well as curves p_j and $\bar{p}_i$ cross at $\omega=\omega_d$. At this intersecting point, the unstable region widens its range as Δ increases. To determine whether the unstable regions exist and, if they do, how many and where they appear, we start with the geometrical discussion about this intersecting point which gives ω_d. For comprehensive discussion of the vibratory system geometrical treatment in $p-\omega$ diagram is simpler than an analytical discussion of the equation $f\bar{f}=0$ of the 8th order in p.

Fig. 6.1 is $p-\omega$ diagram for $\Delta=0$, $i_p=1$, $\delta=1.060$ and $\gamma^2=0.731$. In this diagram roots p_i and $\bar{p}_i=2\omega-p_i$ $(i=1,2,3,4)$ of the frequency equation $f\bar{f}=0$ are shown by full and dotted lines respectively. Regardless of the dimensions of the shaft and the rotor it can be always concluded that (a) the relation $p_1>1>p_2>0>p_3>-1>p_4$ holds and (b) p_1, p_2, p_3, and p_4 respectively approach the value $i_p\omega$, 1, 0, and -1 as ω tends to ∞. It follows from both (a) and (b) that (1) when $i_p<1$, curves p_1 and $\bar{p}_1$, curves p_2 and $\bar{p}_2$ cross at the major ciritical speeds ω_{c1}, ω_{c2} re-

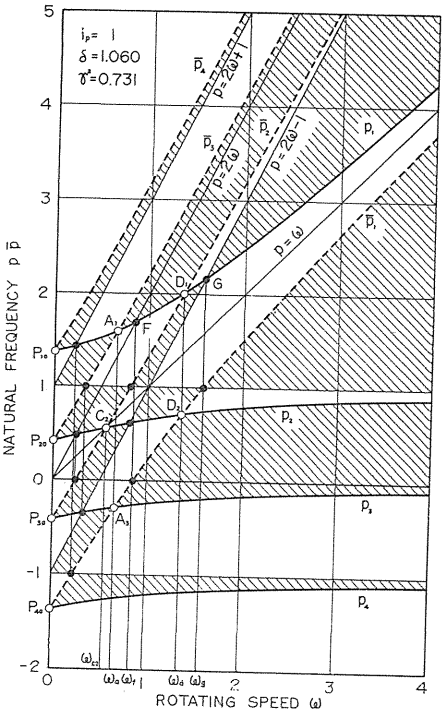

FIG. 6.1. $p-\omega$ diagram when $\Delta=0$.

spectively, and when $i_p \geqq 1$ only curves p_2 and $\bar{p}_2$ cross at ω_{c2} (C_2 in Fig. 6.1); (2) curves p_1 and $\bar{p}_2$ as well as curves p_2 and $\bar{p}_1$ intersect at ω_d (D_1, D_2 in Fig. 6.1); (3) curves p_1 and $\bar{p}_3$ and also curves p_3 and $\bar{p}_1$ cross at ω_a (A_1, A_3 in Fig. 6.1); and (4) curves p_1 and $\bar{p}_4$, curves p_2 and $\bar{p}_3$, curves p_3 and $\bar{p}_2$, and curves p_4 and $\bar{p}_1$ intersect at $\omega=0$ (P_{10}, P_{20}, P_{30}, P_{40} in Fig. 6.1). These are the only possible intersecting points which exist.

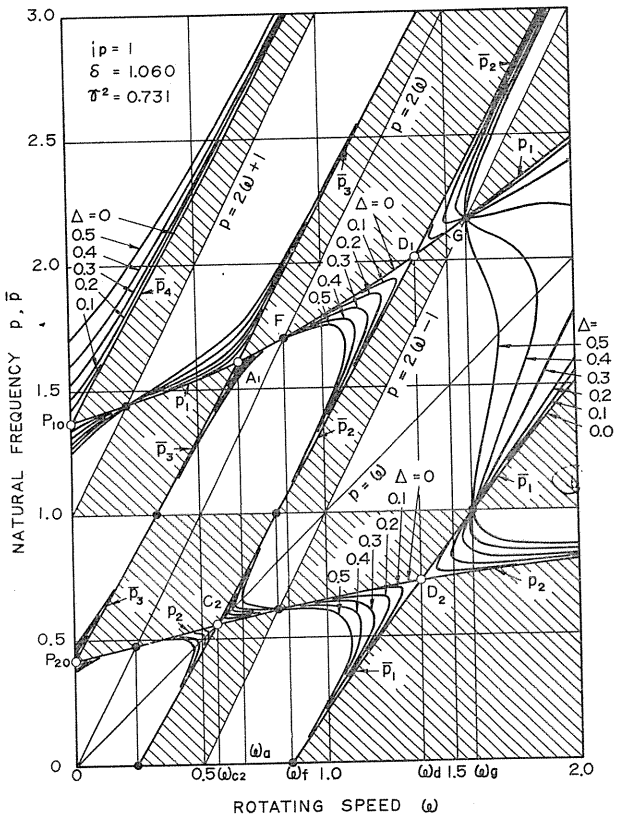

FIG. 6.2. $p-\omega$ diagram for $\Delta=0$, 0.1, 0.2, 0.3, 0.4, 0.5.

The $p-\omega$ plane in Fig. 6.1 is divided into many regions by straight lines of $p=\pm 1$, $p=2\omega$, $p=2\omega\pm 1$ and curves p_i, $\bar{p}_i$, and some of them are shaded. The frequency equation (6.1) is satisfied only when $f\bar{f}\varphi \leqq 0$ because of $\Delta^2>0$. Since $f\bar{f}\varphi$ is positive in the shaded regions and negative in the unshaded regions all $p-\omega$ curves lie only in unshaded regions as shown in Fig. 6.2 where curves for $\Delta=0$, 0.1, 0.2, 0.3, 0.4, and 0.5 are represented. All $p-\omega$ curves pass through points shown by mark ● in Figs. 6.1 and 6.2 where $f\bar{f}=0$ and $\varphi=0$ hold simultaneously. Observing Fig. 6.2 we see that around intersecting points, C_2 cited in (1) as well as D_1 and D_2 in (2), there are some ranges of ω where curves p_1, p_2, $\bar{p}_1$, and $\bar{p}_2$ are lacking if $\Delta \neq 0$. These ranges are the unstable regions where p_i cannot be shown by curves because it becomes a complex number. Near the intersecting points A_1, A_3, P_{10}, P_{20}, P_{30}, and P_{40} cited in (3) and (4) $p-\omega$ curves

exist and unstable regions do not appear. Referring to Eq. (6.1), it has double roots near the points D_1 and D_2 cited in (2) because of $\Phi \cdot \partial^2\Phi/\partial p^2 > 0$. In this situation unstable regions can appear. However, near the intersecting points cited in (3) and (4) $\Phi \cdot \partial^2\Phi/\partial p^2 < 0$ results in no double root and therefore no unstable region.

In summary, we can conclude that in the vibratory shaft system carrying an unsymmetrical rotor, there is always only one unstable region in which two unstable vibrations of frequencies P_1 and $P_2 = 2\omega - P_1$ build up steadily as shown in Eq. (6.6) and Fig. 6.11. Of course we except here the unstable regions near the major critical speeds where unstable vibration with frequency ω takes place.

The value of the rotating speed ω_d at which point the unstable region spreads as Δ increases is given analytically by solving the frequency equation $f\bar{f} = 0$ with reference to $p_1 = \bar{p}_2$:

$$\frac{\omega_d^2}{\omega_a^2} = \frac{i_p^2 + 4(2 - i_p)(1 + \delta) \pm (4 - i_p)\sqrt{i_p^2 + 8(2 - i_p)(\delta - \gamma^2)}}{8(2 - i_p)^2}. \tag{6.8}$$

The natural frequencies p_1 and p_2 at $\omega = \omega_d$ are given as p_{1d}, p_{2d}:

$$\begin{matrix} p_{1d} \\ p_{2d} \end{matrix} = \omega_d \pm \sqrt{\frac{(3i_p - 4)\omega_d^2 + (2 + 2\delta - i_p)}{(4 - i_p)}}. \tag{6.8 a}$$

The value of ω_d increases with the polar moment of inertia i_p and becomes infinite when i_p takes its upper limit value 2. The rotating speed ω_d is plotted against i_p in Fig. 6.3 where $\delta = 1.060$ and $\gamma^2 = 0.731$ as in Figs. 6.1 and 6.2. Curves of the major critical speeds ω_{c1} and ω_{c2} and curves of the rotating speeds ω_f and ω_g at the intersecting points F and G in Figs. 6.1 and 6.2, where curve p_1 crosses the straight lines $p = 2\omega$ and $p = 2\omega - 1$, respectively, as shown in Figs. 6.1 and 6.2, are added in Fig. 6.3. Since $\omega_{c1} > \omega_d > \omega_{c2}$ always holds, curve ω_d lies between curves ω_{c1} and ω_{c2} as shown in Fig. 6.3. Regardless of the magnitude of Δ, curve p_1 always passes through the points F and G as mentioned. Also the unstable region cannot spread beyond the rotating speed ω_f and ω_g of the points F and G, and the unstable region always lies, regardless of the value of the asymmetry Δ, within the shaded space in Fig. 6.3, bounded by the curves ω_f and ω_g.

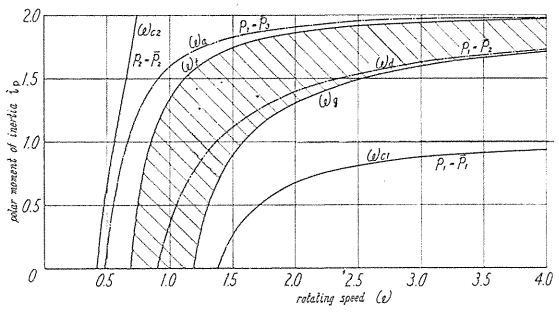

FIG. 6.3. $i_p - \omega_d$ diagram ($\delta = 1.060$, $\gamma^2 = 0.731$)

6.4. Range of unstable region and value of negative damping coefficient

As previously stated, the biquadratic equation (6.4) in p'^2 has a double root

on the boundary of the unstable region and therefore the discriminant D of Eq. (6.4) is equal to zero, *i.e.*,

$$27K_8^6D = 4(12K_0K_3 - 3K_2K_6 + K_4^2)^3 - (27K_2^2K_8 - 72K_0K_4K_8 + 27K_0K_6^2 - 9K_2K_4K_6 + 2K_4^3)^2 = 0. \qquad (6.9)$$

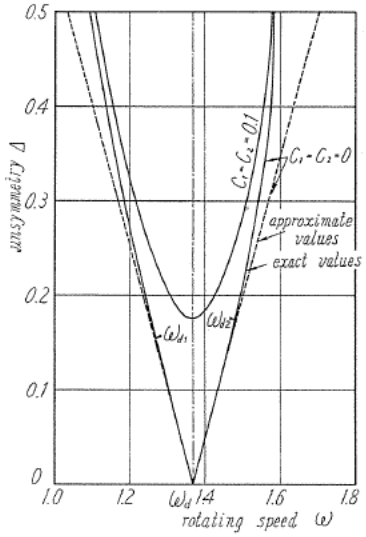

FIG. 6.4. Unstable region near ω_{0d} ($i_p=1$, $\delta=1.060$, $\gamma^2=0.731$, $\omega_d=1.3674$, $|\xi_0|/\Delta=0.6667$, $m_{max}/\Delta=0.3896$)

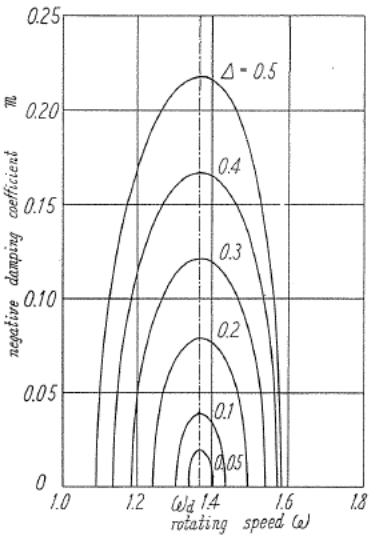

FIG. 6.6. Negative damping coefficient m ($i_p=1$, $\delta=1.060$, $\gamma^2=0.731$, $\omega_d=1.3674$)

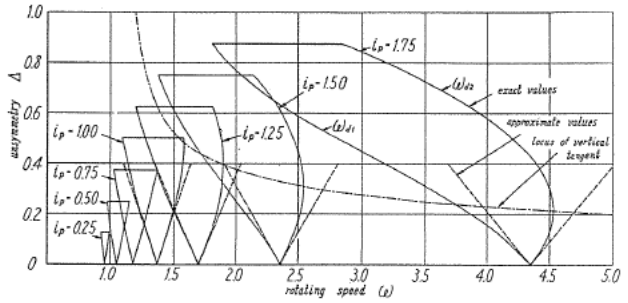

(a)

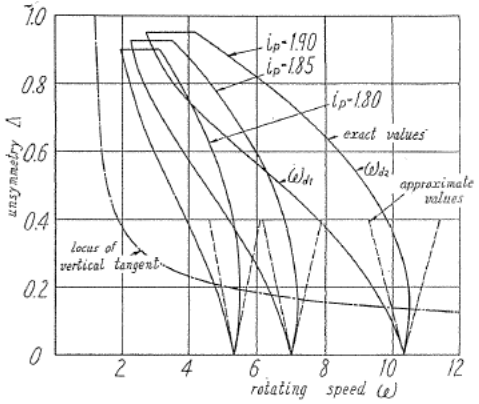

(b)

FIG. 6.5. Unstable regions ($\delta=1.060$, $\gamma^2=0.731$)

The solutions of Eq. (6.9) of the 24th order in ω give the rotating speeds ω_{d1} and ω_{d2} at the boundaries of the unstable region. By numerically solving Eq. (6.9) for the case $\delta=1.060$ and $\gamma^2=0.731$ the boundaries for $i_p=1$ and for the various magnitudes of i_p shown in Figs. 6.4 and 6.5, respectively, are obtained. In Fig. 6.4, ω_{d1} and ω_{d2} are the lower and upper limits of the unstable region and the line $\omega=\omega_d$ is a vertical chain line. The boundary widens its range as the asymmetry Δ or i_p increases. At a rather large polar moment of inertia i_p, the unstable region appears at a higher rotating

speed. For rather large i_p, ω_{d1} decreases steadily as Δ increases. However ω_{d2} has its maximum at a certain value of Δ as shown in Fig. 6.5. At this time the unstable regions bends to the left. Curves connecting the foregoing maximum points of ω_{d2} are shown by the chain line in Fig. 6.5. The equation of this curve is given by inserting the values of ω and p at the point G in Figs. 6.1 and 6.2 into $\partial\Phi/\partial p=0$, *i.e.*, $\Delta^2=-\gamma^2\{(i_p\omega-2p)(1-p^2)^2-2\gamma^2 p\}/2p^2(1-p^2)^2$.

The negative damping m is given by solving Eq. (6.4) and is shown in Fig. 6.6 where $i_p=1$, $\delta=1.060$, and $\gamma^2=0.731$ as were the cases in Figs. 6.1, 6.2, and 6.4. The value of m increases with Δ and takes its maximum value $m_{\max}$ near the center of the unstable region as shown in Fig. 6.6 where the chain line is the line for $\omega=\omega_d$. Value of $m_{\max}$ is plotted against Δ in Fig. 6.7 where it increases with Δ.

6.5. Approximation methods

When the asymmetry Δ is small, boundaries ω_{d1} and ω_{d2}, the negative damping m and $m_{\max}$ and the frequencies P_1 and P_2 of the unstable vibrations can be obtained through the following means based on the expansion of Eq. (6.1) at the point $(\omega=\omega_d+\xi,\ p=p_{1d}+\eta_1)$. Assuming ξ, η_1 and Δ to be small, we have:

$$\Phi(\omega_d+\xi,\ p_{1d}+\eta_1)\fallingdotseq\left(\frac{\partial f}{\partial p}\eta_1+\frac{\partial f}{\partial\omega}\xi\right)\left(\frac{\partial\bar{f}}{\partial p}\eta_1+\frac{\partial\bar{f}}{\partial\omega}\xi\right)+\Delta^2\varphi=0. \tag{6.10}$$

If the inclination angles of the tangents of curves p_1 and $\bar{p}_2$ at the point $D_1(\omega_d,\ p_{1d})$ be α and β respectively we have:

$$\tan\alpha=-\frac{\partial f}{\partial\omega}\Big/\frac{\partial f}{\partial p},\qquad \tan\beta=-\frac{\partial\bar{f}}{\partial\omega}\Big/\frac{\partial\bar{f}}{\partial p}. \tag{6.11}$$

The value of η_1 is given by Eq. (6.10) while $p_1=p_{1d}+\eta_1=P_1\pm im$. Then, referring to Eq. (6.11), we have:

$$P_1=p_{1d}+1/2\cdot(\tan\alpha+\tan\beta)\xi, \tag{6.12}$$

$$m=\frac{1}{2}\sqrt{4\Delta^2\varphi\Big/\left(\frac{\partial f}{\partial p}\cdot\frac{\partial\bar{f}}{\partial p}\right)-(\tan\alpha-\tan\beta)^2\xi^2}, \tag{6.13}$$

here P_1 is the frequency of the unstable vibration. When $\xi=0$, *i.e.*, at $\omega=\omega_d$, m takes its maximum value:

$$m_{\max}=\Delta\sqrt{\varphi\Big/\left(\frac{\partial f}{\partial p}\cdot\frac{\partial\bar{f}}{\partial p}\right)}. \tag{6.14}$$

If ξ be ξ_0 when $m=0$, *i.e.*, at the boundary, we get:

$$\xi_0=\pm 2\Delta\sqrt{\varphi\Big/\left(\frac{\partial f}{\partial p}\cdot\frac{\partial\bar{f}}{\partial p}\right)}\Big/|\tan\alpha-\tan\beta|. \tag{6.15}$$

The upper and the lower limits of the unstable region ω_{d2} and ω_{d1} are clearly represented by $\omega_d+|\xi_0|$ and $\omega_d-|\xi_0|$ and the width of the unstable region $\omega_{d2}-\omega_{d1}$ is equal to $2|\xi_0|$. If we apply the same procedure to the point $D_2(\omega_d,\ p_{2d})$ in Figs. 6.1 and 6.2 we will get the same value of m as in Eq. (6.13) and the following relation:

$$P_2 = p_{2d} + 2\xi - 1/2 \cdot (\tan\alpha + \tan\beta)\xi. \qquad (6.12\,a)$$

Here $p_{2d} = 2\omega_d - p_{1d}$, and P_2 is the frequency of another unstable vibration. From Eqs. (6.12) and (6.12 a) we see that the relation $P_1 + P_2 = 2(\omega_d + \xi) = 2\omega$ is valid. In Eqs. (6.10) through (6.15) we must use the values given at point D_1, *i.e.*, $\omega = \omega_d$, $p = p_{1d}$.

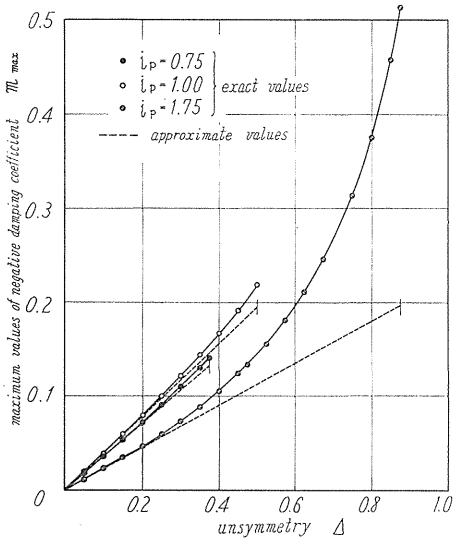

FIG. 6.7. $m_{\max} - \Delta$ diagram ($\delta = 1.060$, $\gamma^2 = 0.731$)

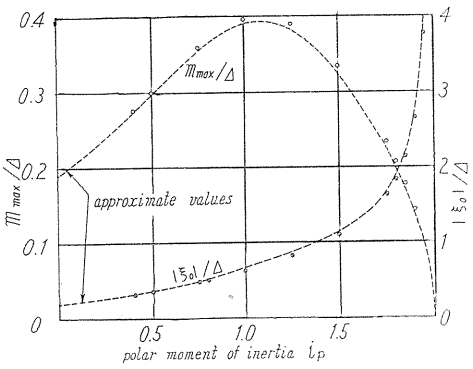

FIG. 6.8. Effects of polar moment of inertia i_p on $m_{\max}$ and $2|\xi_0|$ ($\delta = 1.060$, $\gamma^2 = 0.731$)

The unstable regions and $m_{\max}$ approximately given in Eq. (6.15) and Eq. (6.14) are shown by dotted lines in Figs. 6.4, 6.5, and 6.7 respectively. Approximate values of $|\xi_0|/\Delta$ and $m_{\max}/\Delta$ are plotted against the polar moment of inertia i_p by dotted lines in Fig. 6.8. Exact values for $\Delta = 0.2$ through Eqs. (6.1) and (6.9) are additionally shown by marks ○ and ⦸ which almost agree with the approximate values. Furthermore, Fig. 6.8 shows that the width of the unstable region increases with i_p, while $m_{\max}/\Delta$ is largest at $i_p \fallingdotseq 1.08$ and decreases to zero as i_p tends to its maximum value 2. Consequently, even though the wide unstable region appears when i_p is large, it can be made to disappear easily by little damping because of the small m.

When there is damping, the boundary of unstable region near ω_d is obtained numerically by letting Hurwitz's determinant H_7 of Eq. (3.8) equal to zero[33]. When both damping coefficients c_1 and c_2 are equal to 0.1, the boundary is shown in Fig. 6.4 and there is no unstable region for $\Delta < 0.176$.

6.6. Experimental results

Experimental apparatus is shown in Fig. 6.9. The vertical shaft S of dia., $d = 11.55\phi$, length, $l = 401.9$ mm is supported at its upper end by two self-aligning double-row ball bearings B with 10ϕ bore placed at a distance $l_0 = 36.00$ mm as shown in Fig. 6.9. At the point M, the unsymmetrical rotor R is mounted. By exchanging two attached weights r of the rotor, we can vary the value of asym-

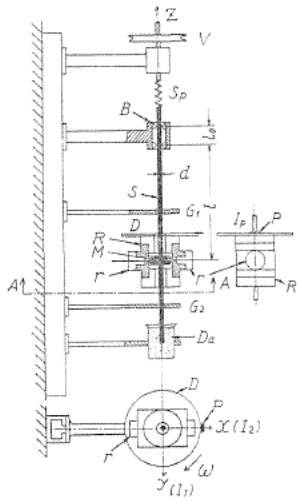

FIG. 6.9. Experimental apparatus

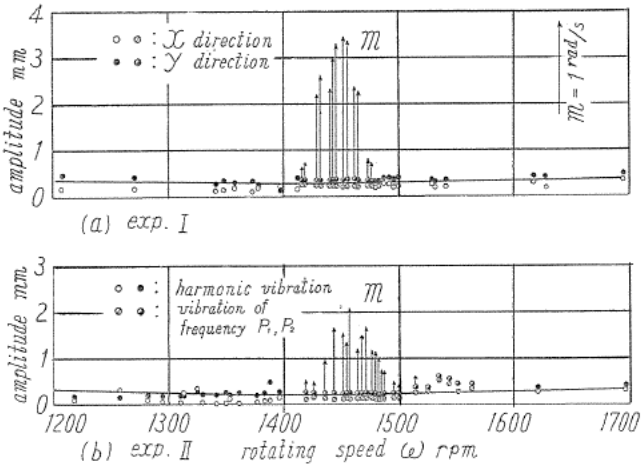

FIG. 6.10. Response curves and negative damping coefficient (experiment I, II)

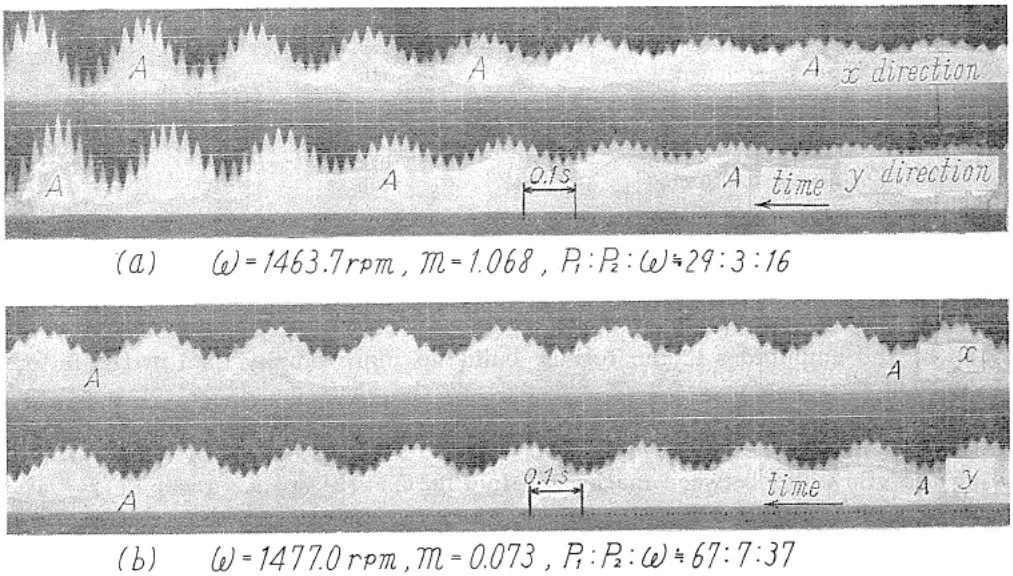

FIG. 6.11. Vibratory waves (experiment I)

metry Δ. When disk D, with a dia. of 280ϕ and a thikness of 3 mm, is put on the rotor, motions at the edge of the disk are recorded optically in both x- and y-directions. By this method the whirl of the rotor can be measured. Guard rings G_1, G_2 are arranged to check the increase of shaft deflection. Using various kinds of oil in vessel D_a in which the lower end of the shaft is merged various damping coefficients are obtained.

Dimensions of our experimental apparatus are as follows:

$$\left.\begin{aligned} &I_p = 0.4300 \text{ kg cm } s^2,\ I_1 = 0.5090 \text{ kg cm } s^3,\ I_2 = 0.3816 \text{ kg cm } s^2,\\ &W = 11.637 \text{ kg},\ \alpha = 3.120\times 10 \text{ kg/cm},\ \gamma = -6.450\times 10^2 \text{ kg/rad},\\ &\delta = 1.777\times 10^4 \text{ kg cm/rad},\ \sqrt{\alpha g/W} = 489.5 \text{ rpm},\ \sqrt{Ig/W} = 6.124 \text{ cm},\end{aligned}\right\} \quad (6.16)$$

$$i_p = 0.9659,\ \Delta = 0.1431,\ \delta = 15.191,\ \gamma^2 = 11.400. \quad (6.17)$$

Unstable vibrations appearing near $\omega_d \fallingdotseq 1450$ rpm are shown in Fig. 6.10. Steady harmonic oscillations in x- and y-directions (cf. Fig. 6.9) are represented by marks ○ and ● respectively. Unstable vibrations steadily growing up in their amplitude are shown by arrows, the length of which is proportional to the magnitude of negative damping m given by vibratory waves as shown in Fig. 6.11. Results of experiment I without damping action by oil in vessel D_a in Fig. 6.9 are given in Fig. 6.10 (a) where the unstable region appears between 1416 and 1480 rpm. Values m in Fig. 6.10 (a) is larger than those in Fig. 6.10 (b) where the results of experiment II with damping by spindle oil in vessel D_a are represented. The unstable vibrations do not occur in experiment IV where oil with high viscosity is used. To estimate damping actions[33] in experiments I, II and IV logarithmic decrements δ_0 in free vibrations of frequencies p_{10}, $\overline{p}_{10}$, p_{20} and $\overline{p}_{30}$, when $\omega = 0$, are experimentally measured and shown in Table 6.1.

TABLE 6.1. Logarithmic Decrement δ_0

Experiment	I	II	IV
$p_{10} = 1727$ cpm	0.0091	0.070	0.31
$\overline{p}_{10} = 1990$ cpm	0.0087	0.077	0.37
$p_{20} = 238.5$ cpm	0.047	0.065	0.35
$\overline{p}_{30} = 243.0$ cpm	0.026	0.073	0.33

Two examples of vibratory waves of unstable vibrations obtained in experiment I are given in Fig. 6.11 where vertical white lines represent rotating marks furnished by P. Negative damping m in Fig. 6.11 (a) is larger than that in Fig. 6.11 (b) and amplitudes in the former build up more rapidly than in the latter. In one interval of marks AA in Fig. 6.11 (a) the shaft makes 16 rotations and vibrations of frequency P_1 oscillates 29 times while the slower vibration of P_2 vibrates 3 times. Therfore we have: $\omega : P_1 : P_2 \fallingdotseq 16 : 29 : 3$ and $P_1 + P_2 = 2\omega$. Observing the vibrations between marks AA in Fig. 6.11 (b) we have: $\omega : P_1 : P_2 \fallingdotseq 37 : 67 : 7$ and also $P_1 + P_2 = 2\omega$.

Negative damping m obtained by experiments I and II are shown by marks ○ and ●, respectively, in Fig. 6.12. In experiment I, $\omega_d = 3.1549$ (1544 rpm) and $|\xi_0|/\Delta = 0.3295$, $m_{\max}/\Delta = 0.2193$ in accordance with Eqs. (6.8), (6.14), and (6.15). The actual range of the unstable region furnished by experiment I comes slightly lower than that induced by the foregoing values calculated under the assumption of the massless shaft. Shifting the relation between m and ω calculated by Eq. (6.4) to the lower speed side by 97 rpm and representing this by dotted lines in Fig. 6.12, we find that it agrees with the experimental results given by marks ○, as shown in Fig. 6.12.

Frequencies P_1 and P_2 of unstable vibrations in experiments I and II are shown in Fig. 6.13.

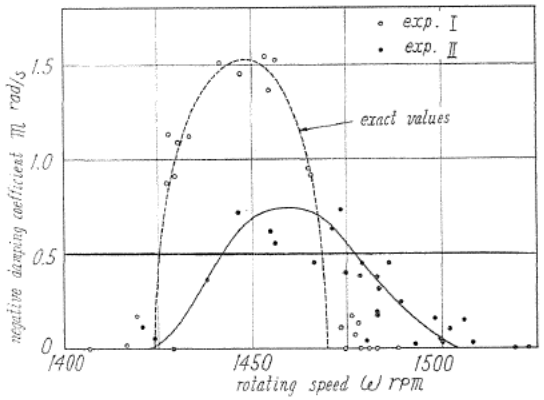

FIG. 6.12. Negative damping coefficient m

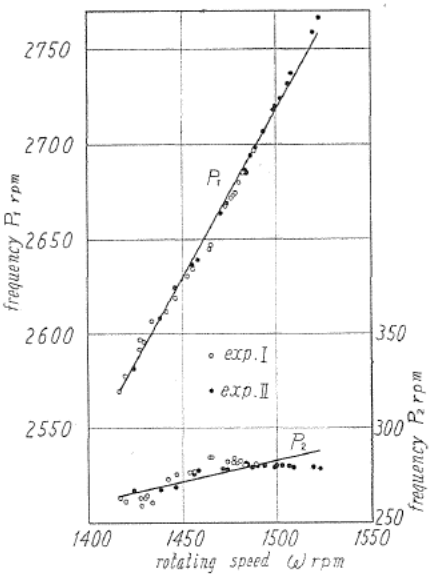

FIG. 6.13. Freqnencies P_1, P_2 of unstable vibrations

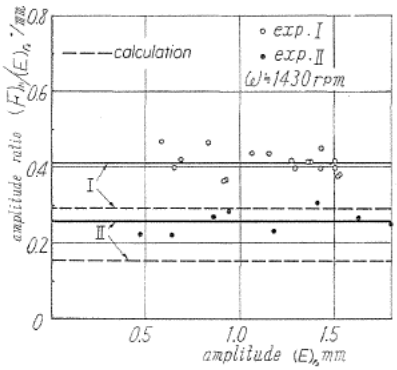

$\leftarrow (E)_{p_2}$ = deflection amplitude of vibration with frequency P_2

$(F)_{p_1}$ = inclination amplitude of vibration with frequency P_1

FIG. 6.14. Amplitude ratio of unstable vibrations

The amplitude ratio $F:E$ between two unstable vibrations of frequencies P_1 and P_2 furnished by experiment I and II is shown by marks ○ and ●, respectively, in Fig. 6.14. The ratio is almost constant during vibrations growing up steadily in their amplitudes, and the ratio of experiment I is larger than that of experiment II. The calculated ratios[33] are added in Fig. 6.14 by broken lines.

6.7. Conclusions

(1) In the vibratory shaft system mounted by an unsymmetrical rotor, one unstable region always appears about ω_d where the relation $p_i=\overline{p}_j=2\omega-p_j$ $(i\neq j)$ holds between the roots of the equation $f\overline{f}=0$.

(2) The rotating speed ω_d always locates between the major critical speeds ω_{c1} and ω_{c2}.

(3) In the unstable region two unstable vibrations with frequencies P_1 and P_2 grow up steadily, and the sum of these P_1+P_2 is equal to 2ω.

(4) The width of the unstable region increases with the asymmetry Δ of the rotor. As the value of the polar moment of inertia i_p increases, the rotating speeds of the unstable region become higher and its range grows wider. For rather large i_p the unstable region shifts to the lower speed side as Δ increases. The unstable region always lies between the rotating speeds ω_f and ω_g where the relations $p_1=2\omega$ and $p_1=2\omega-1$ hold, respectively.

(5) Negative damping m is common to two unstable vibrations of frequencies P_1 and P_2. Near the center of the unstable region m takes its maximum value m_{max}. Values of m and m_{max} increase with the asymmetry Δ, and are largest for a certain intermadiate value of i_p and decrease to zero as i_p tends to its maximum value 2.

(6) The amplitude ratio of two unstable vibrations is held almost constant during the vibrations.

(7) When damping force exists, the unstable region appears only for Δ larger than a certain value. Damping action makes the negative damping m small. Large damping removes the unstable region.

Chapter 7. Effects of a Distributed Mass of Shaft, and of Non-linear Characteristics of Shaft Stiffness on Unstable Vibrations[32]

7.1. Introduction

When a rather long shaft $l \fallingdotseq 100$ cm is used in experiments, another peculiar unstable vibration appears near the rotating speed ω_s higher than major critical speed ω_c as shown in Figs. 7.3 and 7.8. At first we thought that a different flexibility of bearing pedestals in x-, y-directions (treated in Chapter 5) results in new zones of instability near the rotating speeds $\omega=1.730$ (2056 rpm) in Figs. 7.3, 7.4 and $\omega=1.971$ (1677 rpm) in Fig. 7.11 where the relation $p_2=-\overline{p}_1$, *i.e.*, $p_1-p_2=2\omega$ is satisfied, respectively.

Next we changed the flexibility of the lower bearing pedestal A by using the following three pedestals:

Pedestal No. 1 made of cast iron (nearly rigid, $k_{yA}=1.05\times10^4$ kg/cm)

Pedestal No. 2 made of steel (somewhat flexible, $k_{yA}=1.43\times10^3$ kg/cm)

Pedestal No. 3 made of steel (flexible, $k_{yA}=2.65\times10^2$ kg/cm)

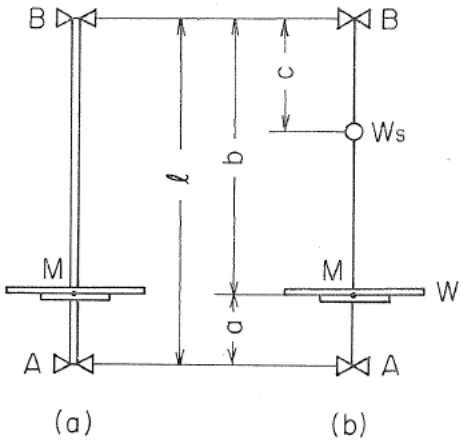

FIG. 7.1. Schematic diagram of shaft system when a mass of shaft is considered

In the experiments using the bearing pedestals No. 1, 2, and 3, the width and location of unstable region, natural frequency P_2 of unstable vibration, and negative damping coefficient m are little affected by changing the flexibility in y-direction. Moreover the shaft itself vibrates violently at the rotating speed $\omega=2.65\sim2.70$ (3150~3200 rpm), and is nearly impossible to pass through the speed, while the rotor seems to be almost at standstill. When a shaft with length $b=83.40$ cm, diameter $d=1.199$ cm is supported freely to incline at one end B and assumed to be fixed at the other end M in Fig. 7.1, natural frequency of first mode of vibration is found to be $p_s=2.73$ (3249 cpm). This fact indicates that the foregoing shaft vibration is the major critical speed of shaft itself and a distributed mass of shaft must be sometimes counted in, though fully neglected through Chapter 1~6.

7.2. Equations of motion and frequency equation

Though a shaft MB with length b in Fig. 7.1 (a) has infinite number of natural frequency, only the fundamental (first) mode of vibration is considered here. The first natural frequency of MB with an equally distributed shaft weight wb is given:

$$p_s^2 = (15.42)^2 EI_z g/(wb^4), \tag{7.1}$$

where the shaft end B is simply supported, and the other end M is assumed to be fixed to the ground.

Let us try to define an equivalent system of six degrees of freedom with a concentrated weight W_s locating on the shaft as shown in Fig. 7.1 (b). If an equivalent shaft weight W_s is located on the shaft at a distance c from shaft end B, a lateral deflection r of shaft MB at a distance z from B due to the centrifugal force $W_s r_s \omega^2/g$ is given:

$$r = \frac{W_s r_s \omega^2 (b-c)^2 \{3b^2 cz - (2b+c)z^3\}}{12 EI_z g b^3}. \tag{7.2}$$

Because an inclination angle of the shaft $\theta = dr/dz$ at the position $z=c$ may be assumed zero, distance c is determined from Eq. (7.2),

$$c = (\sqrt{2} - 1)b. \tag{7.3}$$

Natural frequency p_s of shaft MB in Fig. 7.1 (b) is given:

$$p_s^2 = \frac{12 EI_z g b^3}{W_s c^2 (b-c)^3 (3b+c)}. \tag{7.4}$$

Putting p_s of Eq. (7.1) equal to p_s of Eq. (7.4) and using Eq. (7.3), we can determine W_s according to the following equation,

$$W_s = 0.4286\, wb. \tag{7.5}$$

Let us define the following quantities:

x_s, y_s = lateral displacements of the shaft at $z=c$ in x-, y-directions respectively,

P_x, P_y = forces acting on the center M of rotor in x-, y-directions,

M_{tx}, M_{ty} = moments acting around the MX-, MY-axes,

P_{sx}, P_{sy} = forces acting on the equivalent weight W_s in x-, y-directions.

Influence number a_{ij} and spring constant α_{ij} are defined as follows:

$$\begin{pmatrix} x, & y \\ \theta_x, & \theta_y \\ x_s, & y_s \end{pmatrix} = \begin{pmatrix} a_{11} & a_{12} & a_{13} \\ a_{21} & a_{22} & a_{23} \\ a_{31} & a_{32} & a_{33} \end{pmatrix} \begin{pmatrix} P_x, & P_y \\ M_{ty}, & -M_{tx} \\ P_{sx}, & P_{sy} \end{pmatrix}, \tag{7.6}$$

$$\alpha_{ij} = A_{ij}/\det(a_{ij}), \tag{7.8}$$

where A_{ij} is the cofactor of element a_{ij}, $\det(a_{ij})$ is the determinant consisting of a_{ij}, and the reciprocal relations $a_{ij}=a_{ji}$, $\alpha_{ij}=\alpha_{ji}$ always hold.

Inertia forces P_x, P_y, P_{sx}, P_{sy} and inertia moments M_{tx}, M_{ty} are given by Newton's second law and Euler's equation of motion:

$$\left.\begin{aligned} &\begin{matrix} P_x \\ P_y \end{matrix} = -\left(\frac{W}{g}\right)\begin{matrix} \ddot{x} \\ \ddot{y}, \end{matrix} \quad \begin{matrix} P_{sx} \\ P_{sy} \end{matrix} = -\left(\frac{W_s}{g}\right)\begin{matrix} \ddot{x}_s \\ \ddot{y}_s, \end{matrix} \\ &\begin{matrix} M_{ty} \\ -M_{tx} \end{matrix} = -I\begin{matrix} \ddot{\theta}_x \\ \ddot{\theta}_y \end{matrix} \mp I_p\omega\begin{matrix} \dot{\theta}_y \\ \dot{\theta}_x \end{matrix} + \Delta I\cdot\frac{d}{dt}\left(\dot{\theta}_x\begin{matrix}\cos\\ \sin\end{matrix}2\omega t \pm \dot{\theta}_y\begin{matrix}\sin\\ \cos\end{matrix}2\omega t\right). \end{aligned}\right\} \tag{7.8}$$

Now we introduce the dimensionless quantities,

$$\left.\begin{aligned} &x_s\sqrt{W/(Ig)} = x_s', \quad y_s\sqrt{W/(Ig)} = y_s', \quad t\sqrt{\alpha_{11}g/W} = t', \quad \omega\sqrt{W/(\alpha_{11}g)} = \omega', \\ &p\sqrt{W/(\alpha_{11}g)} = p', \quad W_s/W = m_s, \quad \alpha_{12}\sqrt{W/(Ig)}/\alpha_{11} = \alpha_{12}', \quad \alpha_{13}/\alpha_{11} = \alpha_{13}', \\ &\alpha_{22}W/(\alpha_{11}Ig) = \alpha_{22}', \quad \alpha_{23}\sqrt{W/(Ig)}/\alpha_{11} = \alpha_{23}', \quad \alpha_{33}/\alpha_{11} = \alpha_{33}'. \end{aligned}\right\} \tag{7.9}$$

Using Eq. (7.9) and i_p, Δ, x', y' in Eq. (2.11), and omitting primes on them for convenience, we get the dimensionless equations of motion through Eqs. (7.6), (7.7), and (7.8),

$$\left.\begin{aligned} &\ddot{x} + x + \alpha_{12}\theta_x + \alpha_{13}x_s = 0, \\ &\ddot{y} + y + \alpha_{12}\theta_y + \alpha_{13}y_s = 0, \\ &\ddot{\theta}_x + i_p\omega\dot{\theta}_y + \alpha_{12}x + \alpha_{22}\theta_x + \alpha_{23}x_s - \Delta\cdot\frac{d}{dt}(\dot{\theta}_x\cos 2\omega t + \dot{\theta}_y\sin 2\omega t) = 0, \\ &\ddot{\theta}_y - i_p\omega\dot{\theta}_x + \alpha_{12}y + \alpha_{22}\theta_y + \alpha_{23}y_s - \Delta\cdot\frac{d}{dt}(\dot{\theta}_x\sin 2\omega t - \dot{\theta}_y\cos 2\omega t) = 0, \\ &m_s\ddot{x}_s + \alpha_{13}x + \alpha_{23}\theta_x + \alpha_{33}x_s = 0, \\ &m_s\ddot{y}_s + \alpha_{13}y + \alpha_{23}\theta_y + \alpha_{33}y_s = 0. \end{aligned}\right\} \tag{7.10}$$

Free vibrations of x_s, y_s are represented by

$$\begin{matrix} x_s \\ y_s \end{matrix} = E_s\begin{matrix}\cos\\ \sin\end{matrix}pt + \overline{E}_s\begin{matrix}\cos\\ \sin\end{matrix}\bar{p}t. \tag{7.11}$$

Inserting Eqs. (2.13) and (7.11) into Eq. (7.10) we get the frequency equation:

$$\Phi(\omega, p) = \begin{vmatrix} H & 0 & \alpha_{12} & 0 & \alpha_{13} & 0 \\ 0 & \overline{H} & 0 & \alpha_{12} & 0 & \alpha_{13} \\ \alpha_{12} & 0 & G & -\Delta p\bar{p} & \alpha_{23} & 0 \\ 0 & \alpha_{12} & -\Delta p\bar{p} & \overline{G} & 0 & \alpha_{23} \\ \alpha_{13} & 0 & \alpha_{23} & 0 & H_s & 0 \\ 0 & \alpha_{13} & 0 & \alpha_{23} & 0 & \overline{H}_s \end{vmatrix} = 0, \tag{7.12}$$

where $H=1-p^2$, $\overline{H}=1-\bar{p}^2$, $G=\alpha_{22}+i_p\omega p-p^2$, $\overline{G}=\alpha_{22}+i_p\omega\bar{p}-\bar{p}^2$, $H_s=\alpha_{33}-m_sp^2$, $\overline{H}_s=\alpha_{33}-m_s\bar{p}^2$.

Expansion of Eq. (7.12) gives the same form of frequency equation as Eq. (6.1). In this equation,

$$f = \begin{vmatrix} H & \alpha_{12} & \alpha_{13} \\ \alpha_{12} & G & \alpha_{23} \\ \alpha_{13} & \alpha_{23} & H_s \end{vmatrix}, \quad \bar{f} = \begin{vmatrix} \overline{H} & \alpha_{12} & \alpha_{13} \\ \alpha_{12} & \overline{G} & \alpha_{23} \\ \alpha_{13} & \alpha_{23} & \overline{H}_s \end{vmatrix}, \quad \varphi = -p^2\bar{p}^2\begin{vmatrix} H & \alpha_{13} \\ \alpha_{13} & H_s \end{vmatrix}\cdot\begin{vmatrix} \overline{H} & \alpha_{13} \\ \alpha_{13} & \overline{H}_s \end{vmatrix}. \tag{7.13}$$

If we put $m_s=0$, Eq. (7.12) reduces to Eq. (6.1) of four degrees of freedom system where a distributed mass of shaft is neglected.

To each solution of Eq. (7.12) belongs a set of values E, $\overline{E}$, F, $\overline{F}$, E_s, and $\overline{E}_s$. The ratio of the amplitudes is equal to the ratio of the cofactor A_{ij} of Eq. (7.12) ($j=1, 2, \ldots, 6$), *i.e.*, $E:\overline{E}:F:\overline{F}:E_s:\overline{E}_s=A_{11}:A_{12}:A_{13}:A_{14}:A_{15}:A_{16}$, and

$$\left.\begin{aligned}
A_{11} &= (GH_s-\alpha_{23}^2)\bar{f}-\Delta^2\bar{p}^2\bar{\bar{p}}^2(\bar{H}\bar{\bar{H}}_s-\alpha_{13}^2)H_s,\\
A_{12} &= \Delta\bar{p}\bar{\bar{p}}(\alpha_{12}H_s-\alpha_{13}\alpha_{23})(\alpha_{12}\bar{\bar{H}}_s-\alpha_{13}\alpha_{23}),\\
A_{13} &= -(\alpha_{12}H_s-\alpha_{13}\alpha_{23})\bar{f},\\
A_{14} &= -\Delta\bar{p}\bar{\bar{p}}(\bar{H}\bar{\bar{H}}_s-\alpha_{13}^2)(\alpha_{12}H_s-\alpha_{13}\alpha_{23}),\\
A_{15} &= -(\alpha_{13}G-\alpha_{12}\alpha_{23})\bar{f}+\alpha_{13}\Delta^2\bar{p}^2\bar{\bar{p}}^2(\bar{H}\bar{\bar{H}}_s-\alpha_{13}^2),\\
A_{16} &= \Delta\bar{p}\bar{\bar{p}}(\alpha_{23}\bar{\bar{H}}-\alpha_{12}\alpha_{13})(\alpha_{12}H_s-\alpha_{13}\alpha_{23}).
\end{aligned}\right\} \tag{7.14}$$

Between roots p_i ($i=1\sim6$) derived from $f=0$ of symmetrical rotor, the following relation is held provided $\alpha_{12}\neq0$:

$$p_1>p_{g1}>p_2>p_{g2}>p_3>0>p_4>-p_{g2}>p_5>-p_{g1}>p_6, \tag{7.15}$$

where p_{g1}, p_{g2} are roots of $HH_s-\alpha_{13}^2=0$, *i.e.*,

$$\left.\begin{matrix}p_{g1}^2\\ p_{g2}^2\end{matrix}\right\}=\frac{\alpha_{33}+m_s\pm\sqrt{(\alpha_{33}-m_s)^2+4m_s\alpha_{13}^2}}{2m_s}. \tag{7.16}$$

7.3. Unstable vibrations (experiment I)

7.3.1. Linear vibratory system (when self-aligning double-row ball bearings #1200 are used)

Dimensions of the experimental apparatus used in experiment I are as follows:

$$\left.\begin{aligned}
&I_p=2.179\ \text{kg cm s}^2,\ I_1=1.426\ \text{kg cm s}^2,\ I_2=0.761\ \text{kg cm s}^2,\\
&W=10.433\ \text{kg},\ W_s=0.317\ \text{kg},\ l=99.90\ \text{cm},\ a:b=1:5,\ a=16.50\ \text{cm},\\
&b=83.40\ \text{cm},\ c=34.54\ \text{cm},\ d=1.199\ \text{cm},\\
&\alpha_{11}=1.577\times10^2\ \text{kg/cm},\ \alpha_{12}=-1.960\times10^3\ \text{kg/rad},\ \alpha_{13}=-2.213\times10\ \text{kg/cm},\\
&\alpha_{22}=5.456\times10^4\ \text{kg cm/rad},\ \alpha_{23}=-5.405\times10^2\ \text{kg/rad},\ \alpha_{33}=3.778\times10\ \text{kg/cm},\\
&\sqrt{\alpha_{11}g/W}=1189\ \text{rpm},\ \sqrt{Ig/W}=10.37\ \text{cm};\\
&\alpha=1.434\times10^2\ \text{kg/cm},\ \gamma=-2.257\times10^3\ \text{kg/rad},\ \delta=4.640\times10^4\ \text{kg cm/rad},\\
&\sqrt{\alpha g/W}=1134\ \text{rpm}.
\end{aligned}\right\} \tag{7.17}$$

Dimensionless quantities are obtained by Eq. (7.9):

$$\left.\begin{aligned}
i_p&=1.993,\ \Delta=0.304,\ m_s=0.0319,\ \alpha_{12}=-1.1989,\ \alpha_{13}=-0.1403,\\
\alpha_{22}&=3.2185,\ \alpha_{23}=-0.3306,\ \alpha_{33}=0.2396.
\end{aligned}\right\} \tag{7.18}$$

Another dimensionless quantities used in Chapter 2~6 are got from Eq. (2.11),

$$i_p = 1.993,\ \Delta = 0.304,\ \gamma = -1.517,\ \delta = 3.010. \tag{7.19}$$

Natural frequencies p_i and $\bar{p}_i$ $(i=1\sim6)$ derived from $f=0$ and $\bar{f}=0$ of Eq. (7.13) are shown by full and broken line curves respectively in Fig. 7.2 (a). Since $f\bar{f}\varphi$ is positive in the shaded regions and negative in the unshaded regions, all real $p-\omega$ curves lie only in unshaded regions because real roots p_i make $f\bar{f}\varphi \leqq 0$. In Fig. 7.2 (b) roots p_i and $\bar{p}_i$ of Eq. (7.12) when $m_s=0.0319$ are shown by full line curves. Figs. 7.2 show two unstable regions near major critical speeds C_3 $(p_3=\bar{p}_3=\omega_{c3})$ and C_2 $(p_2=\bar{p}_2=\omega_{c2})$, and one new unstable region near S_2 $(p_2=\bar{p}_3=2\omega-p_3)$, S_3 $(p_3=\bar{p}_2=2\omega-p_2)$ to occur in this shaft system. Width of unstable region $2|\xi_0|$, maximum value of negative damping coefficient $m_{\max}$, and natural frequency P_2, P_3 of unstable vibrations are approximately derived through Eqs. (6.15), (6.14), and (6.12 a, b). In Fig. 7.2 (b) chain line curves are roots of Eq. (7.12) when m_s is put zero, and they show that there exists only one unstable region near $C_3(\omega_{c3})$ if a distributed mass of shaft is ignored.

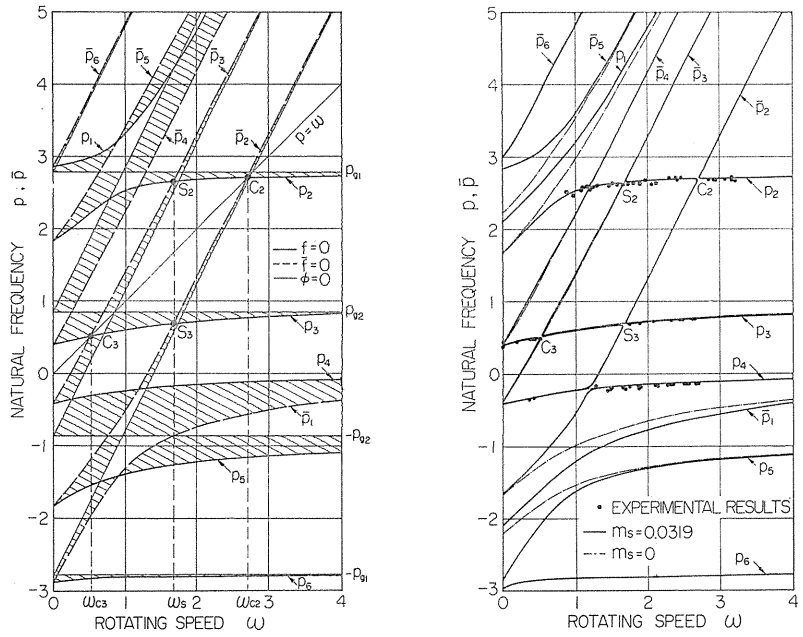

(a) $\Delta=0$, $m_s=0.0319$ (b) $\Delta=0.304$

FIG. 7.2. Natural frequency p, $\bar{p}$ (Experiment I)

By some calculation using Eq. (7.17), (7.18), we can have the abscissa and the ordinates of the cross points S_2, S_3, *i.e.*, $\omega_s=1.670$ (1986 rpm), $p_{2s}=2.655$ (3156 rpm), $p_{3s}=0.685$ (815 rpm), and approximate solutions $2|\xi_0|=64$ rpm, $m_{\max}=2.44$ rad/s. The $m-\omega$ curve and P_2, $P_3-\omega$ curves are respectively shown in Fig. 7.3 where calculated values are shifted by 45 rpm to the lower speed side and experimental results are given by marks ● and ○. Amplitude ratios $|\bar{E}/E|$, $|\bar{F}/F|$, and $|\bar{E}_s/E_s|-\omega$ curves are calculated through Eq. (7.14), and given in Fig. 7.4. Experimental results of $|\bar{E}_s/E_s|$ for p_3 got from shaft vibrations x_s, y_s are given

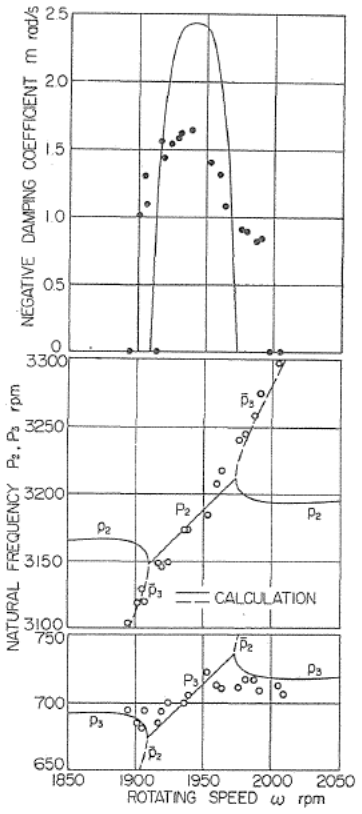

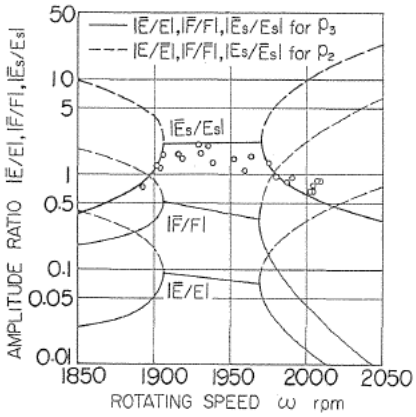

FIG. 7.4. Amplitude ratio of free vibrations near ω_s (I—#1200)

← FIG. 7.3. m, P_2, P_3—ω diagram near ω_s (I—#1200)

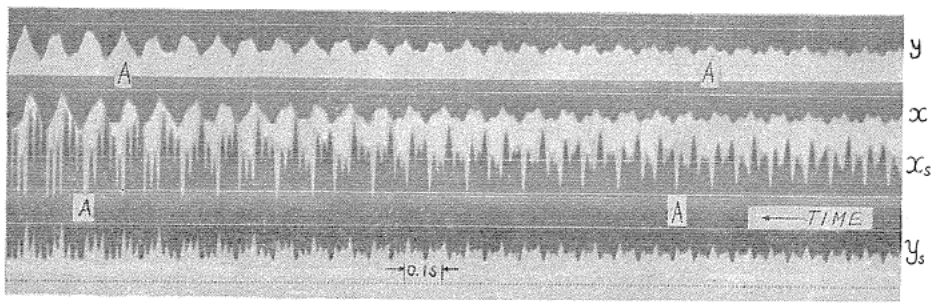

FIG. 7.5. Vibratory waves (Ball bearing #1200 used, ω=1925 rpm, $\omega : P_2 : P_3 \fallingdotseq 50 : 81 : 19$)

by marks ○. One example of vibratory waves is shown in Fig. 7.5 in which amplitudes of vibrations x, y, x_s, and y_s are seen to build up exponentially.

7.3.2. *Non-linear vibratory system (when single-row radial ball bearings are used)*

When both ends of the shaft used in experiment I are supported by single-row radial ball bearings (#6200 with 10ϕ bore) which usually have small "angular clearances" of 0.3°~0.6°, the stiffness of the shaft has non-symmetrical and non-

linear spring characteristics[6]. In experiments using such a shaft system, there exist several critical speeds (i), (ii), (iii), (iv) of rather large amplitudes, all response curves of which are seen of hard spring type.

(i) major critical speed [ω] where two curves $p=\omega$ and $p=p_3$ cross each other in Fig. 7.2 (b).

(ii) sub-harmonic oscillation of order 1/2 [$1/2\cdot\omega$] where two curves $p=\omega/2$ and $p=p_3$ meet.

(iii) "summed and differential harmonic oscillation" [p_3-p_4] where the relation $p_3-p_4=\omega$ holds.

(iv) unstable vibrations near ω_s where the relation $p_2+p_3=2\omega$ is satisfied.

Let us show here some experimental results of (iv). As the rotating speed of shaft ω increases in Fig. 7.6, amplitude of harmonic oscillation moves along AB and reach B (1976 rpm) where steady beats of two vibrations with frequencies P_2, P_3 take place. Amplitude of steady beats gradually enlarges along BC when ω successively increases. When ω is retarded, amplitude of harmonic oscillation moves along FE and jumping phenomenon takes place at E (2064 rpm).

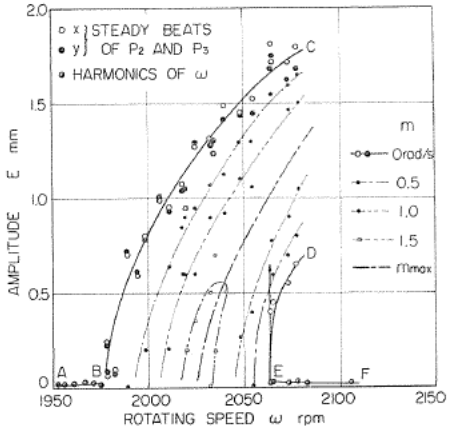

FIG. 7.6. E, $m-\omega$ diagram (I-#6200) [Angular clearances of ball bearings: 0.4° (upper), 0.3° (lower)]

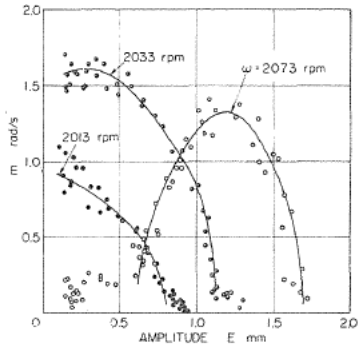

FIG. 7.7. $m-E$ diagram (I-#6200)

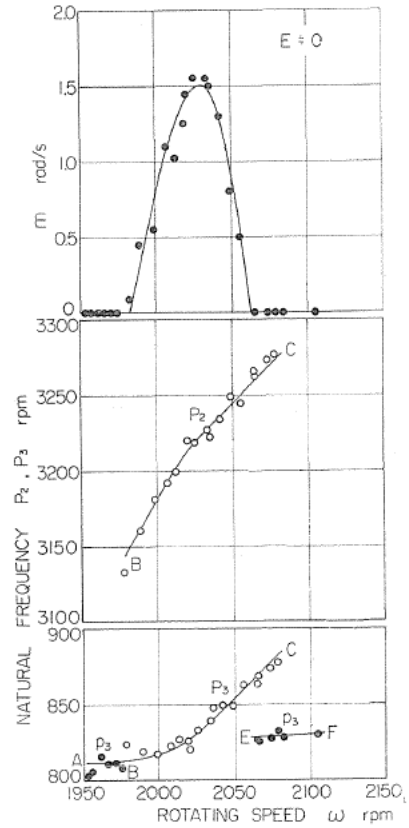

FIG. 7.8. m, P_2 P_3, $-\omega$ diagram (I-#6200)

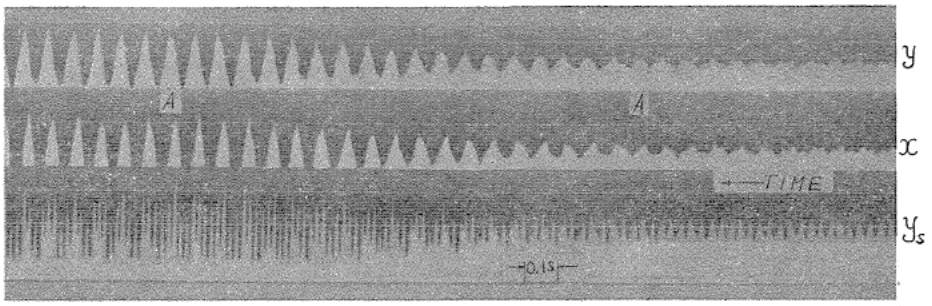

FIG. 7.9. Vibratory waves (Ball bearing #6200 used, $\omega=2033$ rpm, $\omega : P_2 : P_3 \fallingdotseq 47 : 75 : 19$)

When ω is kept constant, negative damping coefficient m varies according to the amplitude of beats as shown in Fig. 7.7. Because it is impossible for both bearing pedestals to be in exact alignment and a small misalignment increases the shaft stiffness, unstable region BE occurs at the higher speed side by 75 rpm than the linear vibratory system shown in Fig. 7.3. When amplitude of beats is nearly zero, estimated negative damping coefficient m is given in Fig. 7.8. The maximum value $m_{\max}$ of Fig. 7.8 is seen to coincide with $m_{\max}$ of Fig. 7.3. Frequencies P_2, P_3 of stable beats along BC are also given by marks ○ in Fig. 7.8. Marks ● indicate frequency p_3 of a small free vibration in the stable region AB and EF. Fig. 7.9 is an example of vibratory waves in which small amplitudes of x, y, y_s are seen to build up rapidly, and then finally attain to certain amplitudes of stable beats BC shown in Fig. 7.6.

7.4. Unstable vibrations (experiment II)

Dimensions of the experiment II are as follows:

$$\left.\begin{aligned}
&I_p = 0.4300 \text{ kg cm } s^2,\ I_1 = 0.5090 \text{ kg cm } s^2,\ I_2 = 0.3816 \text{ kg cm } s^2,\\
&W = 11.637 \text{ kg},\ W_s = 0.304 \text{ kg},\ l = 100.21 \text{ cm},\ a : b = 1 : 4,\\
&a = 20.04 \text{ cm},\ b = 80.17 \text{ cm},\ c = 33.21 \text{ cm},\ d = 1.196 \text{ cm},\\
&\alpha_{11} = 9.420\times 10 \text{ kg/cm},\ \alpha_{12} = -1.142\times 10^3 \text{ kg/rad},\ \alpha_{13} = -2.444\times 10 \text{ kg/cm},\\
&\alpha_{22} = 4.738\times 10^4 \text{ kg cm/rad},\ \alpha_{23} = -5.741\times 10^2 \text{ kg/rad},\ \alpha_{33} = 4.174\times 10 \text{ kg/cm},\\
&\sqrt{\alpha_{11} g/W} = 850.7 \text{ rpm},\ \sqrt{Ig/W} = 6.124 \text{ cm};\\
&\alpha = 7.989\times 10 \text{ kg/cm},\ \gamma = -1.478\times 10^3 \text{ kg/rad},\ \delta = 3.949\times 10^1 \text{ kg cm/rad},\\
&\sqrt{\alpha g/W} = 783.4 \text{ rpm},
\end{aligned}\right\} \tag{7.20}$$

in which both ends of a shaft are assumed to be simply supported, but single-row radial ball bearings are actually used in experiment II. Dimensionless quantities derived from Eqs. (2.11) and (7.9) are as follows:

$$\left.\begin{aligned}
&i_p = 0.9659,\ \Delta = 0.1431,\ m_s = 0.0261,\ \alpha_{12} = -1.9790,\ \alpha_{13} = -0.2595,\\
&\alpha_{22} = 13.412,\ \alpha_{23} = -0.9951,\ \alpha_{33} = 0.4431;\ \gamma = -3.021,\ \delta = 13.180.
\end{aligned}\right\} \tag{7.21}$$

Natural frequencies p_i and $\bar{p}_i$ $(i=1\sim 6)$ derived from $f=0$, $\bar{f}=0$ with use of

the values of Eq. (7.21) are shown by full and broken lines severally in Fig. 7.10. $\varphi=0$ is also shown by straight fine lines. The sign of $f\bar{f}\varphi$ is positive in the shaded region. In the neighborhood of the cross points C_3 (ω_{c3}), C_2 (ω_{c2}), S_2, S_3 (ω_s), D_1, D_3 (ω_d) shown by marks ● where two curves $f=0$ and $\bar{f}=0$ cross each other, unstable regions are likely to occur when $m_s \neq 0$.

When a distributed mass of shaft is neglected, *i.e.*, $m_s=0$, $f=0$, $\bar{f}=0$ curves are shown by chain lines in Fig. 7.10 (cf. Figs. 6.1 and 6.2), and unstable regions are seen to occur only near the cross points C_3, D_{10}, D_{30} (ω_{d0}). Near the rotating speed $\omega_s=2.06$ (1752 rpm) where the relationship $p_2+p_3=2\omega$ is held, two unstable vibrations with frequencies P_2, P_3 are seen to build up as shown in Fig. 7.11.

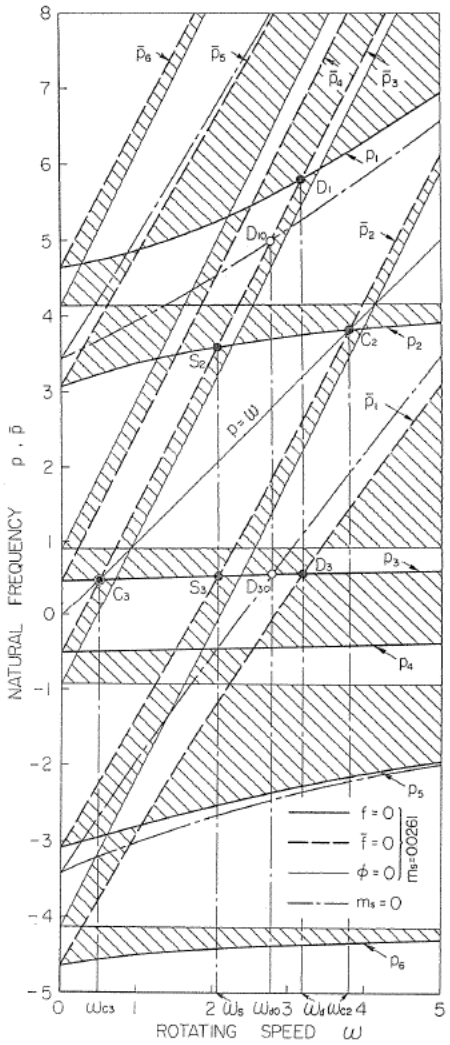

FIG. 7.10. Natural frequency p, $\bar{p}$ (experiment II, $\Delta=0$, $m_s=0.0261$)

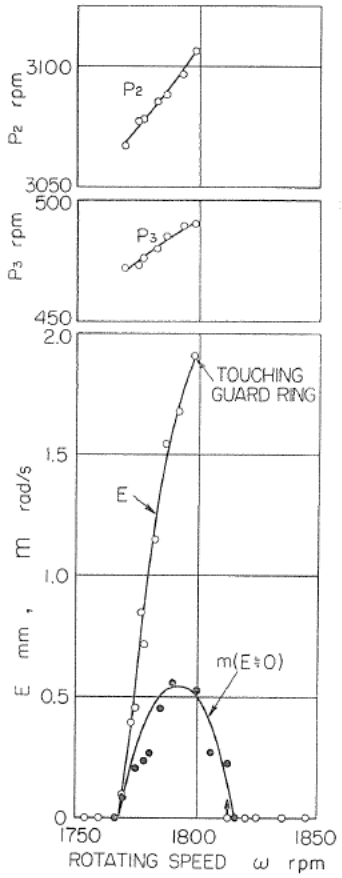

FIG. 7.11. P_2, P_3, m, $E-\omega$ diagram near ω_s (II−#6200) [Angular clearances of ball bearings: 0.5° (upper), 0.4° (lower)]

The response curve of steady beats of two vibrations with frequencies P_2, P_3 can be obtained because of non-linearity in shaft stiffness.

No matter whether m_s is assumed to be zero or not, another unstable region still remains[30]. When a concentrated mass $m_s=0.0261$ is counted in, there exists the unstable region near D_1, D_3 (ω_d), where $\omega_d=3.18$ (2706 rpm) and the relation $p_1+p_3=2\omega$ is satisfied. If m_s is assumed zero, the unstable region appears near D_{10}, D_{30} (ω_{d0}) where $\omega_{d0}=2.77$ (2357 rpm). Experimental results of negative damping coefficient m and frequencies P_1, P_3 are shown in Fig. 7.12.

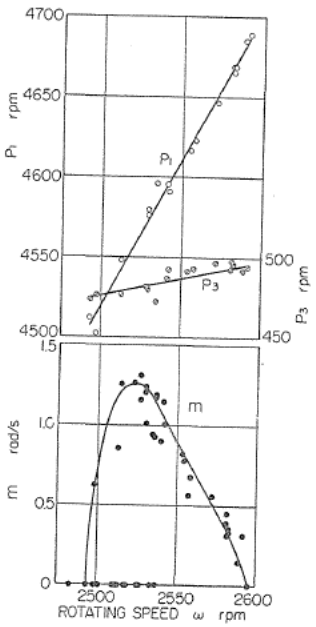

FIG. 7.12. P_1, P_3, m—ω diagram near ω_α (II—#6200)

7.5. Conclusions

(1) When a rather long shaft is used in experiment, and then a natural frequency of first mode of shaft itself is comparatively not so high, there appear new unstable regions.

(2) When a shaft is supported by single-row radial ball bearings which usually have small clearances in inclination angle, the stiffness of the shaft has non-symmetrical and non-linear spring characteristics. The unstable region bends to the higher or lower speed side with increase of the amplitude of steady beats. The response curve and jumping phenomenon are seen because of non-linearity in shaft stiffness.

Chapter 8. Unstable Vibrations of a Shaft with Unsymmetrical Stiffness[27)34)]

8.1. Introduction

Now we proceed to treat the system with variable elasticity corresponding to the system with variable moment of inertia treated so far. There have been many studies[2)3)4)] of the system with a flat shaft. In the present chapter, however, the general system with gyroscopic terms and with a rotor not mounted at mid-point of the unsymmetrical shaft is discussed.

8.2. Equations of motion and forced vibrations

We now denote the spring constants in MX_2-direction $\alpha+\Delta\alpha$, $\gamma+\Delta\gamma$, $\delta+\Delta\delta$, and in MY_2-direction $\alpha-\Delta\alpha$, $\gamma-\Delta\gamma$, $\delta-\Delta\delta$ in Fig. 1.3. Let the displacement of the geometrical center of rotor M be x', y', the inclination angle of MZ_0-axis be θ'_x, θ'_y in MX_2-, MY_2-directions respectively.

The potential energy of the shaft V' should be represented by the following form,

$$V' = \frac{1}{2}(\alpha + \Delta\alpha)x'^2 + (\gamma + \Delta\gamma)x'\theta_x' + \frac{1}{2}(\delta + \Delta\delta)\theta_x'^2$$
$$+ \frac{1}{2}(\alpha - \Delta\alpha)y'^2 + (\gamma - \Delta\gamma)y'\theta_y' + \frac{1}{2}(\delta - \Delta\delta)\theta_y'^2. \tag{8.1}$$

There are the relationships (8.2) between stationary coordinates x, y, θ_x, θ_y and rotating coordinates x', y', θ_x', θ_y':

$$\begin{matrix} x' \\ \theta_x' \end{matrix} = \begin{matrix} x \\ \theta_x \end{matrix} \cos\Theta + \begin{matrix} y \\ \theta_y \end{matrix} \sin\Theta, \quad \begin{matrix} y' \\ \theta_y' \end{matrix} = -\begin{matrix} x \\ \theta_x \end{matrix} \sin\Theta + \begin{matrix} y \\ \theta_y \end{matrix} \cos\Theta. \tag{8.2}$$

Inserting Eq. (8.2) into Eq. (8.1) and using V defined by Eq. (1.9), V' is represented as follows:

$$V' = V - \frac{1}{2}\Delta\alpha\{(y^2 - x^2)\cos 2\Theta - 2xy\sin 2\Theta\}$$
$$- \Delta\gamma\{(y\theta_y - x\theta_x)\cos 2\Theta - (x\theta_y + y\theta_x)\sin 2\Theta\}$$
$$- \frac{1}{2}\Delta\delta\{(\theta_y^2 - \theta_x^2)\cos 2\Theta - 2\theta_x\theta_y\sin 2\Theta\}. \tag{8.3}$$

The kinetic energy of a symmetrical rotor T' is derived from Eq. (1.8a) where ΔI is put zero. Substituting T', V', and F defined by Eq. (1.10) into Lagrange's equation (1.13) and using dimensionless quantities (2.11), (3.1), and (8.4):

$$\Delta\alpha/\alpha = \Delta_{11}, \quad \Delta\gamma/\gamma = \Delta_{12}, \quad \Delta\delta/\delta = \Delta_{22}, \tag{8.4}$$

we have the dimensionless equations of motion of the shaft with unsymmetrical stiffness and viscous damping:

$$\left.\begin{aligned}
&\ddot{x} + c_1\dot{x} + x + \gamma\theta_x - \Delta_{11}(x\cos 2\omega t + y\sin 2\omega t) \\
&\quad - \gamma\Delta_{12}(\theta_x\cos 2\omega t + \theta_y\sin 2\omega t) = e\omega^2\cos(\omega t + \xi), \\
&\ddot{y} + c_1\dot{y} + y + \gamma\theta_y - \Delta_{11}(x\sin 2\omega t - y\cos 2\omega t) \\
&\quad - \gamma\Delta_{12}(\theta_x\sin 2\omega t - \theta_y\cos 2\omega t) = e\omega^2\sin(\omega t + \xi), \\
&\ddot{\theta}_x + i_p\omega\dot{\theta}_y + c_2\dot{\theta}_x + \gamma x + \delta\theta_x - \gamma\Delta_{12}(x\cos 2\omega t + y\sin 2\omega t) \\
&\quad - \delta\Delta_{22}(\theta_x\cos 2\omega t + \theta_y\sin 2\omega t) = (i_p - 1)\tau\omega^2\cos(\omega t + \eta), \\
&\ddot{\theta}_y - i_p\omega\dot{\theta}_x + c_2\dot{\theta}_y + \gamma y + \delta\theta_y - \gamma\Delta_{12}(x\sin 2\omega t - y\cos 2\omega t) \\
&\quad - \delta\Delta_{22}(\theta_x\sin 2\omega t - \theta_y\cos 2\omega t) = (i_p - 1)\tau\omega^2\sin(\omega t + \eta).
\end{aligned}\right\} \tag{8.5}$$

If we substitute particular solutions of forced vibrations (3.3) into Eq. (8.5) we have simultaneous equations of amplitudes A, B, C, and D. Inserting solutions of free vibrations (2.13) into Eq. (8.5) and letting $e=\tau=0$, and $c_1=c_2=0$, we have the frequency equation:

$$\Phi(\omega, p) = \begin{vmatrix} 1-p^2 & -\Delta_{11} & \gamma & -\gamma\Delta_{12} \\ -\Delta_{11} & 1-\bar{p}^2 & -\gamma\Delta_{12} & \gamma \\ \gamma & -\gamma\Delta_{12} & G & -\delta\Delta_{22} \\ -\gamma\Delta_{12} & \gamma & -\delta\Delta_{22} & \bar{G} \end{vmatrix} = 0. \tag{8.6}$$

8.3. Unstable vibrations near ω_c and ω_d

Expansion of Eq. (8.6) gives the following form:

$$\Phi(\omega, p) = f\bar{f} - (1-p^2)(1-\bar{p}^2)\left[\frac{\gamma^2\Delta_{11}}{(1-p^2)(1-\bar{p}^2)} - \gamma^2\left\{\frac{1}{(1-p^2)} + \frac{1}{(1-\bar{p}^2)}\right\}\Delta_{12} + \delta\Delta_{22}\right]^2 + (\delta\Delta_{11}\Delta_{22} - \gamma^2\Delta_{12}^2)^2 = 0. \tag{8.7}$$

When the asymmetries of stiffness Δ_{11}, Δ_{12}, and Δ_{22} are enough small, and the smaller term $(\delta\Delta_{11}\Delta_{22} - \gamma^2\Delta_{12}^2)^2$ in Eq. (8.7) can be neglected, approximation methods used in Section 6.5 may be fully applied to the unstable vibrations of an unsymmetrical shaft by putting $\left[\frac{\gamma^2\Delta_{11}}{(1-p^2)(1-\bar{p}^2)} - \gamma^2\left\{\frac{1}{(1-p^2)} + \frac{1}{(1-\bar{p}^2)}\right\}\Delta_{12} + \delta\Delta_{22}\right]^2$ of Eq. (8.7) in place of $[\Delta p\bar{p}]^2$ of Eq. (6.1).

The second term in Eq. (8.7) has the same sign as that in Eq. (6.1), the derived conclusions in Section 6.3 is fully true to this case. Width of unstable region $2|\xi_0|$ and maximum value of negative damping coefficient $m_{\max}$ are derived from Eqs. (6.15), (6.14) by replacing $\sqrt{-(1-p^2)(1-\bar{p}^2)}\left|\frac{\gamma^2\Delta_{11}}{(1-p^2)(1-\bar{p}^2)} - \gamma^2\left\{\frac{1}{(1-p^2)} + \frac{1}{(1-\bar{p}^2)}\right\}\Delta_{12} + \delta\Delta_{22}\right|$ instead of $\Delta\sqrt{\varphi}$. Only the existence of the positive term $(\delta\Delta_{11}\Delta_{22} - \gamma^2\Delta_{12}^2)^2$ in Eq. (8.7) makes the unstable region of ω_c a little narrow, and makes the unstable region of ω_d slightly wide.

Dimensions of the experimental apparatus with unsymmetrical over-hung shaft are as follows:

$$\left.\begin{aligned} &I_p = 0.1893 \text{ kg cm } s^2,\ I = 0.3461 \text{ kg cm } s^2,\ W = 10.670 \text{ kg},\\ &\alpha \pm \Delta\alpha = 26.586 \pm 2.744 \text{ kg/cm},\ \gamma \pm \Delta\gamma = -545.55 \mp 48.00 \text{ kg/rad},\\ &\delta \pm \Delta\delta = 14993 \pm 1169 \text{ kg cm/rad},\ \sqrt{\alpha g/W} = 471.9 \text{ rpm},\ \sqrt{Ig/W} = 5.64 \text{ cm}. \end{aligned}\right\} \tag{8.8}$$

Dimensionless quantities got by Eqs. (2.11) and (8.4) are:

$$i_p = 0.5470,\ \gamma = -3.639,\ \delta = 17.74,\ \Delta_{11} = 0.1032,\ \Delta_{12} = 0.0880,\ \Delta_{22} = 0.0780. \tag{8.9}$$

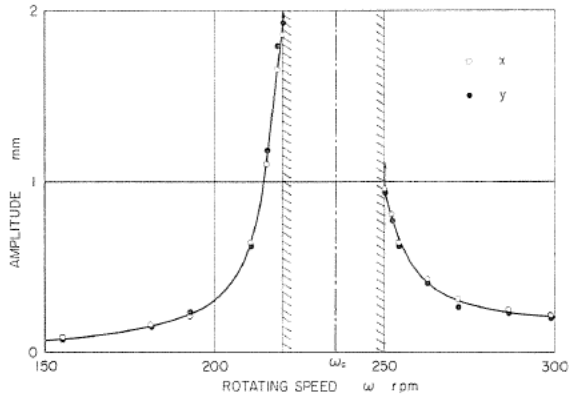

FIG. 8.1. Unstable region near ω_c

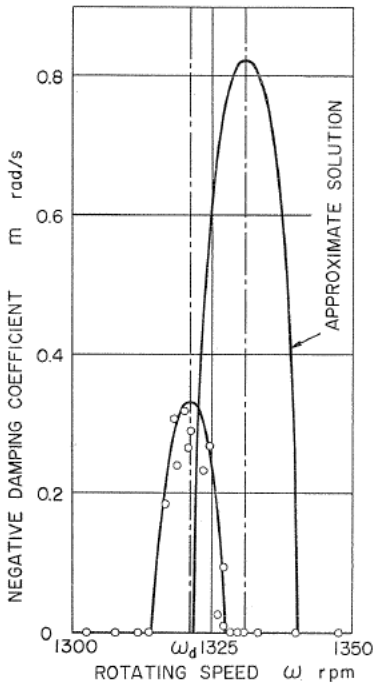

FIG. 8.2. Unstable region near ω_d

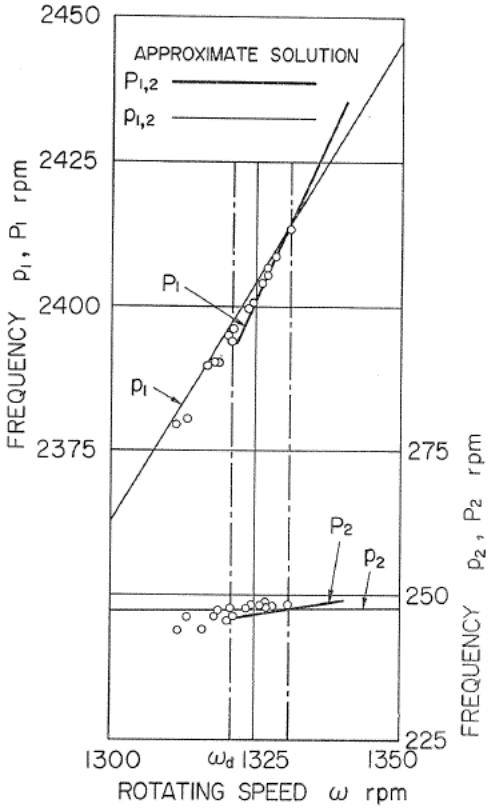

FIG. 8.3. Two vibrations in unstable region near ω_d

The response curve near ω_c is shown in Fig. 8.1, where the shaft becomes unstable at the rotating speed $\omega=220\sim250$ rpm. The calculated values are $\omega_c=$ 235.3 rpm, $2|\xi_0|=27.5$ rpm which coincide well with the experimental results $\omega_c=235$ rpm, $2|\xi_0|=30$ rpm.

The shaft again becomes dynamically unstable at $\omega=1314\sim1327$ rpm, where beats of two vibrations with frequency P_1, P_2 occur. Calculated negative damping coefficient m is given by full line curve in Fig, 8.2 and is compared with experimental results with marks ○. Because of an inevitable damping action existing in the shaft system the experimental value $m_{max}=0.32$ rad/s is fairly smaller than $m_{max}=0.82$ rad/s derived from calculation, but the experimental results of natural frequency P_1, P_2 are almost lying on the calculated full lines as shown in Fig. 8.3.

8.4. Conclnsions

(1) The frequency equation similar to Eq. (6.1) is obtained and the same kinds of unstable vibrations as the unsymmetrical rotor always take place.

(2) Useful approximation methods are also applicable to the shaft with unsymmetrical stiffness.

References

1) A. Watari, "On the Motion of Rotating Shafts", Reports of the Institute of Industrial Science, University of Tokyo, Vol. **2**, No. 4 (1952-3), pp. 114-169.
2) F. Nakanishi, "The Secondary Vibration of Revolving Shafts", Jour. Japan Soc. Mech. Engrs., Vol. **35**, No. 188 (1932-12), pp. 1170-1171.
3) H. D. Taylor, "Critical-Speed Behavior of Unsymmetrical Shafts", Jour. App. Mech. (1940-6), pp. A71-79.
4) W. Kellenberger, "Biegeschwingungen einer unrunden, rotierenden Welle in horizontaler Lage", Ing. Arch., Vol. **26** (1958), pp. 302-318.
5) T. Yamamoto, "On the Critical Speeds of a Shaft", Memoirs of the Faculty of Engineering, Nagoya University, Vol. **6**, No. 2 (1954-11), pp. 106-174.
6) T. Yamamoto, "On the Vibrations of a Rotating Shaft", Memoirs of the Faculty of Engineering, Nagoya University, Vol. 9, No. 1 (1957-5), pp 19-115.
7) T. Yamamoto and S. Hayashi, "Summed and Differential Harmonic Oscillations in Nonlinear Vibratory Systems", Memoirs of the Faculty of Engineering, Nagoya University, Vol. **18**, No. 2 (1966-11), pp. 85-150.
8) S. Fujii, "The roles of Resistance in the Vibration of a Rotating Shaft", Japan National Congress for App. Mech., Vol. **1** (1951), pp. 599-603.
9) B. L. Newkirk and H. D. Taylor, "Shaft Whipping Due to Oil Action in Journal Bearings", General Electric Review, Vol. **28** (1925-8), pp. 559-568.
10) B. L. Newkirk and L. P. Grobel, "Oil-Film Whirl-A Non-Whirling Bearing", Trans. ASME, Vol. **56** (1934), pp. 607-615.
11) Y. Hori, "A Theory of Oilwhip", Jour. App. Mech., Trans. ASME (1959-6), pp. 189-198.
12) A. L. Kimball, "Internal Friction Theory of Shaft Whirling", General Electric Review, Vol. **27** (1924), pp. 244-251.
13) B. L. Newkirk, "Shaft Whipping", General Electric Review, Vol. **27** (1924), pp. 169-178.
14) J. G. Baker, "Self-induced Vibration", Trans. ASME, APM-55-2 (1933), pp. 5-13.
15) F. M. Dimentberg, Flexural Vibrations of Rotating Shafts, (1961), pp. 16-41, Butterworths, London.
16) A. Tondl, Some Problems of Rotor Dynamics, (1965), pp. 17-69. Publishing House of the Czechoslovak Academy of Science.
17) Y. Sawaragi and Y. Iwamoto, "On the 'Shaft Whipping' excited by Dry Friction of Bearings", Trans. Japan Soc. Mech. Engrs., Vol. **17**, No. 57 (1951), pp. 61-66.
18) Y. Sawaragi, T. Matsuda, and K. Sugawara, "On the Forced Vibration of a System with the Restoring Force which is Expressed as a Function of Displacement and Time", Trans. Japan Soc. Mech. Engrs., Vol. **17**, No. 64 (1951), pp. 1-5.
19) D. M. Smith, "The Motion of a Rotor Carried by a Flexible Shaft in Flexible Bearings", Proc. Roy. Soc. London, Series A, Vol. **142** (1933), pp. 92-118.
20) W. R. Foote, H. Poritsky, and J. J. Slade, Jr., "Critical Speeds of a Rotor with Unequal Shaft Flexibilities, Mounted in Bearings of Unequal Flexibilities, I", Jour. App. Mech., Vol. **10** (1943), pp. A77-84.
21) A. Tondl, "The Stability of Motion of a Rotor with Unsymmetrical Shaft on an Elastically Supported Mass Foundation", Ing. Arch., Vol. **29** (1960), pp. 410-418.
22) Y. Yamada, "On the Critical Speeds of a Rotor System Having an Asymmetrical disk", Japan National Congress for App. Mech., Vol. **4** (1954), pp. 381-384.
23) L. Y. Banaf and F. M. Dimentberg, "Flexural Vibration of the Rotating Shaft with a Mounted Disk where Values of Principal Moments of Inertia of Mass are not equal", Izbestiy Akademii Nauk SSSR, Otn, Vol. **6** (1960), pp. 91-97.
24) S. Aiba, "On the Vibration and the Critical Speeds of an Asymmetrical Rotating Shaft", Reports of the Faculty of Engineering, Yamanashi University, No. 13 (1962-12), pp. 30-43.
25) O. N. Romaniv, "Flexural Vibration of the Shaft with a Disk Having Different Moment of Inertia (about the Symmetrical Axes)", Izbestiy Akademii Nauk SSSR, Otn, Vol. **6** (1960), pp. 98-104.

26) S. H. Crandall and P. J. Brosens, "On the Stability of Rotation of a Rotor with Rotationally Unsymmetric Inertia and Stiffness Properties", Jour. App. Mech., Trans. ASME, Vol. **28**, No. 4 (1961-12), pp. 567-570.
27) T. Yamamoto and H. Ōta, "On the Vibrations of the Shaft Carrying an Asymmetrical Rotating Body", Bulletin of JSME, Vol. **6**, No. 21 (1963-2), pp. 29-36.
28) T. Yamamoto and H. Ōta, "Unstable Vibrations of the Shaft Carrying an Unsymmetrical Rotationg Body (Vibrations Induced by Flexibility of Bearing Pedestals)", Bulletin of JSME, Vol. **6**, No. 23 (1963-8), pp. 404-411.
29) T. Yamamoto and H. Ōta, "On the Forced Vibrations of the Shaft Carrying an Unsymmetrical Rotating Body (Response Curves of the Shaft at the Major Critical Speeds)", Bulletin of JSME, Vol. **6**, No. 23 (1963-8), pp. 412-420.
30) T. Yamamoto and H. Ōta, "On the Unstable Vibrations of a Shaft Carrying an Unsymmetrical Rotor", Jour. App. Mech., Trans. ASME, Vol. **31**, Series E, No. 3 (1964-9), pp. 515-522.
31) T. Yamamoto, H. Ōta, and K. Sato, "On the Forced Vibrations of the Shaft Carrying an Unsymmetrical Rotor (Forced Vibrations Having the Circular Frequencies Differing from the Rotating Angular Velocity of the Shaft)", Bulletin of JSME, Vol. **9**, No. 33 (1966-2), pp. 58-66.
32) T. Yamamoto, H. Ōta, and K. Kakida, "The Effects of a Distributed Mass of Shaft and of Non-linear Characteristics of Shaft Stiffness on Unstable Vibrations", Preprints for General Meeting of Tokai Branch, Japan Soc. Mech. Engrs. (1966-3), pp. 45-48.
33) T. Yamamoto and H. Ōta, "The Damping Effect on Unstable Whirlings of a Shaft Carrying an Unsymmetrical Rotor", Memoirs of the Faculty of Engineering, Nagoya University, Vol. **19**, No. 2 (1967-11), pp. 197-217.
34) T. Yamamoto, H. Ōta, and K. Kōno, "On the Unstable Vibrations of a Shaft With Unsymmetrical Stiffness Carrying an Unsymmetrical Rotor", Jour. App. Mech., Trans. ASME, Vol. **35**, Series E, No. 2 (1968-6), pp. 313-321.